AUTOMATIC PHYSICAL FATIGUE ASSESSMENT FOR CONSTRUCTION WORKERS BASED ON COMPUTER VISION AND PRESSURE INSOLE SENSOR

YANTAO YU

PhD

The Hong Kong Polytechnic University

2020

The Hong Kong Polytechnic University

Department of Building and Real Estate

AUTOMATIC PHYSICAL FATIGUE ASSESSMENT FOR CONSTRUCTION WORKERS BASED ON COMPUTER VISION AND PRESSURE INSOLE SENSOR

Yantao YU

A thesis submitted in partial fulfilment of the requirements

for the degree of Doctor of Philosophy

January 2020

CERTIFICATE OF ORIGINALITY

I hereby declare that this thesis is my own work and that, to the best of my knowledge and belief, it reproduces no material previously published or written, nor material that has been accepted for the award of any other degree or diploma, except where due acknowledgement has been made in the text.

Yantao Yu

January 2020

Abstract[1]

The construction industry around the globe has unsatisfactory occupational health and safety records. One of the major reasons is attributed to high physical demands and hostile working environments. Construction work always requires workers to work for a long duration without sufficient breaks to recover from overexertion, and to work under harsh climatic conditions and/or in confined workspaces. Such circumstances can increase the risk of fatigue, which may lead to work-related musculoskeletal disorders (MSDs) and accidents on construction sites. With a growing proportion of older workers in many countries/regions, it is paramount to improve the occupational health and safety of construction workers in order to sustain the current construction workforce. Since fatigue poses a major challenge to occupational health and safety, fatigue monitoring and management has become an issue of utmost prominence.

Traditionally, physical fatigue monitoring in the construction domain relies on self-reporting or subjective questionnaires. These methods require the manual collection

[1] Abstract is based on a published study and being reproduced with the permission of Elsevier.
Yu, Y., Li, H., Yang, X., Kong, L., Luo, X., & Wong, A. Y. L. (2019). An automatic and non-invasive physical fatigue assessment method for construction workers. Automation in Construction, 103, 1–12. https://doi.org/10.1016/j.autcon.2019.02.020

of responses and are impractical for continuous fatigue monitoring. Some researchers have used on-body sensors for fatigue monitoring (such as heart rate monitors and surface electromyography (sEMG) sensors). Although these devices appear to be promising, they are intrusive, requiring sensors to be attached to the worker's body. Such on-body sensors are uncomfortable to wear and could easily cause irritation. Considering the limitations of these methodologies, the authors propose a novel non-intrusive method to monitor whole-body fatigue by combining computer vision technology and smart insoles for construction workers. Specifically, a computer vision-based 3D motion capture algorithm was developed to model the motion of various body parts using an RGB camera. Further, smart insoles capable of monitoring the reaction forces of feet generated by a work-pattern was applied with a self-charging capacity. A fatigue assessment indicator was developed using the force data from the insoles, the 3D model data from the developed motion capture algorithm and inverse dynamics modeling. A series of laboratory experiments demonstrate the accuracy and feasibility of the data collection methods and physical fatigue assessment (PFA) method. Field experiments demonstrate that the proposed method can not only be easily used by the construction industry to monitor the risk of overexertion and fatigue among workers but also contribute to improving construction site layout and schedule management aiming at improving construction workers safety.

Publications

*An asterisk * indicates corresponding author.*

Journal Papers (Published)

1. **Yu, Y.**, Yang, X., Li, H., Luo, X., Guo, H., & Fang, Q. (2019). Joint-Level Vision-Based Ergonomic Assessment Tool for Construction Workers. Journal of Construction Engineering and Management, 145(5), 04019025. https://doi.org/10.1061/(ASCE)CO.1943-7862.0001647
2. **Yu, Y.**, Li, H., Umer, W., Dong, C., Yang, X., Skitmore, M., & Wong, A. Y. L. (2019). Automatic Biomechanical Workload Estimation for Construction Workers by Computer Vision and Smart Insoles. Journal of Computing in Civil Engineering, 33(3), 04019010. https://doi.org/10.1061/(ASCE)CP.1943-5487.0000827
3. **Yu, Y.**, Li, H., Yang, X., Kong, L., Luo, X., & Wong, A. Y. L. (2019). An automatic and non-invasive physical fatigue assessment method for construction workers. Automation in Construction, 103, 1–12. https://doi.org/10.1016/j.autcon.2019.02.020
4. **Yu, Y.**, Guo, H., Ding, Q., Li, H., & Skitmore, M. (2017). An experimental study of real-time identification of construction workers' unsafe behaviors. Automation in Construction, 82, 193–206. https://doi.org/10.1016/j.autcon.2017.05.002
5. Kong, L., Li, H., **Yu, Y.***, Luo, H., Skitmore, M., & Antwi-Afari, M. F. (2018). Quantifying the physical intensity of construction workers, a mechanical energy approach. Advanced Engineering Informatics, 38, 404–419. https://doi.org/10.1016/j.aei.2018.08.005

6. Guo, H.**, Yu, Y.,** Ding, Q., & Skitmore, M. (2018). Image-and-Skeleton-Based Parameterized Approach to Real-Time Identification of Construction Workers' Unsafe Behaviors. *Journal of Construction Engineering and Management*, *144*(6), 04018042. https://doi.org/10.1061/(ASCE)CO.1943-7862.0001497

7. Guo, H., **Yu, Y.**, & Skitmore, M. (2017). Visualization technology-based construction safety management: A review. *Automation in Construction*, *73*, 135–144. https://doi.org/10.1016/j.autcon.2016.10.004

8. Guo, H., **Yu, Y**., Xiang, T., Li, H., & Zhang, D. (2017). The availability of wearable-device-based physical data for the measurement of construction workers' psychological status on site: From the perspective of safety management. *Automation in Construction*, *82*, 207–217. https://doi.org/10.1016/j.autcon.2017.06.001

9. Yang, X., **Yu, Y.**, Li, H., Luo, X., & Wang, F. (2017). Motion-based analysis for construction workers using biomechanical methods. *Frontiers of Engineering Management*, *4*(1), 84. https://doi.org/10.15302/J-FEM-2017004

10. Guo, H., **Yu, Y.**, Liu, W., & Zhang, W. (2014). Integrated appliation of BIM and RFID in construction safety manangement. *Journal of Engineering Management*, (4). https://doi.org/10.13991/j.cnki.jem.2014.04.018

11. X. Luo, H. Li, **Y. Yu**, C. Zhou, D. Cao, Combining deep features and activity context to improve recognition of activities of workers in groups, Computer-Aided Civil and Infrastructure Engineering. (2020) mice.12538. doi:10.1111/mice.12538.

12. M.F. Antwi-Afari, H. Li,, W. Umer, **Y. Yu**, X. Xing, Construction Activity Recognition and Ergonomic Risk Assessment Using a Wearable Insole Pressure System, Journal of Construction Engineering and Management. 146 (2020) 04020077. doi:10.1061/(ASCE)CO.1943-7862.0001849.

13. Yang, X., Li, H., **Yu, Y.**, Luo, X., Huang, T., & Yang, X. (2018). Automatic Pixel-Level Crack Detection and Measurement Using Fully Convolutional Network. *Computer-Aided Civil and Infrastructure Engineering*, *33*(12), 1090–1109. https://doi.org/10.1111/mice.12412

14. Antwi-Afari, M. F., Li, H., **Yu, Y.**, & Kong, L. (2018). Wearable insole pressure system for automated detection and classification of awkward working postures in construction workers. *Automation in Construction*, *96*, 433–441. https://doi.org/10.1016/j.autcon.2018.10.004

15. Luo, X., Li, H., Cao, D., **Yu, Y**., Yang, X., & Huang, T. (2018). Towards efficient and objective work sampling: Recognizing workers' activities in site surveillance videos with two-stream convolutional networks. *Automation in Construction*, *94*, 360–370. https://doi.org/10.1016/j.autcon.2018.07.011

16. Luo, X., Li, H., Yang, X., **Yu, Y.**, & Cao, D. (2018). Capturing and Understanding Workers' Activities in Far-field Surveillance Videos with Deep Action Recognition and Bayesian Nonparametric Learning. *Computer-Aided Civil and Infrastructure Engineering*. https://doi.org/10.1111/mice.12419

17. Fang, Q., Li, H., Luo, X., Ding, L., Rose, T. M., An, W., & **Yu, Y**. (2018). A deep learning-based method for detecting non-certified work on construction sites. *Advanced Engineering Informatics*, *35*, 56–68. https://doi.org/10.1016/j.aei.2018.01.001

18. Guo, H., **Yu, Y.**, Liu, W., & Zhang, W. (2014). Integrated application of BIM and RFID in construction safety management. Journal of Engineering Management, (4). https://doi.org/10.13991/j.cnki.jem.2014.04.018

Journal Papers (Under review)

1. **Yu, Y.**, Li, H., Yang, X., & Antwi-Afari, M. F. (2019). Posture data collection methods for construction workers: A review. Automation in Construction. Manuscript ID: AUTCON_2019_1244 (Under Review).
2. Umer, W., Li, H., **Yu, Y.**, Antwi-Afari, M. F., Luo, X., & Anwer, S. (2019). Physical exertion modeling using combined cardiorespiratory and thermoregulatory measures for construction tasks: A case study. Automation in Construction. Manuscript ID: AUTCON_2018_1067_R4 (Under Review).

Conference Papers (Published)

1. **Yu, Y.**, Li, H., & Yang, X. (2019). 3D Posture Estimation from 2D Posture Data for Construction Workers. In M. Al-Hussein (Ed.), 2019 Proceedings of the 36th ISARC (pp. 26–34). Banff, AB, Canada: The International Association for Automation and Robotics in Construction. https://doi.org/10.22260/ISARC2019/0004
2. **Yu, Y.**, Li, H., & Wong, Y. L. A. (2019). A non-intrusive method for measuring construction workers' muscle fatigue. In T. Linner & T. Bock (Eds.), Proceedings of the CIB W119 workshop on Automation and Robotics in Construction (pp. 26–36). Hong Kong: International Council for Resaerch and Innovation in Building and Construction. https://doi.org/10.14459/2019md1519198
3. **Yu, Y.**, Li, H., Yang, X., & Umer, W. (2018). Estimating Construction Workers' Physical Workload by Fusing Computer Vision and Smart Insole Technologies. In 2018 Proceedings of the 35th ISARC (pp. 1212–1219). Berlin: International Association for Automation and Robotics in Construction. https://doi.org/10.22260/ISARC2018/0168

4. **Yu, Y.**, Zhang, J., & Guo, H. (2017). Investigation of the Relationship between Construction Workers' Psychological States and Their Unsafe Behaviors Using Virtual Environment-Based Testing. In Computing in Civil Engineering 2017 (pp. 417–424). Reston, VA: American Society of Civil Engineers. https://doi.org/10.1061/9780784480847.052
5. Yang, X., Wang, F., Li, H., **Yu, Y.**, Luo, X., & Zhai, X. (2019). A Low-Cost and Smart IMU Tool for Tracking Construction Activities. In M. Al-Hussein (Ed.), 2019 Proceedings of the 36th ISARC (pp. 35–41). Banff, Alberta, Canada: The International Association for Automation and Robotics in Construction. https://doi.org/10.22260/ISARC2019/0005

Honors and Awards

1. **Best Paper Award** in the 35th International Symposium on Automation and Robotics in Construction (ISARC 2018) conference, June 2018, Berlin, Germany. Paper title: Estimating Construction Workers' Physical Workload by Fusing Computer Vision and Smart Insole Technologies
2. **Outstanding Paper Award** in the Chartered Institute of Building (Hong Kong) Outstanding Paper Award 2018, September 2018, Hong Kong, China. Paper Title: Automatic biomechanical workload estimation for construction workers by computer vision and smart insoles
3. **Best Paper Award** in the 1st BIM-CIM Innovation Competition for College Students in Guangdong-Hong Kong-Macao Great Bay Area, Shenzhen, China, December 2018. Paper Title: IMU-based real-time monitoring system for construction quality of concealed concrete projects

Acknowledgements

First and foremost, I want to thank my supervisor Professor Heng Li. It has been an honor to be his Ph.D. student. He has taught me, both consciously and unconsciously, how good research is done and what a good researcher should be. His passion on research motivated me a lot during my PhD study. He cares not only my research progress, but also my career development in the long run. I really appreciate all his contributions of ideas, time and patience.

I would like to thank Dr Arnold Wong, my co-supervisor, for his assistance on my research. He taught me experiment methods, revised my paper word by word, and helped me to find supports when my research encountered difficulties. His rigorous research attitude and hardworking has encouraged me to be an excellent young researcher like him.

I also want to thank my second co-supervisor, Professor Xiaoming Tao. She supported me a lot on learning material science, which broaden my views and provided me new research ideas and opportunities. I am also thankful for the excellent example she has provided as a successful female scientist and professor.

I would like to thank Research Grants Council (RGC) of Hong Kong and the Hong Kong PhD Fellowship Scheme (HKPFS) and The Hong Kong Polytechnic University for supporting me in pursuing my PhD study.

My sincere thanks also go to Dr. Xincong Yang, Dr. Xiaochun Luo and Mr. Xintao Yang. They gave me many valuable suggestions and technical supports. Without their help, my research could not progress so smoothly. I also appreciate all my colleagues in the Smart Construction Lab, their kindness and accompany makes my Ph.D. life colorful and unforgettable.

Last but not the least, I would like to thank my parents for their endless love, support and encouragement.

Table of Contents

List of Figures

List of Tables

List of Abbreviations

2D	Two Dimensional
3D	Three Dimensional
ANN	Artificial Neural Network
ATP	Adenosine Triphosphate
BVH	Bio-Vision Hierarchy
CNN	Convolutional Neural Network
DH	Denavit-Hartenberg
FC	Fully-connected
GRF	Ground Reaction Force
HOG	Histograms of Oriented Gradients
HSV	Hue-Saturation-Value
IMU	Inertial Measurement Unit
KIM	Key Item Method
KNN	K-Nearest Neighbor
LA	Left Ankle
LDA	Latent Dirichlet allocation
LE	Left Elbow
LH	Left Hip
LN	Left Knee
LS	Left Shoulder
LSTM	Long Short Term Memory
LW	Left Waist
MPJPE	Mean Per Joint Position Error

NIOSH	National Institute for Occupational Safety and Health
OCRA	Occupational Repetitive Actions
OSH	Occupational Safety and Health
OWAS	Ovako Working Posture Analysis System
PATH	Posture, Activity, Tools and Handling
PFA	Physical Fatigue Assessment
QEC	Quick Exposure Check for musculoskeletal risks
RA	Right Ankle
RANN	Residual Artificial Neural Network
RE	Right Elbow
REBA	Rapid Entire Body Assessment
ReLU	Rectified Linear Unit
RGB	Red-Green-Blue
RH	Right Hip
RK	Right Knee
RS	Right Shoulder
RULA	Rapid Upper Limb Assessment
RW	Right Waist
sEMG	Surface Electromyography
SIFT	Scale Invariant Feature Transform
SURF	Speeded Up Robust Features
SVM	Support Vector Machine
WMSD	Work-related MusculoSkeletal Disorder
WMSE	Weighted Mean Square Error

List of Symbols

$\boldsymbol{DH}_{\mathrm{C}}$	Denavit-Hartenberg matrix of a child joint	
$\boldsymbol{DH}_{\mathrm{P}}$	Denavit-Hartenberg matrix of a parent joint	
$\boldsymbol{F}_{\mathrm{C}}$	Joint reaction force at child joint	N
$\boldsymbol{F}_{\mathrm{P}}$	Joint reaction force at parent joint	N
$\boldsymbol{G}$	Gravity	N
$\boldsymbol{H}^{(\mathrm{k})}$	The k^{th} hidden layer in RANN	
$\boldsymbol{H}_{\mathrm{R}}^{(\mathrm{k})}$	The output of residual unit	
$\boldsymbol{I}_{3}$	Unit matrix	
$\boldsymbol{J}_{\mathrm{C}}$	3D cartesian coordinates of a child joint with an additional element 1	
$\boldsymbol{J}_{\mathrm{P}}$	3D cartesian coordinates of a parent joint with an additional element 1	
$\boldsymbol{R}_{\mathrm{x}}$	Rotation matrix around x-axis	
$\boldsymbol{R}_{\mathrm{y}}$	Rotation matrix around y-axis	
$\boldsymbol{R}_{\mathrm{z}}$	Rotation matrix around z-axis	
$\boldsymbol{S}_{\mathrm{3D}}$	Original 3D posture	
$\boldsymbol{S}'_{\mathrm{3D}}$	Rotated 3D posture	
$\boldsymbol{S}_{\mathrm{2D}}$	Projected 2D posture	
$\boldsymbol{T}$	Transformation matrix	
$\boldsymbol{W}^{(\mathrm{k})}$	Weight matrix connecting the $(\mathrm{k\text{-}1})^{\mathrm{th}}$ layer and the k^{th} layer in RANN	
$\boldsymbol{E}$	Information in an RGB image	
$\boldsymbol{F}_{\mathrm{L}}$	Ground reaction force of left foot	
$\boldsymbol{F}_{\mathrm{R}}$	Ground reaction force of right foot	
$\boldsymbol{\Gamma}$	Joint torque	N·m

$\boldsymbol{\Gamma}_{\mathrm{P}}$	Joint torque at parent joint	N·m
$\boldsymbol{\Gamma}_{\mathrm{G}}$	Torque produced by $\boldsymbol{G}$	N·m
$\boldsymbol{\Gamma}_{\boldsymbol{F}_{\mathrm{C}}}$	Torque produced by $\boldsymbol{F}_{\mathrm{C}}$	N·m
$\boldsymbol{\Gamma}_{\boldsymbol{F}_{\mathrm{P}}}$	Torque produced by $\boldsymbol{F}_{\mathrm{P}}$	N·m
$\boldsymbol{\Gamma}_{\mathrm{max}}$	Maximum joint capability	N·m
$\boldsymbol{\Gamma}_{\mathrm{cem}}$	Current joint capability	N·m
$\boldsymbol{b}^{(\mathrm{k})}$	Bias	
$\boldsymbol{f}_{\mathrm{L,q}}$	Pressure value measured by the sensor q in the left insole	N/m^2
$\boldsymbol{f}_{\mathrm{R,q}}$	Pressure value measured by the sensor q in the right insole	
$\boldsymbol{h}$	Row vector of $\boldsymbol{H}^{(\mathrm{k})}$	
$\overline{\boldsymbol{h}}$	Mean vector of all row vectors in $\boldsymbol{H}^{(\mathrm{k})}$	
$\hat{\boldsymbol{h}}$	Normalized row vector of $\boldsymbol{H}^{(\mathrm{k})}$	
$\boldsymbol{h}_{\mathrm{BN}}$	Output vector of batch normalization	
$\boldsymbol{w}$	Weight vector of all joints	
$\boldsymbol{s}_{\mathrm{n,j}}$	Ground truth 3D location of joint j in data item n	
$\hat{\boldsymbol{s}}_{\mathrm{n,j}}$	Estimated 3D location of joint j in data item n	
$\boldsymbol{a}$	Upper body plane generated by neck joint and two hip joints	
$\boldsymbol{b}$	Lower body plane generated by waist joint and two knee joints	
$\boldsymbol{c}$	Sagittal plane	
$\boldsymbol{l}$	Intersecting line of plane $\boldsymbol{a}$ and $\boldsymbol{c}$	
$\boldsymbol{n}$	Normal vector of plane $\boldsymbol{a}$	
$\boldsymbol{v}$	A three-dimensional vector	
$\boldsymbol{x}$	2D joint locations	
$\boldsymbol{y}$	3D joint locations	
$\boldsymbol{\chi}_1$	Scaling coefficient vector	
$\boldsymbol{\chi}_2$	Shifting coefficient vector	
$\boldsymbol{\mu}$	Unit vector representing the anterior direction of human body	
$\boldsymbol{\upsilon}$	Unit vector representing the positive direction of x-axis	

$\boldsymbol{\kappa}$	The normal vector of $\boldsymbol{\mu}$ and $\boldsymbol{\upsilon}$	
A	Plantar contact area	m^2
CF	Cumulative joint physical fatigue index	
IF	Instantaneous joint physical fatigue index	
L	The number of neurons in a layer of RANN	
N	The number of data items in training dataset	
Q	Largest sensor number in each insole	
$\overline{AB}$	Vector from point A to point B	
c_1	Age coefficient for joint capability regression	
c_2	Weight coefficient for joint capability regression	
c_3	Height coefficient for joint capability regression	
c_4	Gender coefficient for joint capability regression	
c_5	Joint muscle fatigue coefficient	
c_6	Joint muscle recover coefficient	
e_{n}	Mean per joint position error for the n^{th} posture in the dataset	
$h^{(\mathrm{k})}_{\mathrm{m,l}}$	The value of an element in a hidden layer $\boldsymbol{H}^{(\mathrm{k})}$	
j	The serial number of a joint	
l	The column number of an element in a hidden layer	
l_{bone}	Force arm	m
$loss_{\mathrm{n}}$	The loss of the n^{th} posture in the training dataset	
$loss$	Training loss	
m	The row number of an element in a hidden layer	
n	The serial number of a data item in training dataset	
$p_{\mathrm{n,j_0}}$	2D coordinates of the $\mathrm{j}_0^{\mathrm{th}}$ joint in the n^{th} posture in the training dataset	
q	The number of each sensor in an insole	
r	Location of the center of mass	
r_{x}	Roll angle around x-axis	rad

r_y	Pitch angle around y-axis	rad
r_z	Yaw angle around z-axis	rad
t	Time	
w_j	The weight of joint j	
α	Angle of plane $\boldsymbol{a}$ and plane $\boldsymbol{b}$	rad
β	Trunk flexion angle	rad
η	Upper arm flexion angle	rad
γ	Trunk side angle	rad
ϵ	Constant for preventing being division by zero	
ϕ	Upper arm abduction angle	rad
σ^2	Variance	
θ_1	Horizontal projection angle	rad
θ_2	Vertical projection angle	rad
$\boldsymbol{g}(\bullet)$	ReLU function	
$\boldsymbol{F}(\bullet)$	Batch norm and ReLU function	
$\boldsymbol{R}(\bullet)$	RANN function	
$\circ$	Hadamard product, or element-wise product	

PART I INTRODUCION AND LITERATURE REVIEW

Chapter 1 Introduction[2]

1.1 Fatigue in the construction industry

The construction industry around the globe is affected by unsatisfactory occupational health and safety records [1]. One of the major reasons is fatigue due to the high physical demands of construction tasks. Construction workers need to work for a prolonged period without sufficient breaks, and/or work in harsh climatic conditions/confined workspaces. Such working patterns may heighten the risk of developing fatigue in construction workers. If workers continue to work under the fatigue condition, they may be at the risk of developing work-related musculoskeletal disorders (WMSDs), making mistakes, reducing productivity and quality of work, as well as having accidents or fall incidents on construction sites. According to the Bureau of Labor Statistics [2], 33% of all occupational injuries

[2] This chapter is based on a published study and being reproduced with the permission of Elsevier.

Yu, Y., Li, H., Yang, X., Kong, L., Luo, X., & Wong, A. Y. L. (2019). An automatic and non-invasive physical fatigue assessment method for construction workers. Automation in Construction, 103, 1–12. https://doi.org/10.1016/j.autcon.2019.02.020

and illnesses on the US construction sites were related to fatigue. Therefore, fatigue is a severe occupational health and safety problem [3].

Manpower shortage, which has been listed as one of the core challenges facing the industry, may increase physical fatigue. A study predicted that there would be a shortfall of 10,000 to 15,000 construction workers from 2019 to 2021 in Hong Kong [4], which accounts for approximately 5.4% to 8.1% of the total construction workforce in Hong Kong [5]. Manpower shortage has brought negative effects to the industry. For example, Hong Kong was ranked the third most expensive place build on the planet in 2018 for stretched labor supply driving up construction costs [6]. In addition, aging manpower aggravates the situation. According to a survey in 2018, 42% of the registered construction workers in Hong Kong were at or over the age of 50. The rate was even higher at 56% for skilled workers [6]. Given the fact that older workers are more prone to fatigue due to declining physical work capacity, it is paramount to optimize the sustainability of the current construction workforce by improving their occupational health and safety.

In the future, while the continuous growth of the construction industry is expected to generate significant socio-economical value, it places pressures on the manpower and exacerbate the situations. In short, fatigue brings negative effects on safety, health and productivity to the global construction industry due to high workloads, manpower shortage and aging population. As a result, it is important to provide accurate fatigue level monitoring and prevention for construction workers for better safety, health and productivity performance.

1.2 Research scope

This section aims to narrow the research scope from fatigue to physical fatigue assessment. First, the reason why physical fatigue, rather than mental fatigue, is selected as the topic is given. Then, the importance of assessment is explained and narrows the research topic to physical fatigue assessment.

1.2.1 From fatigue to physical fatigue

Fatigue has been defined as the failure to maintain power output [7]. Fatigue experiences result from the reduction of each of the three types of energetic resources: physical, mental and emotional. Consequently, fatigue is categorized as physical fatigue, mental fatigue and emotional fatigue [8]. Mental and emotional fatigue are the temporary inability to maintain optical cognitive and emotional performance. Mental and emotional fatigue are multidimensional and multicausal, e.g. high pressure, sleep disorders, mood changes, social environment [9,10]. These factors are difficult to quantified and closely related to social cultural atmosphere.

Physical fatigue, or muscle fatigue, is biomechanically defined as the decrease of the muscles' ability to generate forces. Physical fatigue has closed relations with job task characteristics, such as external load, awkward postures and work durations [11,12]. Thus, physical fatigue could be interfered with construction site management. In addition, construction workers had lower levels of mental health than general population, but higher levels of physical health [13]. This study focuses on physical fatigue considering its prevalence and the opportunity to intervene it through constriction site management.

1.2.2 The importance of assessment in physical fatigue prevention

Performance assessment, or performance measurement, is quite important in workplace safety and health management, which is applied to monitor, benchmark and improve performance. Physical fatigue, as a critical cause of safety and health problems on construction site, should also be quantitatively measured [14], so that construction professionals could better understand the development of physical fatigue and make prevention measurements. Serving as the first step of physical fatigue prevention, physical fatigue assessment (PFA) is selected as the topic of this research.

1.3 Research problem statement

Considering the prevalence of physical fatigue among construction workers and its severe negative effects, many methods have been proposed for physical fatigue assessment. The utility and accuracy of PFA are decided by indicator design and data collection method [15].

Research problems of indicator design. Both qualitative and quantitative indicators have been used in previous studies. For example, workers' descriptions about their perception of fatigue level are qualitative indicators, which are subjective and may lead to biased results. Quantitative indicators provide more objective results. Ergonomic risk score is one of the most widely used quantitative indicators for PFA, which assesses ergonomic risk based on joint angles, posture duration and repetition. Ergonomic risk score was developed and has been widely applied in the manufacturing industry, where the manpower works with regular and repetitive postures in tidy indoor environments. The working environments and working activities in the construction industry, on the contrary, are complex and dynamic. Therefore, the ergonomic risk scores developed in the manufactory industry cannot be applied in the construction industry.

What's more, physical fatigue level is closely related to a worker's physical capability. For instance, when doing the same task, aged workers usually have higher physical fatigue level than young workers. However, above indicators fail to consider the individual differences in physical capability. Therefore, a new PFA indicator is needed in the construction industry for individualized evaluation with no limitations on work postures.

Research problems of data collection. A number of approaches have been proposed to provide PFA-related data. For example, self-reported questionnaires and systematic observation are traditionally used to evaluate workers' fatigue [16,17]. On-body sensors, mainly physiological sensors and motion sensors, have been introduced for automatic assessment [18–22]. Although prior studies have proven the concept, attaching multiple sensors to construction workers' bodies inevitably interfere their work performance. Further, these sensors may be uncomfortable to wear and may cause skin irritation. Considering complex field environments and dynamic construction workers activities, an automatic and non-invasive data collection method should be developed.

In conclusion, the research problems are that 1) there lacks a PFA indicator which considers both irregular working patterns and individual difference in physical capability; and 2) there lacks a method to collect the data for PFA from construction workers in an automatic, accurate and non-invasive manner.

1.4 Research aim and objectives

This research aims to develop a PFA method for construction workers which suits the complex and dynamic nature of construction activities. Specifically, the objectives of this research are:

1) to develop a physical fatigue indicator which provides quantitative and individualized results for irregular construction activities,
2) to identify the data demanding of above indicator and develop relative data collection methods,
3) to test the accuracy of the data collection methods and the physical fatigue indicator,
4) to validate the usability of the PFA method on construction sites.

1.5 Research significance

One intended outcome of the study, on a theoretical level, is to provide continuous and quantitative physical fatigue measurements of construction workers, which contribute to the understanding of construction workers physical fatigue development, such as the relations between physical fatigue and construction site layouts and schedules.

On a practical level, a second intended outcome of the study is a non-invasive data collection method which is suitable for construction field environments. In addition to satisfying the data demands in this study, the proposed data collection method also contributes to other construction worker-related studies, such as detecting safe behavior and assessing productivity.

Further, a third intended outcome contributes to occupational health in the construction industry. From the perspectives of construction workers, the method could provide individualized joint-level PFAs, which could help them to have a better understanding of the health risks during working. From the perspectives of site managers, the method could help in evaluating the physical fatigue level under different site layouts or work schedules and contributes to better construction health management.

Overall, this study will: (1) improve the understanding of physical fatigue development of workers on construction sites, (2) provide continuous and accurate posture data and external load data from workers, and (3) assist in reducing the possibility of overexertion and fatigue-induced injuries among workers.

1.6 Research instruments

The following research instruments are applied in this study to answer the following research questions.

1) **Literature review**. Relative publications, mainly peer-reviewed journal papers and conference papers, were reviewed to gain an understanding of the knowledge of PFA and previous techniques for construction workers' data collection. Available techniques and research gaps were identified based on the literatures review.
2) **Laboratory experiments**. A series of laboratory experiments were conducted in this research for assessing the accuracy and improving the performance of the proposed data collection methods.
3) **Field experiments.** Field experiments were used to test the feasibility of the proposed PFA method on real construction sites and demonstrated the method in application in construction site management.

1.7 Overview of the thesis

The rest of this thesis consists of three parts and eight chapters. The rest of the PART I is a literature review of relevant background knowledge about physical fatigue assessment. Part II explains the building of the PFA method, where Chapter 3 outlines the PFA method and relevant assumptions, Chapter 4 proposes a 3D posture data collection method based on computer vision, and Chapter 5 brings an external forces estimation method and the development of the new PFA indicator. At last, PART III describes the experiment settings and results in Chapter 6 and investigates the applications of the PFA method in construction site management in Chapter 7. The discussion of this study and possible future research directions are given in Chapter 8.

Chapter 2 Literature Review[3]

This section reviews existing studies on physical fatigue assessment indicators in section 2.1, physical fatigue development theories in section 2.2, data collection methods in section 2.3. Finally, research gaps are revealed in section 2.4.

2.1 Physical fatigue assessment indicators

Indicators are the core of assessment methods, which define the effectiveness and efficiency of assessment results, and determine the data needed for the assessment methods. Accordingly, physical fatigue indicators are the foundation upon which PFA methods are built. The aim of the section is (1) to summarize and compare

[3] This chapter is based on a published study and being reproduced with the permission of Elsevier, International Council for Research and Innovation in Building and Construction, and The International Association for Automation and Robotics in Construction.

Yu, Y., Li, H., Yang, X., Kong, L., Luo, X., & Wong, A. Y. L. (2019). An automatic and non-invasive physical fatigue assessment method for construction workers. Automation in Construction, 103, 1–12. https://doi.org/10.1016/j.autcon.2019.02.020

Yu, Y., Li, H., & Wong, Y. L. A. (2019). A non-intrusive method for measuring construction workers' muscle fatigue. In T. Linner & T. Bock (Eds.), Proceedings of the CIB W119 workshop on Automation and Robotics in Construction (pp. 26–36). Hong Kong: International Council for Research and Innovation in Building and Construction. https://doi.org/10.14459/2019md1519198

Yu, Y., Li, H., & Yang, X. (2019). 3D Posture Estimation from 2D Posture Data for Construction Workers. In M. Al-Hussein (Ed.), 2019 Proceedings of the 36th ISARC (pp. 26–34). Banff, AB, Canada: The International Association for Automation and Robotics in Construction. https://doi.org/10.22260/ISARC2019/0004 previous PFA indicators and related theories in multiple disciplinaries, and (2) to reveal the limitations of the previous indicators if applied to the construction industry. Accordingly, section 2.1.1 summarized subjective PFA indicators, while section 2.1.2 and section 2.1.3 summarized objective PFA indicators including physiological indicators and ergonomic indicators. Section 2.1.4 reviewed the indicator based on joint torques. Then, through comparing the application scenarios of above indicators, section 2.1.5 analyzes the limitations of existing PFA indicators and reveals that a new PFA indicator is necessary for construction workers.

2.1.1 Subjective PFA indicators

Subjective PFA indicators rely on workers' subjective feelings of self-perceived physical fatigue, which is usually quantified by self-report-scales. *Borg rate of perceived exertion (RPE) scale* and *Borg CR10 scale* are two commonly used scales asking workers regarding their perception of fatigue on a scale from 6 to 20 or from 0.0 to 12.0 [23], where higher scores indicate more fatigue. Self-report-scales are easy to implement but not suitable for investigating construction workers' physical fatigue because: (1) the reporting process may interrupt the normal work activity; (2) the scales only provide final fatigue status rather than monitoring the fatigue development process; and (3) the reported data may be inaccurate/inconsistent due to distorted memory and dishonest answer.

2.1.2 Physiological indicators

Physical fatigue involves a physiological process, which can be monitored by physiological indicators such as cardiovascular indicators and electronic indicators. Cardiovascular indicators include heart rate, skin temperature and breathing rate, which usually increase as a consequence of high physical strains [21,24,25]. These indicators can be measured by wearable sensors tied/attached to workers' bodies. However, these sensors may hinder workers' performance during work routine. In addition, these sensors need to be charged every "several hours" within a day, making it difficult to monitor physical fatigue for a prolonged period [3].

A widely-used electronic indicator for physical fatigue detection is surface electromyography (sEMG) [26]. SEMG measures the myoelectric activity during muscle contraction and relaxation cycles [27]. The myoelectric signals are captured by electrodes, then amplified, filtered and transferred to digital signals. When a muscle develops fatigue, the median frequency of the digital signal will decrease [28]. Previous studies have used sEMG to measure construction worker's muscle fatigue in laboratories [18,29]. Although sEMG can accurately measure muscle fatigue, the method may not be applicable on the construction sites. Since a pair of sEMG electrodes should be attached to the skin of each target muscle group, it is infeasible to attach a lot of electrodes to workers for whole-body muscle/physical fatigue measurements. Further, as sweating and body movement can cause significant artifacts to sEMG signals, it is impossible to monitor muscle fatigue accurately on construction sites.

In summary, while physiological indicators can objectively assess physical fatigue, workers need to wear some sensors in order to detect physiological changes, which may hinder work performance, cause discomfort, and may have questionable accuracy for continuous PFAs for construction workers. In addition, some physiological indicators, such as heart rate, are affected by both physical and mental fatigue. As a result, measuring physical fatigue with physiological indicators may lead to biased results.

2.1.3 Ergonomic indicators

Ergonomics indicators estimate physical fatigue based on workers' kinematics data. Numerous studies have adopted posture-based methods and computation models to assess/estimate workers' physical fatigue.

Unergonomic postures are a critical cause of physical fatigue. Previous research evaluated physical fatigue based on working postures [3]. Some studies assessed physical fatigue based on joint angles. By observing the joint angles of various body parts in a given work posture (e.g. trunk flexion/extension angles, shoulder flexion/abduction angles, and elbow/knee flexion angles), each joint angle was classified into a particular range of motion category, which is given a specific physical fatigue score [30–32]. Another method is to first identify the working posture (e.g. standing up, back bending, squatting, etc.) through observation and then estimate the corresponding physical fatigue based on the posture [33]. Although awkward postures may increase physical fatigue level, other factors (e.g., lifting construction materials, or using heavy tools) may also modify the risk of developing physical fatigue. Therefore, using the posture-based method alone without considering other factors may underestimate physical fatigue.

In addition to postures, some studies also took exerted forces into account. Several ergonomic scales have been developed, including Key Item Method (KIM) [34], The National Institute for Occupational Safety and Health (NIOSH) lifting equation [35], Ovako Working Posture Analysis System (OWAS) [36], Occupational Repetitive Actions (OCRA) [37], Rapid Upper Limb Assessment (RULA) [38], and Rapid Entire Body Assessment (REBA) [39]. When assessing exerted forces, the external forces/loadings are classified into different categories according to the absolute value, such as 0~5kg, 5~10kg and over 10kg. The overall physical fatigue score is calculated by summing the posture-based score and the exerted force-based score. Some scales also consider the work pattern. For example, RULA and REBA take the work repetitiveness and duration into account. The final physical fatigue score will be higher if a task is repeated more than four times per minute or lasts for more than a minute.

While these scales are easy to use and can provide quantitative workload assessments, they may not be suitable for construction workers. First, some of these scales only assess a particular body part (e.g. OCRA evaluates the upper body only), but the construction workers usually get whole-body fatigue. Further, these scales were originally developed to evaluate the works of manufacturing workers, whose works mainly involve repetitive motions with external forces in a static posture.

However, the works of construction workers are more diverse and less repetitive, making it difficult to assess physical fatigue based on repetitiveness or duration alone. Importantly, since using different scales may yield different results [34], it is difficult to compare findings across studies.

Another defect of ergonomic indicators in PFA lies in the difference between ergonomic risk and physical fatigue. Though unergonomic postures may lead to physical fatigue, other factors may also cause physical fatigue. For example, if performing the same posture with the same exerted forces, workers with high physical capability are less prone to feel physical fatigue than those with low physical capability; workers who just have a sufficient rest are less prone to feel physical fatigue than those who work continuously. In short, ergonomic indicators consider only a part of external factors of physical fatigue, while ignore internal factors and other external factors, which may lead to biased physical fatigue assessment results.

2.1.4 Joint torques as PFA indicators

Biomechanical calculation could provide more detailed and accurate PFA through calculating joint forces or joint torques based on exerted forces and postures. Several types of software have been developed to provide joint forces and torques given postures and exerted forces, including 3DSSPP, OpenSim, and AnyBody Modelling System [40–42]. In addition, above software could also provide personalized PFA by comparing joint torques to workers' joint capacities.

In construction management, 3DSSPP and OpenSim have been applied to assess workers' ergonomic risks and physical fatigue [43,44]. However, the software could only be used in laboratory or virtual environments due to the limitations on data collection. For example, a typical whole-body motion sensor set for OpenSim requires the acquisition of 50 markers' data on the participant's body using multiple cameras [45]. It is impractical for workers' fatigue monitoring on construction sites.

2.1.5 Comparison of PFA indicators

Based on the above analysis, this section summarizes and compares the limitations of PFA indicators as shown in Table 2-1. Except for Myoelectric indicators, all of the above indicators could be used on whole-body level. In addition, joint torque indicators could provide PFAs on both whole-body level and body segment level. For working patterns, all the methods have no limitations on the repetition or duration of postures except for ergonomic scales. Ergonomic scales are usually suitable for simple and repetitive postures. For working environment, some methods, such as myoelectric indicator and biomechanical software analysis, could only be used in laboratory environments because the measurement requires complex sensors which could only be used in laboratories.

Besides, pervious PFA methods, excepted for joint torque indicators, have been limited to general guidelines without considering individual differences. It is a fact that peoples are varied in physical capabilities. For example, aging people are more prone to get physical fatigue then young people. Other factors, such as gender,

Table 2-1 The comparison of physical fatigue assessment indicators

PFA Indicators				Body parts	Working pattern	Environment	Individualized assessment	Dynamic assessment
Subjective	Self-report		Self-perception of physical fatigue	Whole-body	No restriction	Outdoor	×	×
Objective	Physiological indicators	Cardiovascular indicators	Heart rate, skin temperature or breathing rate	Whole-body	No restriction	Outdoor	×	×
		Myoelectric indicator	The median frequency of sEMG signals	Low back	No restriction	Lab	×	×
	Ergonomic indicators	Pose or/and exerted forces-based assessments (Ergonomic scales)	Ergonomic risks due to awkward postures, large exerted forces, and prolonged or repetitive task patterns	Whole-body	Repetitive and regular	Outdoor	×	×
	Joint torque indicators	Biomechanical software analysis	Joint-level physical fatigue	Whole-body/body segments	No restriction	Lab	√	×

height and weight have also prove to be related to physical capabilities [46]. In addition, work history also affects physical capabilities. People usually have higher capability after having a rest. The reviewed indicators, however, failed to consider individual differences on working physical capabilities.

2.1.6 Summary

Most PFA indicators have restrictions on regular working patterns, certain body parts, or laboratory environments. Besides, these PFA indicators fail to consider individual differences and temporal variations of workers' physical ability. As a result, few of them suits construction site environments. Based on above considerations, there exists a lack of a PFA indicator which is accurate and suitable for construction tasks. The indicator should 1) has no limitations on body part or working pattern; 2) be suitable for outdoor environments; 3) allow individualized assessment; and 4) consider the dynamic variations of worker's capability.

The following section reviews theoretical models about physical fatigue development with the hope to find a model suitable for the PFA indicator in construction industry.

2.2 Physical fatigue development models and human body kinetics

It has been argued in section 2.1 that previous PFA indicators are not suitable for the construction industry. In order to build a new PFA indicator, this chapter investigates the background knowledge of physical fatigue development, aiming at finding out a model that could be used in the PFA for construction industry.

Section 2.2.1 reviews fatigue development mechanisms [47], and compares them according to their usability in construction industry. The comparison results show that joint-torque-model has the potential to be transformed into a PFA indicator. Section 2.2.2 further reviews relevant biomechanical knowledge about join torque calculation, and analyzes the data requirements.

2.2.1 Physical fatigue development models

A number of theories have been proposed to explain the development of physical fatigue, such as calcium ions cross-bridge mechanism model and force-PH relation model [48,49]. Mathematical models were built to simulate the physical fatigue development in the above theories. However, it is infeasible to measure the construction workers' calcium ions or intracellular pH on construction sites continuously and non-intrusively due to the bulky equipment and the intrusiveness.

Joint torques could be used to predict physical fatigue [50]. The model was first theoretically built based on the muscle motor unit theory [51]. The theory assumes that a muscle consists of many motor units with different force generation capabilities and recovery properties [51]. Some motor units generate large forces and develop fatigue quickly, but they also recover quickly after fatigue. Conversely, some motor units generate smaller amount of forces for a longer duration, but they recover slowly after contraction. As a result, when a muscle contracts, the muscle capacity should first decrease rapidly then slowly; and during the recovery process, the muscle capacity should also increase first rapidly then slowly. Muscle fatigue decreases the capacity of corresponding body segments to cope with the external force, which can be expressed as the physical fatigue level of a joint in the model. The model simulates the suggested joint fatigue and recovery process through the modelling of joint torques, maximum voluntary contraction and fatigue/recovery rate.

The model was validated in a series of human studies on the elbow joint fatigue during some static tasks [50,52]. In addition, the model has been applied in virtual construction environments to assess the fatigue level of shoulder joints of construction workers, in which the shoulder joint torques were estimated based on shoulder joint angle and external forces [53].

Above theories reveal the mechanism of physical fatigue development, and provide theoretical foundations for PFA indicators. However, if applied on construction sites, the model has to be simple enough so that its data requirements could met with data collection methods. Calcium ions cross-bridge mechanism model, for example, requires nearly 20 variables to estimate the fatigue level of a single muscle, which is too complex to be applied on construction sites. Force-PH relationship model requires intracellular pH, which is difficult to measure on construction sites.

Joint torque model is more suitable for PFA in the construction industry. Firstly, the model is built based on the definition of physical fatigue, i.e. the decline of a muscle's ability to generate forces, which means it has no limitation of working patterns or body parts. Besides, the model is based on joint torques, which could be calculated according to posture data and exerted forces data. In addition, compared with calcium ions amounts and pH values, postures and external forces are more closely connected with construction site factors such as working postures and the weight of materials or tools.

Joint torque calculation is the core issue of joint torque physical fatigue development model. The following section introduces relevant biomechanical knowledge with the hope to find out the data requirements for joint torque calculation.

2.2.2 Joint torque calculation

Joint torque calculation is one of the core issues in biomechanics, which applied mechanics and the structure of the living body to explain body movements [54].

Joint torques are generated by the neuromusculoskeletal system [55], which includes muscles and tendons. Muscles are able to generate forces and are attached to bones by tendons, which transform the forces generated by muscles to bones and generates torques. The skeletal systems consist of the bones, joints and ligaments. Bones provide the structure for the body and are connected with joints. Ligaments are the tissue that stabilizes the joints. At a joint, the interaction forces among bones and ligaments also generate torques. In short, joint torques are the complex outcomes of muscles, tendons, joints and bones [55].

Biomechanical models of various levels of detail (LOD) have been developed to calculate joint torques. In highly detailed models, muscles, tendons, bones and ligaments are regarded as materials with different elasticities and structures (i.e. shape, thickness and density), which are measured with computer tomography scans [56]. Finite element models are applied to simulate their interactive reactions, and engineering software is required to perform finite element simulation [57]. Due to the huge amount of computation, such detailed models can only be applied on certain joints.

The models with medium LOD focus on the simulation of the movement simulation of human body segments or the whole human body, where the neuromusculoskeletal system is simplified as bones connected with joints and springs. Given the temporal series of joint location data, the model could find the joint velocities and accelerations that best reproduce the location data based on human body movement constrains such as finite degree of freedom (DOF) and bone length constrains. Then inverse dynamics is used to calculate muscle forces and joint torques according to the velocities and accelerations [41]. Though the model complexity has been reduced compared to the highly detailed models, simulating the movement of bones with the constrains of muscles and tendons is still a challenging task. For example, 80 muscles were included in a model for human gait simulating with a DOF of 37 [58]. High DOF represents large data input. Even a relatively simple whole-body model requires at least the 3D accelerations and locations of 50 joints [59].

In low LOD models, the human bodies are simplified as rigid bones connect with hinge joints, ignoring muscles and tendons. Such models contain only main joints (i.e. head, neck, chest, shoulders, elbows, wrists, hips, knees and ankles) and the bones linking the joints [60]. Given the 3D coordinates of the main joints and external forces (usually the forces in hands and ground reaction forces), the joint torques could be calculated with statics. Due to the simplicity, the model has been widely used in industries for ergonomic job design [11,61]. However, the models could only be applied in slow movements because they do not consider accelerations.

Table 2-2 is a comparison of the data demand of above biomechanical models. Apparently, models with higher LOD has more strict requirements on input data but result in more accurate results. Since it might not feasible to satisfy the data demands of the models with the high and middle LODs, this study selected the model with the low LOD.

Table 2-2 The data demand of joint torque calculation

Model LOD	**Data demand**	**Body parts**	**Accuracy**	**References**
High	• computer tomography scan results • elasticity • shape • thickness • density	One joint	High	[56,57]
Middle	3D accelerations and locations of at least 50 joints and external forces	Whole body	Middle	[41,58,59]
Low	3D locations of the joints and external forces	Whole body	Low	[11,60,61]

2.2.3 Summary

Existing physical fatigue model are reviewed to provide a theoretical foundation for a new PFA indicator. Joint torque model was found more suitable for construction industry. Then the biomechanical models for joint torque calculations are reviewed, and the model with a low LOD was selected, whose data demand for the whole-body torque calculation consists of postures and external forces, directing towards the review of posture and external force collection methods in the next chapter.

2.3 Data collection method for PFA

It was argued in the last chapter that external forces and posture data collection is the key issue for joint-torque-based PFA. The aim of this chapter, therefore, is to investigate how previous external force and posture data collection methods used in studies or industries, with the hope that a suitable data collection method for construction sites could be found, or the gaps between previous posture data collection methods and construction field application could be revealed.

First of all, external force measurements are introduced in section 2.3.1. Then the principles and applications of three types of posture data collection methods, i.e. manual methods, contact-sensor-based methods and non-contact methods are reviewed in section 2.3.2, 2.3.3 and 2.3.4, respectively. Then section **Error! Reference source not found.** compares the three types of methods from data quality, intrusiveness and cost, and prove computer vision methods to be a suitable posture data collection method for construction workers. Based on the comparison results, section **Error! Reference source not found.** reviewed previous computer vision algorithms for posture data collection from algorithm design, dataset structure and accuracy, revealing the reasons for lacking accurate posture data collection algorithms for construction workers.

2.3.1 External force measurements

The external forces of a worker are mainly the forces in hands and the ground reaction forces [60]. It is extremely challenging to measure the forces generated by hands, because our hands have broad range of forces and movements. In practice, hand dynamometers and goniometers are used to measure the hand forces of simple, static and unnatural postures [62]. The hand postures of construction workers are much more diverse, so an ideal hand force measurement tool should suit the flexibility and continuous variations of hand postures.

Wearable sensors are introduced to measure hand forces continuously in dynamic cases. sEMG sensors have been used to measure the force generated by the forearm through monitoring the muscle activities [28]. However, sEMG sensors are not able to provide accurate results, because the strength of sEMG signals are affected by electrode placement, signal simplifying and filtering, muscle ability, etc. [63]. In addition, sEMG electrodes require dry skin surface and are connected with wire to a signal processor, which limits its application on construction sites.

Thin and flexible force sensors provide an alternative way. These sensors are extremely light weight and soft enough to cover curved surfaces, which are usually attached to gloves to measure grasp forces [64,65]. The gloves have been applied for improving athletes' performance and robots torch feelings, where the weights of the objects hold in hands are light. Construction workers, however, usually need to carry heavy load. In addition, the gloves were tested in laboratory environments in rather short time period. Their performance in harsh construction site environments for long periods is still unknown. What's more, most of such gloves are still under development in laboratories and not commercially available.

In studies on medicine and sports, ground reaction forces are usually measured with force platforms. Single pedestal force platforms are suitable for measuring GRF in static cases or in a small area. For example, some studies have applied single pedestal force platforms to evaluate construction workers' static balance control through measuring the differences in GRF between the feet [66]. For studies about movements, multiple pedestal force platforms have to be used to cover the movement area. For example, to measure the GRF of a human going upstairs, all the stairs need to be covered by a pedestal.

Wearable plantar pressure sensor systems provide a more flexible way of GRF measurement. The system consists of a pair of insoles with pressure sensors and a wireless data transmission module. The system could continuously measure and record plantar pressure distributions and calculate GRF in vertical directions [67]. In addition, a number of wearable plantar pressure sensor systems are commercially available, which are easy to use and comfortable to wear. These systems have been applied in the construction industry to measure workers' plantar pressures accurately and continuously [68–70].

In summary, for measuring forces in hands, most instruments are applied in laboratories to measure light weight with simple hand postures. For GRF measurement, force platforms directly measure the GRF but need to cover all the movement area; wearable pressure sensor systems estimate GRF in the vertical direction based plantar pressure distribution. The advantages of wearable pressure sensor systems are comfortableness and few restrictions on movement area.

2.3.2 Manual posture data collection methods

Manual posture data collection methods are the most conventional approaches to collecting posture data on construction sites. There are mainly two kinds of approaches, i.e. self-report and systematic observation.

Self-report methods ask the workers to recall their postures during construction tasks and answer questions about the postures. The data is usually collected through questionnaires or interviews, which have low initial cost and are easy to conduct. A variety of posture-related data has been collected with self-report methods, such as the occurrence of awkward hand postures and moving heavy materials [71,72], the durations of the fall-prone postures[73], and the frequency of extreme working postures [74].

Despite the wide usage of self-report methods, there are several shortcomings of self-report methods. First, self-report methods have validity problems. Workers might misremember the materials covered by the survey and result in biased results. Second, self-report methods cannot collect posture data continuously, making it difficult to provide timely feedback for construction site management. Finally, with the increase number of participants, self-report methods become labor- and time-consuming, making it impossible to collect "big data" on construction sites.

Systematic observation is an objective and well-ordered method for the close examination of some aspects of behaviors so as to obtain reliable data unbiased by observer interpretation [75]. In systematic observation, working postures are recorded and assessed through on-site observation or recorded video clips [33]. For example, Rose et al. (2001) records the occurrence of awkward postures and the construction workers' endurance time of the postures based on field observations [76], while Sporrong et al. (1999) first recorded the working postures with video then collected posture data through frame sampling [77].

Systematic observation typically involves specifications about what and how variables should be recorded, making the results more objective and comparable. Posture, Activity, Tools and Handling (PATH) is a working posture sampling method specially designed for construction tasks [78]. PATH uses seven-digit codes to record construction postures. Four digits describe the postures of back, arm, leg and hand load, while the rest three digits describe construction working activity, tool use and grasp type. PATH has been successfully applied in the construction industry to record the working postures of laborers, carpenters, ironworkers, plasterers and tilers, facilitating the posture duration analysis and the ergonomic risk assessment [79,80].

In addition to PATH, the systematic observation methods developed by other fields were also applied to the construction industry to collect workers' posture data, such as Ovako Working Posture Analysis System (OWAS) [36], Quick Exposure Check for musculoskeletal risks (QEC) [81] and Rapid Upper Limb Assessment (RULA) [38].

Compared with self-report methods, systematic observation methods are more objective because the specific rules of data coding and recording increase the level of detailedness of the collected data. However, as the categorization of the postures is based on the observers' subjective judgement, the error resulting from subjective judgment cannot be avoided [82]. In order to eliminate the subjective errors in posture data collection, automatic methods have been developed to provide accurate results, as shown in section 2.3.3 and 2.3.4.

2.3.3 Contact-sensor-based posture data collection methods

Contact-sensor-based pose data collection methods use body attached sensors or markers to collect construction workers' posture-related data. The sensors calculate joint angles or joint positions using joint kinematic data, i.e., linear/angular acceleration/velocity/displacement.

I. Inertial Measurement Unit (IMU) and Electro-goniometers

IMU is a sensor system that uses measurement systems, e.g., gyroscopic sensors and accelerometers, to estimate relative position, velocity and acceleration [83]. IMU has been widely used to study construction workers' joint kinematics. Commercially available IMU can reach an orientation accuracy of $\pm 1^{\circ}$ for dynamic conditions and all orientations [84]. If attached to the workers' waistline, IMU helped to distinguish common tasks and postures with different fall-risk profiles in construction according to stability metrics [85]. With the data obtained by IMU attached to the back at waist level, a previous study identified safety hazards according to the three-axis acceleration data measured by IMU [86]. In addition to IMU, electro-goniometers could also measure joint kinematics. For example, a Lumbar Motion Monitor System, which is a portable tri-axial electro-goniometer, was used to evaluate the potential of tools to reduce awkward postures in drywall installers. The system was attached to the worker's back and continuously documented time and posture data in the lumbar region in three human body reference planes (the sagittal plane, the coronal plane and the transverse plane) [87].

Multiple IMUs attached to key human body joints constitute an IMU system. IMU systems have been widely used to collect construction workers' posture-related data for behavioral analysis. For example, an IMU system was developed to monitor a construction worker's postures during a brick-laying task. The system employed eight IMUs, covering upper/lower back, arms, and upper/lower legs for examining the motions in detail [88]. Another system used 17 IMU sensors to track the locations of 28 joints at the same time [89]. Special algorithms were designed to extract information from the data for various research goals. For example, a Support Vector Machine (SVM) was trained to discriminate expert masons from novice masons [89]. Besides, a motion tensor decomposition approach was designed to compress the full-body 3D poses and accurately differentiate the postures [90].

II. Marker-based motion capture system

Marker-based motion capture systems (e.g., the VICON system and OptiTrack) are commonly used in laboratories for 3D motion capture and analysis. A marker-based motion capture system usually contains cameras and reflective markers. The cameras are equipped with infra-red lights and set up in a laboratory around the individual. The markers are retro-reflective balls put on the designated location of the human body and can be illuminated with the infra-red lights mounted on the cameras. The system estimates the 3D position and the movement trajectory of each marker based on the signals of the reflective marker captured by the cameras. Chiou et al. (2007) used a marker-based motion capture system to analyze the gait of construction workers while wearing safety shoes or stilts at different heights [91]. Simeonov et al. (2011) applied a marker-based motion capture system to collect the upper-body kinematics data for postural stability assessment [92].

Compared with manual posture data collection methods, contact-sensor-based methods have strong advantages in posture data collection. First of all, if attached to the construction workers, the sensors could measure and record postures automatically without manual observations or records. Secondly, the collected posture data is objective and accurate, which benefits the posture-based analysis for safety, health and productivity management. Finally, with the help of the sensors, the data could be collected continuously in a high frequency, which provides the data foundation for posture analysis and timely feedback. However, there are several shortcomings of the contact sensors that limit the application on construction sites. The contact sensors need to be tied tightly to construction workers trunks and limbs, leading to uncomfortableness and unwillingness to wear. Besides, addition labors and costs are needed for recharging and maintaining the sensors. For non-invasive data collection, previous studies developed non-contact methods as shown in section 2.3.4.

2.3.4 Non-contact posture data collection methods

Non-contact-sensor-based methods could collect construction workers' pose data in a non-invasive way. They usually use images or videos of construction sites, which contain visual information related to human pose estimation. Human pose estimation is a classical task in computer vision aiming at "obtain 2D pixel positions of human body joints from an image" [93], which is referred to as *2D pose estimation* in the rest of the review. The output of 2D pose estimation is 2D skeletons consisting of the 2D coordinates of human body joints. *3D pose estimation* is the "the task of producing a 3-dimensional figure that matches the spatial position of the depicted" given an image of a human being. The results of 3D pose estimation is 3D skeletons consisting of 3D coordinates of human body joints. *2D pose estimation* and *3D pose estimation* are collectively referred to as *pose estimation.* Reviewed articles indicate depth cameras and Red-Green-Blue (RGB) cameras are the two popular tools for human pose estimation for non-contact-sensor-based-methods.

I. Depth camera

Depth cameras generate range images or 3D point clouds. In a range image, each pixel corresponds to a numerical value representing the distance from the camera, i.e. the depth of the pixel. Some cameras have both an RGB camera and a system to measure depth, which can generate RGBD images. In an RGBD image, a pixel is represented by a four-digit number, where three digits represent the color (red, green, and blue) and the fourth digit represents the depth, i.e., the distance between the pixel and the depth camera. There are a variety of different types of depth cameras, such as structured light depth cameras, stereo depth cameras and time-of-light (TOF) depth cameras.

Structured light depth cameras project light patterns on to a scene and extract depth information by analyzing the distortion of the observed patterns [94]. Kinect V1, is a typical structured light depth camera, which relies on infrared light patterns to estimate depth and was applied in the construction industry to estimate the joint locations trajectories of construction workers [95].

Stereo depth cameras perceive depth by simulating the human binocular vision system. A stereo depth camera captured images with at least two image sensors and calculate depth by estimating disparities between matching key-points in the images. A previous study developed a stereo depth camera consisting of two common smartphones, and applied it to estimate 3D human skeletons [96]. Another study applied commercially available stereo cameras to detect the 2D locations of human body joints and compute the 3D positions of the joints using triangulation [97].

TOF depth cameras determine depth according to the speed of light. A depth camera emits light and measures how long the light takes to get back to the camera, and depth equals the light of speed multiplies by the duration. Kinect V2 contains a TOF camera, where the light is infrared. Kinect V2 was used in construction to collect 3D human body skeletons for unsafe behavior detection [98,99]. Light Detection and Ranging (LiDAR) sensors are another type of TOF depth cameras which use laser light to calculate depth. LiDAR sensors have been applied to recognize human postures for in-home application scenarios according to the topological information embedded in the 3D point cloud [100].

Compared with contact-sensor-based-methods, range images are less invasive, as the workers need not wear any sensors. The benefit of non-invasiveness is significant in whole-body 3D pose estimation, where contact-sensor-based-methods require workers to wear over ten IMU sensors. However, it is difficult to estimate 3D skeletons from range images as accurate as those methods allowing for direct measurement of joints using wearable sensors. One of the reasons is that infrared depth cameras are highly sensitive to environments. Sunlight and far distances between workers and cameras will severely affect the depth estimation of a depth camera [101].

II. RGB camera

Widespread surveillance cameras on the construction sites provide vast amounts of information for pose estimation. However, unlike depth images containing the depth information of each pixel, the images captured by RGB cameras contain only 2D information, i.e., the color information of each pixel, making it a challenge to estimate poses from RGB images. Based on the 2D information in an image, researchers utilized hand-crafted features or deep learning algorithms to detect workers, recognize postures and estimate 2D or 3D poses. The rest of the section summarizes the algorithms, including feature-based algorithms and deep-learning algorithms.

III. Computer vision algorithms for posture-related data collection from Depth cameras and RGB cameras

The reviewed algorithms that extract posture-related data from construction images or videos are classified into three categories based on the outputs, including worker detection, posture classification, and pose estimation.

Worker detection aims to find workers from an RGB image, which could answer the question "if there are any construction workers in the image." The reviewed studies selected regions of interest first by detecting moving objects from a series of RGB images or using sliding detection window; then extracted hand-crafted features, such as histograms of oriented gradients (HoG) and color features, from the selected regions [102,103]. Machine learning algorithms, such as Supported Vector Machine (SVM) and K-Nearest Neighbor (KNN), were applied to train classifiers based on the extracted features to differentiate construction workers from other objects [102,103].

Worker posture classification takes a step further, which classifies postures of the detected workers from RGB images or depth images. In some previous studies, the first step of posture recognition was worker detection [104,105]. [104] applied a similar strategy to [102] to detect workers, i.e., using motion features to detect the moving objects and using color features to identify workers from all the moving objects. After worker detection, a silhouette was created for each worker, which was then thinned to generate a skeleton. An Artificial Neural Network was designed to classify the skeleton into effective, contributory, and ineffective categories. In terms of RGBD images, depth information was employed to detect workers. [105] computed the median image from a set of depth images to subtract the background and find the largest bounding boxes for clusters of connected pixels to detect the worker. The depth values of the pixels surrounded by the bounding box was then rescaled and reshaped into a vector, which will be used to for posture classification. Linear discriminant analysis was applied in [105] to classify postures into standing, squatting, sitting, stooping, bending and crawling.

Worker pose estimation includes 2D pose estimation and 3D pose estimation. In terms of 2D pose estimation, a two-branch CNN was applied in [31] to estimate the

2D skeletons of construction workers from RGB site images, where the first branch detected body parts and second the branch predict body part association. However, 2D poses are view variant, making it difficult to assess work performance based on 2D poses. For example, in [31], view-invariant features, are required for ergonomic posture classification according to 2D poses. 3D pose estimation predicts 3D joint locations of human bodies and thus solve the problem of view variance. [96] used two cameras to record working scenarios at the same time from different point of views. Then HSV color features and optical flow were applied to track 2D body joints from each of the image sequences captured by the two cameras. Then SIFT and SURF were used to match the 2D skeletons in the two image sequences, and finally, paired body joints were triangulated to compute 3D joint positions. Other methods estimated 3D poses from monocular RGB images, such as [106] and [107]. Both of the two studies applied CNN, in which estimating 2D poses and inferring 3D poses based on the 2D poses play an important role. [106] applied a multi-stage CNN to estimate the 3D poses of workers from construction site video frames. In each stage, a 2D joint predictors generated belief maps of human body joints, then a probabilistic 3D pose model estimated 3D pose based on the 2D belief maps. After that, the estimated 3D pose was projected back onto the image plane to generate a new set of 2D belief maps. Next, a fusion layer fused the two sets of 2D belief maps, which are passed to the next stage for 2D joint location prediction. After six stages, the probabilistic 3D pose model generated a 3D pose according to the final set of 2D joint belief maps. [107] used another CNN architecture to estimate the 3D poses of construction workers from site images. The network includes two parts. The first part is a CNN, named Stacked Hourglass network, to estimate 2D poses from the images, while the second part is a separate neural network which inferred 3D poses based on 2D poses and bone length constraints.

Table 2-3 summarizes the above algorithms. Before 2016, most of the algorithms used hand crafted features to represent images or videos and applied machine learning algorithms onto the features. With the development of deep learning, more sophisticated algorithms such as CNN and Long Short-Term Memory (LSTM) have been applied, which generated the optimal features and weights through a training process. Besides, due to the high complexity, the deep learning networks have better presentation ability and could finish challenging tasks, such as action recognition and 3D pose estimation. In terms of dataset, Table 2-3 compares above studies based on data collection environments, participants, data categories and the total number of training examples. For real construction site applications, a dataset should consider the variety of working environments (indoors and outdoors), trades and actions or poses. However, nearly half of the previous studies were conducted in indoor environments, limiting the application in outdoor construction fields. In addition, the generalization ability of a practical learning algorithm is important. The difference between the distributions of the training data and test data results in poor generalization ability [108]. In Table 2-3, only four studies included more than ten workers; three studies included more than three construction trades, which means there might exist test data different from the training data and leads to biased predictions.

Table 2-3 Comparison of computer vision algorithms for construction worker pose estimation

Task	Input	Algorithm	Dataset				Performance evaluation	Ref
			Environments	Participant	Labeling	No. of data samples		
Worker detection	RGB image	1. Motion features for foreground blobs recognition 2.HOG and SVM for human body identification 3.HOC (RGB/HSV) and KNN for construction worker detection	Field	5 workers	Positive and negative examples of standing workers	2700 images	99.00% (Precision)	[102]
	RGB image	1.Multi-scale sliding detection windows 2.HOG and HOC (HSV) as features 3.SVM for worker/non-worker classification	Field	Multiple workers on 5 construction sites		8000 images	98.83% (Accuracy)	[103]
Posture classification	RGB image	1.Motion segmentation algorithm for identifying moving objects 2.Color variance for extracting workers 3.Region growing technique for creating silhouette 4.Fast parallel algorithm for creating 2D skeletons 5. ANN for posture classification	Field	2 rebar workers	3 types of postures	2000 images	99.00% and 81.00% for each worker (Accuracy)	[104]
	Depth image (Infra-red)	1.Extracting person using pixel depth 2.Linear discriminant analysis (LDA) for posture classification	Laboratory	1 student	4 postures	22226 images	0.33% (highest error rate)	[105]
2D Pose estimation	RGB image	Two-branch CNN - 1st branch for body part detection - 2nd branch for body part association	Field	-	-	-	-	[31]

3D Pose estimation	Depth image (Stereo)	1. HSV features and optical flow for 2D skeleton estimation 2. SIFT and SURF for 2D skeleton matching and triangulation for 3D skeleton reconstruction	Laboratory	1 student	2 actions	1000 images	3.80 cm (Average error of bone length measurements)	[96]
	RGB image	Multi-stage CNN architecture that combines the Convolutional Pose Machine and a probabilistic 3D joint estimation mode	Field	11 people	3D joint locations of daily actions	Human 3.6M dataset	8.93 cm (Mean per joint position error)	[106]
	RGB image	CNN for 2D pose estimation and 3D pose reconstruction	Field	11 people	3D joint locations of daily actions	Human 3.6M dataset	3.90 cm (Mean per joint position error)	[107]

2.3.5 Comparison of data collection methods

This section compares previous posture data collection methods from the aspects of data quality, intrusiveness and cost. If a posture data collection method is used in PFA, data quality determines the accuracy and detailedness of the assessment results; intrusiveness and cost determine the feasibility of the assessment method on construction sites.

I. Data quality

Data quality is the fitness of for "its intended uses in operations, decision making and planning" [109]. The following dimensions are selected in this study: accuracy, reliability, precision and timeliness [109], as shown in Table 2-4

Data accuracy represents the degree to which data correctly describe the real postures. In the reviewed posture data collection methods, the accuracy of the descriptive data is low for data collectors' subjective judgement and non-standard data presentation. Automatic methods perform better in accuracy. Marker-based motion capture system contributes to the best accuracy with a joint error as small as 2 mm. The best performance of motion sensors is 1 degree. For non-contact methods, the joint location error ranges from 3 cm to 5 cm.

Data reliability means the degree to which data is measured and collected consistently. Manual methods, for example, are of low reliability, because the classification of postures relies on manual judgement. As a result, the same postures may be classified into various categories by different observers. Automatic methods, on the contrary, collected posture data according to predefined rules, which helps to maintain high consistency.

Data timeliness is the degree to which data represent reality from the required point in time. Manual methods are of low timeliness, since neither self-report nor system observation provides continuous results. One of the advantages of automation is excellent timeliness. Even the lowest frequency of the outputs from the reviewed automatic methods is up to 25 fps, which means the posture data could be retrieved every 0.04 s. Good data timeliness provides the prerequisite for near-real-time PFA.

Data precision is the degree to which data describes the detailedness of the real postures. Joint kinematic data could provide the most detailed joint data such as joint 3D locations and 3D accelerations, which benefits the biomechanical analysis of the joint torques. 3D skeletons only contain the 3D locations of joints without acceleration information. Though acceleration could be calculated as the second derivative of location, some 3D location data collection methods, such as depth camera and RGB camera, are not accurate enough. Then is 2D skeletons, which only contain the 2D location of the key joints. Descriptive posture data contains only posture classifications.

It should be noted that one data format could generate another format. Figure 2-1 represents such relations among the data formats. Given the bone length constrains, 3D joint acceleration and 3D joint angular acceleration are mutually transferrable.

3D joint location could be generated by the double integral of 3D joint acceleration on time. 2D joint locations could be generated through projecting 3D joint locations on a certain plane. Finally, given the classification rules, posture category could be generated with 3D joint locations. In short, if a method could collect 3D joint locations, it could generate 2D joint locations and posture categories. Further, if a method could provide acceleration data, it could generate all the other data formats.

II. Intrusiveness

Intrusiveness means the negative effects of the posture data collection methods on the workers' normal working operations. Previous posture collection methods are intrusive. The intrusiveness of interviewed and self-reported posture data is positively correlated to the data collection frequency. Some researchers collected data twice a day during the workers' rest period, which has few effects on construction working but the collected data might not be accurate enough [110]. To increase data accuracy, observers and interviewer have to collect data frequently, which will interrupt normal construction works. Wearable sensors are also intrusive, as they need to be tied tightly to workers' body segments, which will make to worker feels uncomfortable [3]. In addition, some sensors need to be calibrated frequently, which also limits its application on real construction sites [111]. Observation, on the contrary, could collect data continuously without any sensors attached to the workers. However, it is reported that being observed during working might result in workers' higher stress and less trust in managers [112–114].

Table 2-4 Outputs of different posture data external collection methods

Method	**Output**	**Accuracy**	**Reliability**	**Timeliness Frequency [FPS]**	**Precision** Posture category	2D joint location	3D joint location	3D joint acceleration	3D joint angular velocity/acceleration
Manual method	Descriptive postures	Low	Low	Not real time	√				
Marker-based motion capture system	3D skeleton	High (2mm)	High	120-360	√	√	√	√	√
Motion sensor	3D skeleton	High (1 degree)	High	200	√	√	√	√	√
Depth camera	3D skeleton	Middle (5.5 cm)	High	30	√	√	√		
RGB camera	2D/3D skeleton	Middle (3.9 cm)	High	25-30	√	√	√		

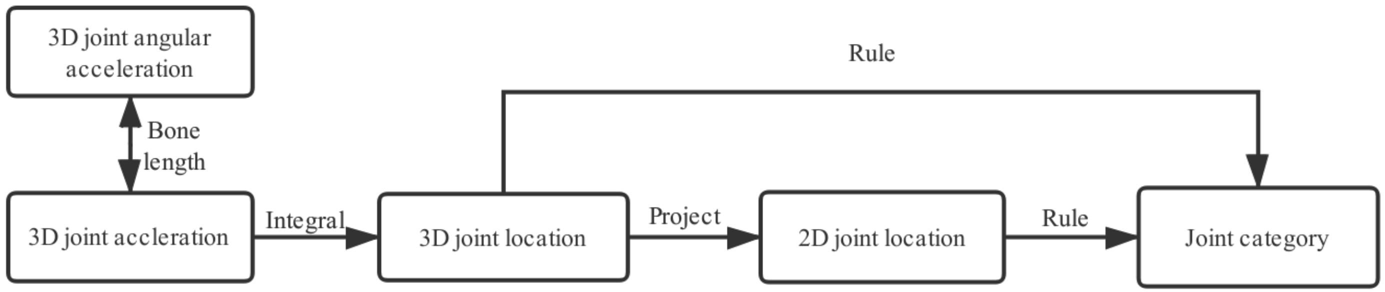

Figure 2-1 Data transferability of different data formats

III. Cost

Costs of a pose data collection method include labor cost, time cost, and hardware cost. Manual-based methods, such as self-report, interview, and manual observation, have little hardware cost but are extremely labor and time costs. Automatic methods, on the contrary, are less labor- and time-consuming but will increase the cost of purchasing and maintaining hardware. The price of different hardware varies a lot. Table 2-5 summaries the price of four categories of pose data collection devices, including wearable motion sensor systems, marker-based motion capture systems, depth cameras and CCTV cameras. Each category includes three example products.

In wearable motion sensors systems, commercially available products have been developed, which usually consist of IMU sensors, data dongles, drivers, software, and accessories. Such a system is user-friendly. The users could easily capture 3D pose data by following the instructions without complex system configurations or algorithm development. The price of each IMU ranges from 206 to 1000 USD. Assuming a wearable motion sensor system for whole-body 3D pose data collection includes 17 IMU sensors, the price of the whole system will be at least 3499 USD. Considering that each system could only capture the pose data of one worker, the cost is too high for field application.

The price of a marker-based motion capture system is closely related to the number of cameras. Dense camera arrangement ensures that each marker is visible to at least four cameras for 3D localization, and thus results in high accuracy. Besides, camera resolution, frame rate and synchronization method (wire/wireless) also influent the cost. The price of an eight-camera-system varied from 20,000 to 100,000 USD, which is much higher than wearable motion sensor systems.

As for cameras, the price of the example depth cameras is between 177 and 350 USD. Depth cameras provide depth maps. Algorithms are required to extract 3D human body skeletons from depth maps. Fortunately, the three depth cameras listed in Table 2-5 have equipped with software development kits, which allow users to obtain 3D joint positions with several lines of codes.

The price of the CCTV cameras in Table 2-5 ranges from 24 to 200 USD. The cameras could provide both RGB videos and infrared videos and have commonly used for field surveillance. However, special algorithms need to be trained so that 3D pose data could be retrieved from the videos [115,116]. In addition to cameras, the cost of a complete CCTV system also includes surveillance hard disks, cables, and installation fees. According to an agent's quotation, the total price of installing a CCTV system including eight high-resolution cameras on construction sites are about 12,000 USD.

Table 2-5 The price of cameras or sensors applied in posture data collection

Automatic pose data collection method	Example Product	Price [USD]	Reported application	References
Wearable motion sensor system	3-Space™ MoCap Starter Bundle (17 IMUs, sensor straps, 3 wireless dongles, drivers and software)	3499 (About 206 per camera)	3D skeleton data of one person	[84]
	Xsens MVN	600 per IMU		[117]
	Motion Node	Over 1000 per IMU		[118]
Marker-based motion capture system	OptiTrack (8-camera system)	About 20,000	3D skeleton data of single person with millimeter accuracy	[119]
	Nokov (8-camera system)	About 40,000		[120]
	Vicon (8-camera system)	About 100,000		[121]
Depth camera	Kinect for Windows V2	248	3D skeleton data of at most six people in 0.5~4.5 m	[122]
	Intel RealSense Depth Camera D435	177	3D skeleton data in 10 m	[123]
	TVico	350	3D skeleton data in 0.6~5.0m	[124]
CCTV camera (including RGB camera)	Hikvision DS-2CE56C0T-IT3	About 70	RGB videos for large area surveillance. 3D skeleton data could be extracted from the captured video frames with computer vision algorithms.	[125]
	Dahua 2PM Eyeball	About 34		[126]
	Hikvision DS-2DE3304W-DE	205		[127]

2.4 Summary and research gaps

Construction workers' external forces and postures play a vital role in joint-torque-based PFA. For external forces, commercially available wearable plantar sensor systems could measure ground reaction forces (GRF) continuously and non-intrusively. For forces in hands, there are few tools that could be used outsides laboratories.

In terms of posture data, wearable sensors and depth cameras have been applied to collect construction workers' 3D posture data. Though the tools could collect accurate data, their usability on real construction sites is limited due to the intrusiveness and the outdoor environments of construction sites. 3D posture estimation from 2D images provides a feasible alternative to solve the problem. However, previous 3D posture estimation algorithms performed not very well when estimating the postures of construction workers. The gaps are 1) there lacks a 3D working posture dataset for construction workers, and 2) a deep learning network need to be specially designed for the dataset.

According to above analysis, the research gaps are identified as below.

1) There lacks a physical fatigue indicator that could estimate the whole-body physical fatigue for construction workers without limitations on working patterns.
2) There exists a lack of feasible data collection methods to satisfy the data demanding of above indicator and suit construction site environments. The data includes ground reaction forces, forces in hands, and 3D posture data.
3) There lacks a computer vision algorithm to generate accurate 3D posture data from construction site videos, and
4) There lacks a posture dataset for construction workers to train the above algorithm.

PART II DEVELOPMENT OF PFA METHOD

Chapter 3 Research outline

3.1 Research outline

This study aims to develop a PFA method for construction workers, which could provide personalized PFA in an automatic, continuous and non-invasive manner in outdoor environments.

To develop a new quantitative PFA method for construction workers, it involves four steps (Figure 3-1). The first step is to collect 3D motion data automatically and non-invasively using an ordinary 2D RGB camera. Considering previous 2D posture estimation methods' good performance and the successful application in the construction industry [106], this research focuses on estimating 3D postures from the results of 2D posture estimation. The second step involves the measurements of external forces and human body parameters, which enables the estimation of joint torques in the third step. The fourth step is the estimation of a PFA indicator based on a joint-torque-based physical fatigue development model. Laboratory experiments were conducted to test the accuracy of 3D posture estimation, external force measurement and the PFA indicator. Field experiments validated the feasibility of the proposed method on construction sites and its potential in assisting fatigue-prevention-oriented construction site management.

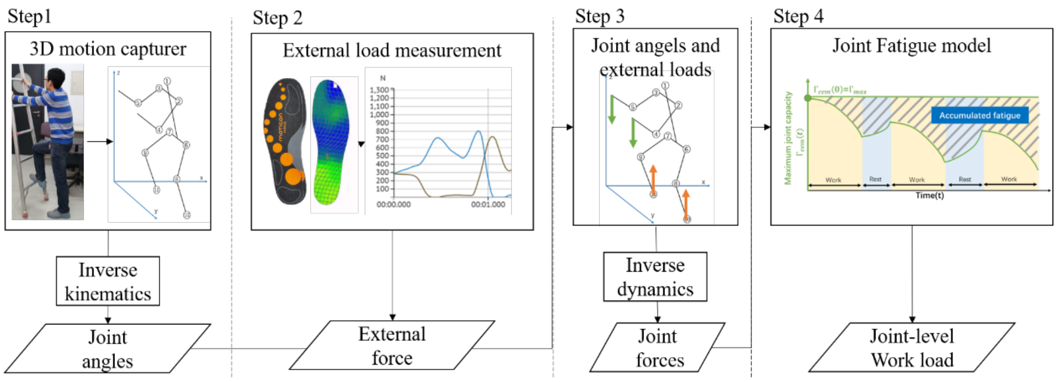

Figure 3-1 An overview of the PFA method

3.2 Key assumptions

The following research assumptions were made to simplify and narrow the research questions during the PFA method development and experiment validation.

Assumption 1: human body was simplified as a lever system connected with hinge joints. This assumption aims to simplify posture data collection and joint-level fatigue analysis. The assumption is commonly used in previous studies on pose estimation and biomechanics [115,128].

Assumption 2: workers' motions on construction sites are assumed to be slow and steady, which meant the lever system was in an equilibrium status. The assumption simplifies the joint torque calculation from a dynamics problem to a static problem, which means the proposed PFA method does not consider the influence of accelerations.

The following assumptions were made in data collection:

Assumption 3: the worker's posture has no acceleration in the vertical direction. Otherwise, the ground reaction force measured with the insoles does not equal to the weight of worker and any external forces.

Assumption 4: all the worker's weights and external forces act on his/her feet. The method measures external forces with smart insoles by subtracting self-weight from total ground reactions forces. As a result, this method is unsuitable for postures such as leaning, sitting and kneeling.

In the laboratory experiments, the author assumed that:

Assumption 5: there is no mental fatigue during the experiments. Fatigue is a complex and comprehensive phenomenon which consists of physical fatigue and mental fatigue. As physical fatigue is the focus of the research, the following methods were involved in the experiments to exclude the influence of mental fatigue: 1) all the participants were required to sit still for five minutes before each experiment, and 2) all participant were allowed to stop the experiment at any time in case that they felt bored. Another aim of the five-minute still sitting is to recover the participants' joint capacity to the maximum, as this research assumes that the participants have no physical fatigue at the start of each task.

Chapter 4 3D construction working posture estimation from 2D images[4]

4.1 Introduction

Posture data collection is one of the key issues of developing the new PFA method for construction workers. This chapter aims at a deep-learning-based 3D working posture data collection method. To develop a deep learning algorithm, question modelling, dataset, network architecture and training method are the key problems. Section 4.2 to 4.5 solve above four problems respectively.

4.2 Problem formulation

Denoting the information in an RGB image as $\boldsymbol{E}$, estimating the probability of 3D joint locations $\boldsymbol{y}$ from $\boldsymbol{E}$ can be formulated as:

[4] This chapter is based on the following published study and being reproduced with the permission of Elsevier.

Yu, Y., Li, H., & Yang, X. (2019). 3D Posture Estimation from 2D Posture Data for Construction Workers. In M. Al-Hussein (Ed.), 2019 Proceedings of the 36th ISARC (pp. 26–34). Banff, AB, Canada: The International Association for Automation and Robotics in Construction. https://doi.org/10.22260/ISARC2019/0004

$$p(\boldsymbol{y},\boldsymbol{x},\boldsymbol{E}) = p(\boldsymbol{y} \mid \boldsymbol{x},\boldsymbol{E}) \cdot p(\boldsymbol{x} \mid \boldsymbol{E}) \cdot p(\boldsymbol{E}). \tag{4-1}$$

Assuming that the prediction of $\boldsymbol{y}$ given $\boldsymbol{x}$ is independent of $\boldsymbol{E}$ [116], the problem could be formulated as

$$p(\boldsymbol{y},\boldsymbol{x},\boldsymbol{E}) = p(\boldsymbol{y} \mid \boldsymbol{x}) \cdot p(\boldsymbol{x} \mid \boldsymbol{E}) \cdot p(\boldsymbol{E}), \tag{4-2}$$

where $p(\boldsymbol{x} \mid \boldsymbol{E})$ means the probability of the 2D joints locations based on the RGB image, which could be accurately estimated with OpenPose [129]. So, this study mainly focuses on $p(\boldsymbol{y} \mid \boldsymbol{x})$, i.e., predicting $\boldsymbol{y}$ given $\boldsymbol{x}$. Since $\boldsymbol{y}$ is a continuous variable, the problem is modelled as the regression problem in equation (4-3).

$$\boldsymbol{y} = \boldsymbol{R}(\boldsymbol{x}) \tag{4-3}$$

To ensure the non-intrusive collection of 3D motion data for biomechanical analyses, the 3D motion data of the target worker must be collected accurately and automatically without interfering work activities. To reach the goal, this study 1) developed a 3D working posture dataset, ConPose, for construction workers, which including 67,976 3D postures covering 6 working activities (climbing, masonry, material handling, plastering, rebar typing and scaffolding); 2) designed a deep neural network, which is an Residual Artificial Neural Network (RANN), for 3D posture estimation for construction workers. This method makes it possible to continuously collect 3D posture data from construction site videos and contributes to 3D-pose-data-based behavior management, such as identifying unsafe behavior postures, estimating joint workloads and assessing labor productivity. Figure 4-1 layouts the framework of the algorithm.

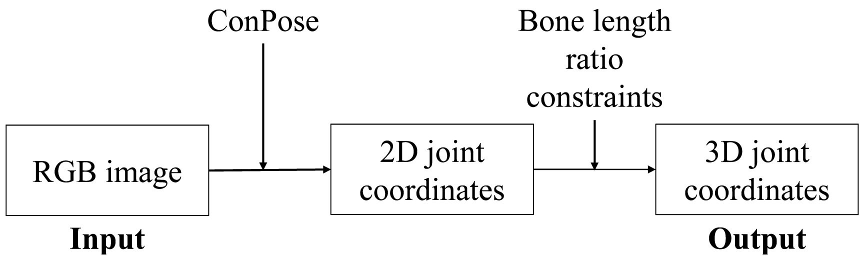

Figure 4-1 The single RGB camera-based 3D motion capture algorithm

4.3 Establishing 3D construction working posture dataset

To establish the 3D construction working posture dataset, 3D working posture data were collected with inertial measurement units (IMUs) through six construction tasks, including climbing, masonry, plaster, material handling, plaster, rebar tying and scaffold. Then 2D working postures were generated through projecting the 3D postures on different planes.

4.3.1 Collecting 3D posture data

Participants: Two participants (one healthy male worker and one healthy male graduate student) were recruited to perform construction tasks. Table 4-1 is the demographic parameters of the workers.

Table 4-1 The demographic parameters of the participants

Participant	Gender	Height [m]	Weight [kg]	Age [years]
#1	Male	1.78	69.3	37
#2	Male	1.70	65	29

Equipment: The participants were required to wear the IMU system (3-Space™ sensor, Yost Labs', Ohio, US) to determine the ground truth for the 3D motion data. Each sensor includes triaxial gyroscope, accelerometer, and compass sensors, and provides orientation data in real-time. The IMU sensor has an accuracy of 1° [130]. Thirteen sensors were tightly tied to the head, chest, back, waist, upper arms, forearms, thighs and shanks to determine the joint positions as shown in Figure 4-2. The sampling frequency of the IMU system was 50 Hz.

Figure 4-2 Thirteen IMU sensors tied to head, chest, back, waist, upper arms, forearms, thighs and shanks (T-shape calibrating)

Construction tasks: After putting on the IMU system, the participants were instructed to perform construction tasks. To calibrate the IMU system before the task, the participants were required to stand with both feet closed together and both arms stretched out to the sides and held parallel to the ground to form a T shape. Figure 4-3 are the representative frames during the experiment.

Figure 4-3 Representative frames of scaffolding, masonry and climbing

In the climbing task, the participants climbed and dismounted from a three-meter-height bilateral ladder for in four different postures (normal climbing, backward-facing climbing, climbing with an object and reaching far to a side). Each posture was repeated for five times. For the masonry task, the participants were asked to build a concrete block wall. Each concrete block weighted approximately 16kg. Concrete blocks were placed 1 m away from the target concrete block wall location. The thickness of the wall was 190 mm and the height was 1,520 mm. The wall comprised eight layers. The width of each layer was either 780 mm or 970 mm. To build the wall, the participants first bent knees to pick up a block, then turned around to lay the block. The motion was repeated until a layer of the brick wall had been properly placed. Then the participants checked the layer with a level and evened it out with a thicker layer of mortar. The procedure was repeated until the target wall was built. In the plaster task, the participants were instructed to perform a simulated material handling task through mimicking the motion of plastering an area of 5 meters width and 2 meters height. The material handling task involved picking up 4 bricks from the floor with both hands and then carry the bricks to to a target place on the floor 3 meters away. The participants needed to repeat the task for 10 times. In the simulated rebar tying task, the participants tied a mesh of plastic bars at every intersection. The mesh of the plastic bars consisted of 5 × 5 bars placed perpendicular to one aonther to form a mesh. The distance between the bars in both direction was 30 cm. Finally, for the scaffolding task, the participants were instructed to construct a cube with two-meter-long steel tubes and couplers. The working area was the location where the cube was built. The storage area was the place where the steel tubes and couplers were stored. The straight-line distance from the storage area to the work area was about 6 m. During the experiment, the participant first carried a tube weighted approximately 12 kg from the storage area to the working area, then assembled the tubes with couplers. This process was repeated for 16 times to finish the task. Table 4-2 shows the duration and number of frames of each task.

Table 4-2 The duration and number of frames of each task

Construction task	**Duration [sec.]**	**No. of data frames**
Climbing	150	4500
Masonry	379	11365
Material handling	113	3400
Plaster	47	1397
Rebar tying	137	4100
Scaffold	1440	43214
Sum	2266	67976

4.3.2 Data processing

I. Transferring joint location description from Euler angles to positions

It is a general practice to evaluate the accuracy of a pose estimation algorithms with the distance between predicted joint locations with the ground truth [131]. However, the posture data were represented by Euler angles of each joints in the data from IMU system, which needs to be transferred to 3D joint coordinates.

The results of the IMU system are postures stored in a BVH file, which contains the joints' three dimensions relative to original position and the offset of one child joint to its parent joint. The BVH structure is presented in Figure 4-4. The root joint is hip joint, which contains six parameters in raw data, including three-dimensional positions and three-dimensional rotations. The arrows start at parent joints and end at child joints. The chest point gives an example of the data structure of all the joints except for the hip/root joint. Each joint contains the offsets along three dimensions relative to the original posture and three-dimensional rotation angles relative to the original posture at time t.

Denavit-Hartenberg (DH) matrix was used to transfer Euler-angle-postures to 3D-joint-locations-postures. The matrix separates a screw displacement into the product of a pure translation along a line and a pure rotation about the line [132]. The motion of each joint was seen as a screw displacement relevant to its parent joint, which was separated to pure translations and pure rotations along x, y and z-axis. Equation (4-4) illustrates the calculation process, where $\boldsymbol{J}_{\mathrm{C}}$ and $\boldsymbol{J}_{\mathrm{P}}$ are the 3D cartesian coordinates of a child joint and its parent joint with an additional element 1; $\boldsymbol{DH}_{\mathrm{C}}$ means the Denavit-Hartenberg matrix of a child joint; $\boldsymbol{DH}_{\mathrm{P}}$ means the Denavit-Hartenberg matrix of its parent joint; $\boldsymbol{R}_{\mathrm{x}}$, $\boldsymbol{R}_{\mathrm{y}}$ and $\boldsymbol{R}_{\mathrm{z}}$ are the rotation matrices around x-, y- and z-axis, respectively; $\boldsymbol{R}$ is the rotation matrix; $\boldsymbol{T}$ is the transformation matrix; $\mathrm{r}_{\mathrm{x}}, r_y. r_z$ are the rotation angles around the x-, y- and z-axis; $\Delta x,\ \Delta y,\ \Delta z$ are the offsets of a child joint to its parent joint along x-, y- and z-axis.

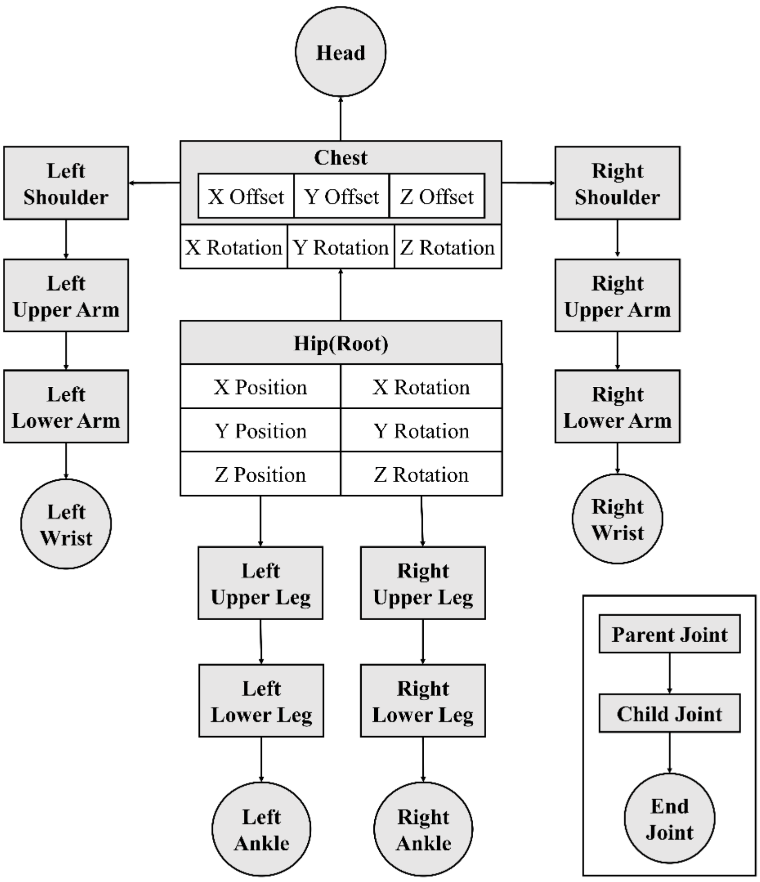

Figure 4-4 The data structure of a frame in the BVH file

$$
\begin{aligned}
&\boldsymbol{J}_{\mathrm{C}} = \boldsymbol{J}_{\mathrm{P}} \cdot \boldsymbol{DH}_{\mathrm{C}} \\
&\boldsymbol{DH}_{\mathrm{C}} = \boldsymbol{DH}_{\mathrm{P}} \cdot \boldsymbol{R}_{\mathrm{z}}\boldsymbol{R}_{\mathrm{y}}\boldsymbol{R}_{\mathrm{x}} \cdot \boldsymbol{T} \\
&\boldsymbol{R}_{\mathrm{z}} = \begin{bmatrix} \cos r_{\mathrm{z}} & -\sin r_{\mathrm{z}} & 0 & 0 \\ \sin r_{\mathrm{z}} & \cos r_{\mathrm{z}} & 0 & 0 \\ 0 & 0 & 1 & 0 \\ 0 & 0 & 0 & 1 \end{bmatrix} \\
&\boldsymbol{R}_{\mathrm{y}} = \begin{bmatrix} \cos r_{\mathrm{y}} & 0 & -\sin r_{\mathrm{y}} & 0 \\ 0 & 1 & 0 & 0 \\ \sin r_{\mathrm{y}} & 0 & \cos r_{\mathrm{y}} & 0 \\ 0 & 0 & 0 & 1 \end{bmatrix} \\
&\boldsymbol{R}_{\mathrm{x}} = \begin{bmatrix} 1 & 0 & 0 & 0 \\ 0 & \cos r_{\mathrm{x}} & -\sin r_{\mathrm{x}} & 0 \\ 0 & \sin r_{\mathrm{x}} & \cos r_{\mathrm{x}} & 0 \\ 0 & 0 & 0 & 1 \end{bmatrix} \\
&\boldsymbol{T} = \begin{bmatrix} \boldsymbol{I}_3 & \boldsymbol{J}_{\mathrm{C}} - \boldsymbol{J}_{\mathrm{P}} \\ \boldsymbol{0} & 1 \end{bmatrix},
\end{aligned}
\tag{4-4}
$$

II. Generating 2D postures from 3D postures

The 3D postures ($\boldsymbol{S}_{3\mathrm{D}}$) were first rotated to the front view ($\boldsymbol{S}'_{3\mathrm{D}}$), then projected to 2D postures ($\boldsymbol{S}_{2\mathrm{D}}$). Rodrigues's rotation formula, an efficient algorithm for rotating a three-dimensional vector given a rotation axis and a rotation angle, as shown in equation (4-5). In this study, $\boldsymbol{\mu}$ represents the anterior direction of human body and is defined as normal vector of the plane determined by left hip, right hip and neck joint. The front view was generated through rotating the 3D posture so that the $\boldsymbol{\mu}$ was along the positive unit vector of the x-axis, denoted as $\boldsymbol{\upsilon}$. The rotation angle is the angle between $\boldsymbol{\mu}$ and $\boldsymbol{\upsilon}$, denoted by $\langle \boldsymbol{\mu}, \boldsymbol{\upsilon} \rangle$; the axis of rotation is the normal vector of $\boldsymbol{\mu}$ and $\boldsymbol{\upsilon}$, which is represented by a unit vector $\boldsymbol{\kappa}$.

$$\boldsymbol{S}'_{3\mathrm{D}} = \boldsymbol{S}_{3\mathrm{D}} \cos\langle \boldsymbol{\mu}, \boldsymbol{v} \rangle + (\boldsymbol{\kappa} \times \boldsymbol{v}) \sin\langle \boldsymbol{\mu}, \boldsymbol{v} \rangle + \boldsymbol{\kappa}(\boldsymbol{\kappa} \cdot \boldsymbol{v})(1 - \cos\langle \boldsymbol{\mu}, \boldsymbol{v} \rangle) \tag{4-5}$$

Then the 2D joint locations were calculated based on the 3D joint locations with projection matrix. The generated 2D joint locations are related to the location of the camera. Given the location of horizontal angle θ_1 and vertical angle θ_2, the 2D postures could be generated through rotating the original 3D coordinate system to a new one whose z-axis is along the direction of the original z-axis. Given a 3D point (x, y, z) in the original coordinate system, the 2D projection is given in equation (4-6).

$$\boldsymbol{S}_{2\mathrm{D}} = \boldsymbol{S}'_{3\mathrm{D}} \begin{bmatrix} -\cos\theta_1 \cos\theta_2 & -\sin\theta_1 \cos\theta_2 \\ \sin\theta_1 & \cos\theta_1 \\ \cos\theta_1 \sin\theta_2 & -\sin\theta_1 \sin\theta_2 \end{bmatrix}, \tag{4-6}$$

4.3.3 Dataset structure

The construction working posture dataset includes 3D working posture data and the corresponding 2D working posture data. In addition, each item also includes the name of the task that generates the data. The structure was shown in Figure 4-5. The data was first grouped by task and camera projection angle, then in each group, 70% of the data items were randomly selected as training data, 20% as validation data and 10% as test data.

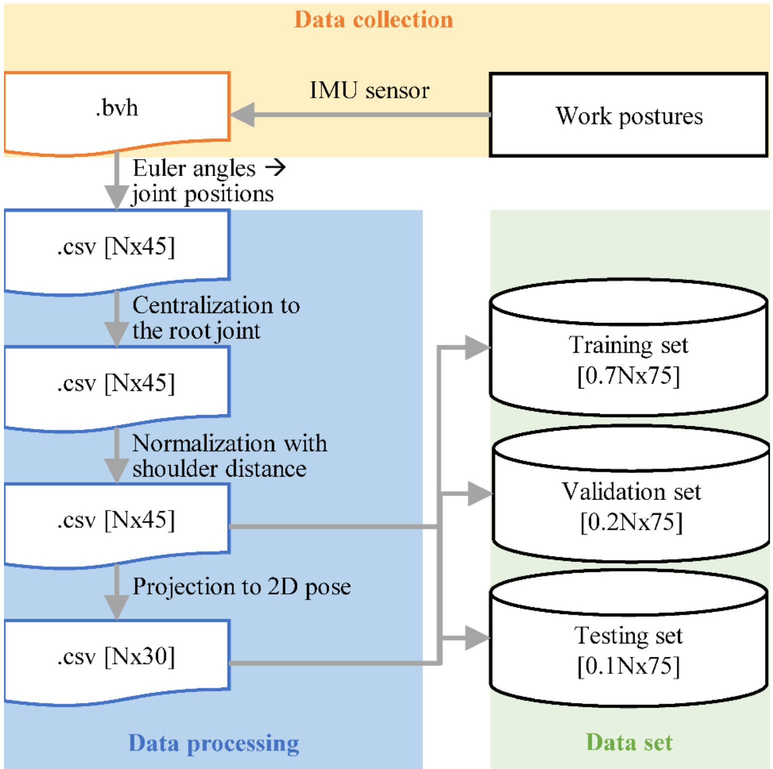

Figure 4-5 Dataset structure

4.4 Network design

4.4.1 Residual artificial neural network architecture (RANN)

The architecture of the neural network is shown in Figure 4-6. The network includes input module, residual module and output module. The input module aims to increase the dimension from 30 to L and is composed of a fully-connected layer, a batch norm layer and a Rectified Linear Unit (ReLU) layer. The residual module aims to find the relations between the input module and the output module and is composed of N residual units. Each unit includes a fully-connected layer, a batch norm layer, a ReLU layer and a residual layer. The output module aims to decrease the dimension from a large number to 45 and includes only one fully-connected layer.

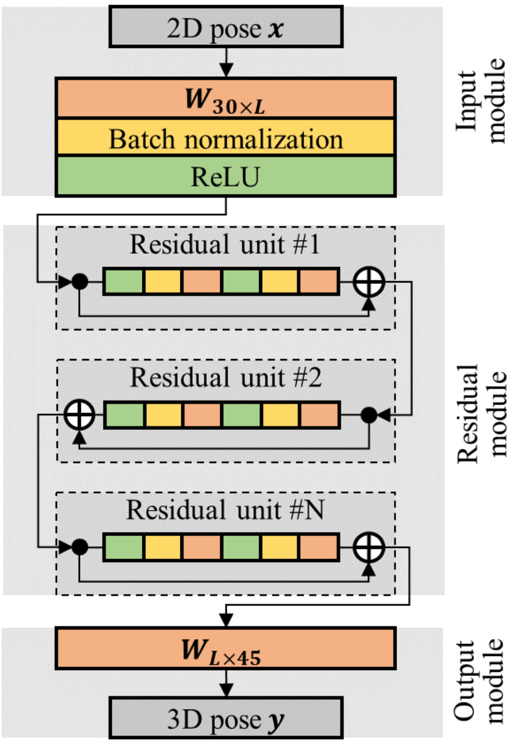

Figure 4-6 The architecture of the residual artificial neural network (RANN)

Fully-connected (FC) layers are the basic layers in neural networks. In an FC layer, the output and input are fully pairwise connected, and the output neurons are the weighted sums of the input neurons. An FC layer could be represented as

$$\boldsymbol{H}^{(k)} = \boldsymbol{H}^{(k-1)}\boldsymbol{W}^{(k)} + \boldsymbol{b}^{(k)}, \tag{4-7}$$

where $\boldsymbol{W}^{(k)}$ is the weight matrix connecting the $(k\text{-}1)^{th}$ layer $\boldsymbol{H}^{(k-1)}$ and the k^{th} layer $\boldsymbol{H}^{(k)}$. $\boldsymbol{b}^{(k)}$ is the bias.

Activation layer is used to increase the non-linearity of a neural network. ReLU (Rectified Linear Unit) was used in the proposed neural network. Equation (4-8) is the ReLU function. Given the value of $h^{(k)}_{m,1}$, which is the element located at the m^{th} row and the l^{th} column $h^{(k)}_{m,1}$ in a hidden layer $\boldsymbol{H}^{(k)}$, ReLU function will compare the value with 0. If $h^{(k)}_{m,1} > 0$, the function will return $h^{(k)}_{m,1}$; if $h^{(k)}_{m,1} \le 0$, the value will be zero.

$$\boldsymbol{g}(h^{(k)}_{m,l}) = \max(0, h^{(k)}_{m,l}), \tag{4-8}$$

Batch norm layer was added between FC layer and ReLU layer. During the training process, the network parameters, i.e. $\boldsymbol{W}^{(k)}$ and $\boldsymbol{b}^{(k)}$ were updated continuously, leading to the continuous variation of the input of the next layer. As a result, the next layer must adapt to such variation, making the network very unstable and difficult to reach consistent. Batch norm is introduced to solve the problem [133]. The procedure of batch norm was shown in equation (4-9) and (4-10):

$$\hat{\boldsymbol{h}} = \frac{\boldsymbol{h} - \overline{\boldsymbol{h}}}{\sqrt{\sigma^2 + \epsilon}}, \tag{4-9}$$

$$\boldsymbol{h}_{BN} = \chi_1 \circ \hat{\boldsymbol{h}} + \chi_2, \tag{4-10}$$

where $\boldsymbol{h}$ is a row vector of $\boldsymbol{H}^{(k)}$; $\overline{\boldsymbol{h}}$ is the mean vector of all row vectors in $\boldsymbol{H}^{(k)}$; $\hat{\boldsymbol{h}}$ is the result of normalization with mean $\overline{\boldsymbol{h}}$ and variance σ^2. A small constant ϵ was added to prevent being division by zero. To calculate the output of batch norm layer $\boldsymbol{h}_{\mathrm{BN}}$, $\hat{\boldsymbol{h}}$ is scaled by $\boldsymbol{\chi}_1$ and shifted by $\boldsymbol{\chi}_2$, which are two learnable parameter vectors introduced to recover the information lost due to normalization.

Residual layer has been widely-used in human pose identification to get better consistency [116,134]. The residual layer means slip connections and was used in the residual units. Equation (4-11) shows the principles of residual layer. $\boldsymbol{H}_{\mathrm{R}}^{(\mathrm{k})}$ is the output and $\boldsymbol{H}^{(\mathrm{k})}$ is the input. $\boldsymbol{F}\left(\boldsymbol{H}^{(\mathrm{k})}\right)$ is the result of batch normalization and ReLU. Compared with learning a direct mapping from $\boldsymbol{H}^{(\mathrm{k})}$ to $\boldsymbol{H}_{\mathrm{R}}^{(\mathrm{k})}$, it is easier for the stacked non-linear layers to push the residual to zero, i.e., to make $\boldsymbol{F}\left(\boldsymbol{H}^{(\mathrm{k})}\right)=\boldsymbol{H}_{\mathrm{R}}^{(\mathrm{k})}-\boldsymbol{H}^{(\mathrm{k})}=0$. So the residual layers contribute to better consistency [134].

$$\boldsymbol{H}_{\mathrm{R}}^{(\mathrm{k})}=\boldsymbol{F}\left(\boldsymbol{H}^{(\mathrm{k})}\right)+\boldsymbol{H}^{(\mathrm{k})}, \tag{4-11}$$

Network complexity is controlled by the width of layers and the number of residual units. The width of layers means the number of neurons in each layer. Increasing layer width and the number of residual units will increase network complexity. Complex network could increase the accuracy but is prone to overfitting and computationally expensive. In this study, various combinations of the layer width and the numbers of the residual units were tested to decide the proper complexity.

4.4.2 Loss function

The loss function of the network is weighted mean square error (WMSE). The original mean square error is calculated as the average of the squared differences between the output of the network and the ground-truth-value. However, the limb joints (e.g. wrists, ankles, elbows and knees) usually have a larger range of motion than the torso joints (e.g. shoulders, hips, waist, chest), which means the locations of the limb joints are more difficult for the network to infer, so the loss function should focus more on the limb joints. WMSE was applied as the training loss function to distribute the weight to each joint according to the standard deviation of the coordinates of the joints. For a certain joint j_0, the corresponding weight w_{j_0} is calculated as equation (4-12),

$$w_{\mathrm{j}_0} = \frac{1}{\sum_{\mathrm{j}=1}^{15} w_{\mathrm{j}}} \sqrt{\frac{1}{N} \sum_{\mathrm{n}=1}^{\mathrm{N}} \left(p_{\mathrm{n},\mathrm{j}_0} - \frac{1}{N} \sum_{\mathrm{n}=1}^{\mathrm{N}} p_{\mathrm{n},\mathrm{j}_0} \right)^2}, \tag{4-12}$$

where j is the serial number of a joint; n is the serial number of a data item in training dataset; N is the number of data items in training dataset; $p_{\mathrm{n},\mathrm{j}_0}$ represents the 2D coordinates of the $\mathrm{j}_0^{\mathrm{th}}$ joint in the n^{th} posture in the training dataset.

Denoting the weight vector of all joints as $\boldsymbol{w}$, the training loss, $loss$, is calculated as equation (4-13) and (4-14),

$$loss_n = \boldsymbol{w}\left[\left(\hat{\boldsymbol{s}}_{\mathrm{n,j}} - \boldsymbol{s}_{\mathrm{n,j}}\right)\circ\left(\hat{\boldsymbol{s}}_{\mathrm{n,j}} - \boldsymbol{s}_{\mathrm{n,j}}\right)\right], \tag{4-13}$$

$$loss = \frac{1}{N}\sum_{\mathrm{n=1}}^{\mathrm{N}}\left\|loss_n\right\|, \tag{4-14}$$

where $\boldsymbol{s}_{\mathrm{n,j}}$ and $\hat{\boldsymbol{s}}_{\mathrm{n,j}}$ are the ground truth and estimation of the 3D location of joint j in data item n, respectively. $loss_{\mathrm{n}}$ is the loss of the $\mathrm{n^{th}}$ posture in the training dataset, and *loss* represents training loss. $\circ$ represents the Hadamard product, or element-wise product.

4.5 Network training

The aim of the experiment is to decide the proper network complexity and the weight of each node in the network. In the following training process, the loss function is defined as mean-squared loss and optimized with Adam algorithm [135]. The dropout rate is 0.5. The max-norm constraint is 1. 70% of the data items were used to train the network, while the rest of the dataset was used for validation and test.

4.5.1 Network complexity

The complexity of the network has a great influence on the network performance. High complexity may result in overfitting and poor generalization ability, which means the network could achieve high accuracy only in the trained dataset and may fail to provide accurate predictions if used on another dataset. Besides, high complexity means a large number of parameters in the network, which will increase the time spent in training and prediction. Low complexity, on the contrary, may lead to poor prediction accuracy but short training time.

This experiment aims to find the proper network complexity. The author changed the depth and width of the network through editing the number of basic units (2, 3, 4) and the number of nodes in each linear layer (512, 1024, 2048). As a result, nine different networks were generated. In this experiment, the initial learning rate was set as 0.01, and the batch size was set as 64. Each network was trained for 50 epochs.

Figure 4-7 compares the nine networks according to training loss, validation loss, training error and validation error. Training loss represents the final value of loss function. A smaller training loss is preferable. The trained network was then used to estimate the 3D joint locations according to the inputs data in the validation dataset. The estimation results were then compared with the target data. The validation error is defined as the mean of the distances between the estimated 3D location and the target 3D locations of the 16 joints. The last subfigure is the time spent on estimating the 3D joint locations for one frame. Based on the comparison of the nine networks in Figure 4-7, it could be found that the model with 1024 neurons within each layer and 2 residual units has the lowest training loss, validation loss, validation error and validation time. As a result, the complexity "1024×2" was selected in the following training process.

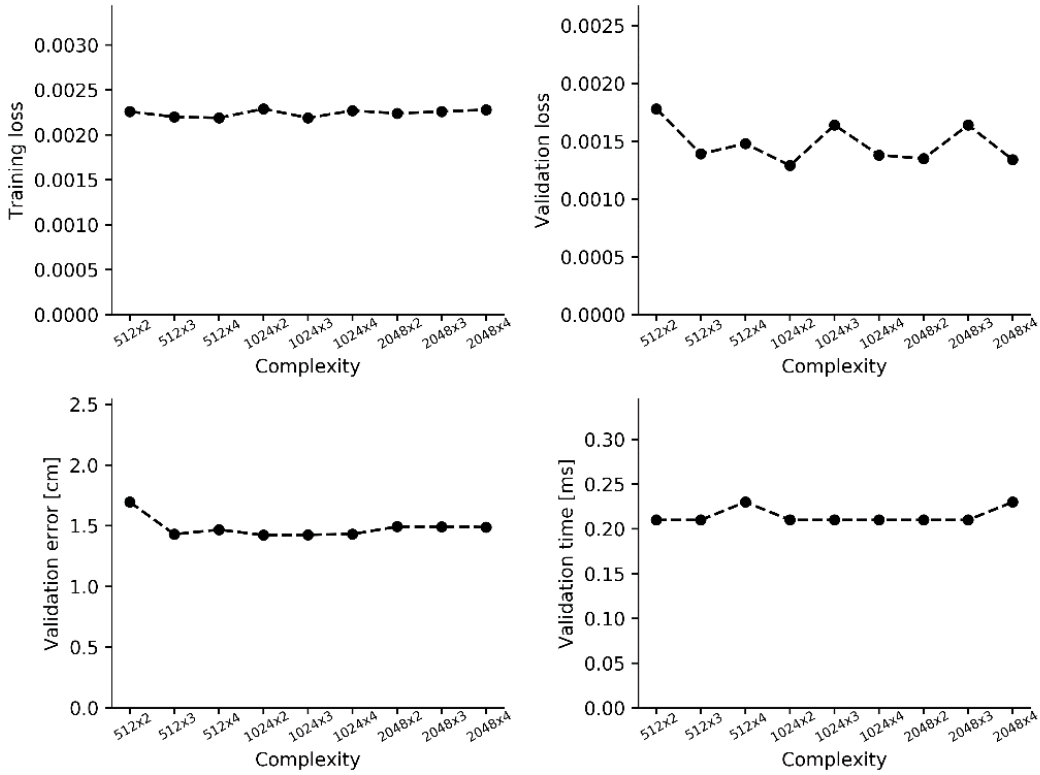

Figure 4-7 The training results of different network complexities

4.5.2 Learning rate

The goal of the training process is to find an extreme point of the loss function, where the gradient of the loss function equals to zero. Learning rate controls how much the weights were adjusted in each step. High learning rates may lead to missing the extreme point and the divergence of the loss function, while low learning rates may extend the training process and make the network trapped in local extrema. Consequently, it is important to find a suitable learning rate. Four learning rates were tested, and the results are shown in Figure 4-8. It could be found that setting the learning rate as 0.001 provided the smallest training loss and the lowest validation error. The learning rate was set as 0.001 in the following experiments.

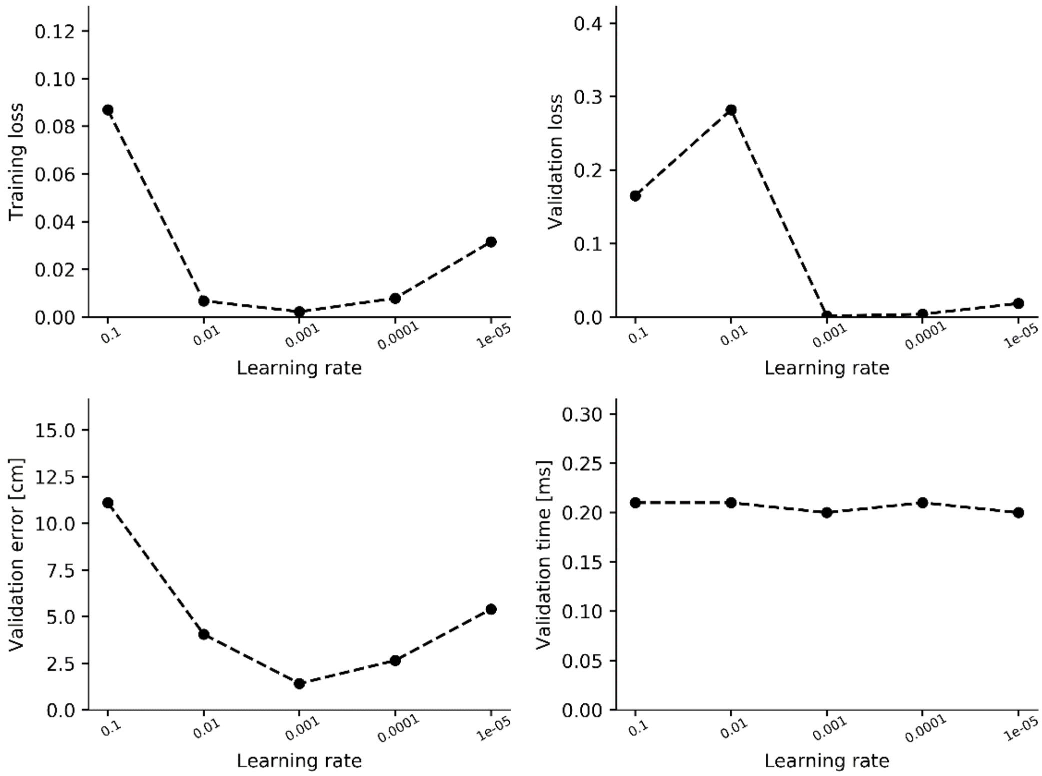

Figure 4-8 The training results of different learning rates

4.5.3 Batch size

Mini-batch gradient descent was applied to find the extreme of the loss function. The algorithm splits the training dataset into small batches to calculate the loss function gradients and update the weights. A larger batch size means that more examples could be used to decide the decrease direction of the loss gradient but requires more memory. A smaller batch size, on the contrary, requires less memory, but may increase the randomness of the gradient decrease direction and make the loss function trapped in local minimum. Different batch sizes (8, 16, 32, 64, 128, 256, 512) were tested in this experiment. The results are provided in Figure 4-9. When the batch size is 64, the training process returns the smallest training loss, the lowest validation error, a relatively small validation loss and the shortest validation time.

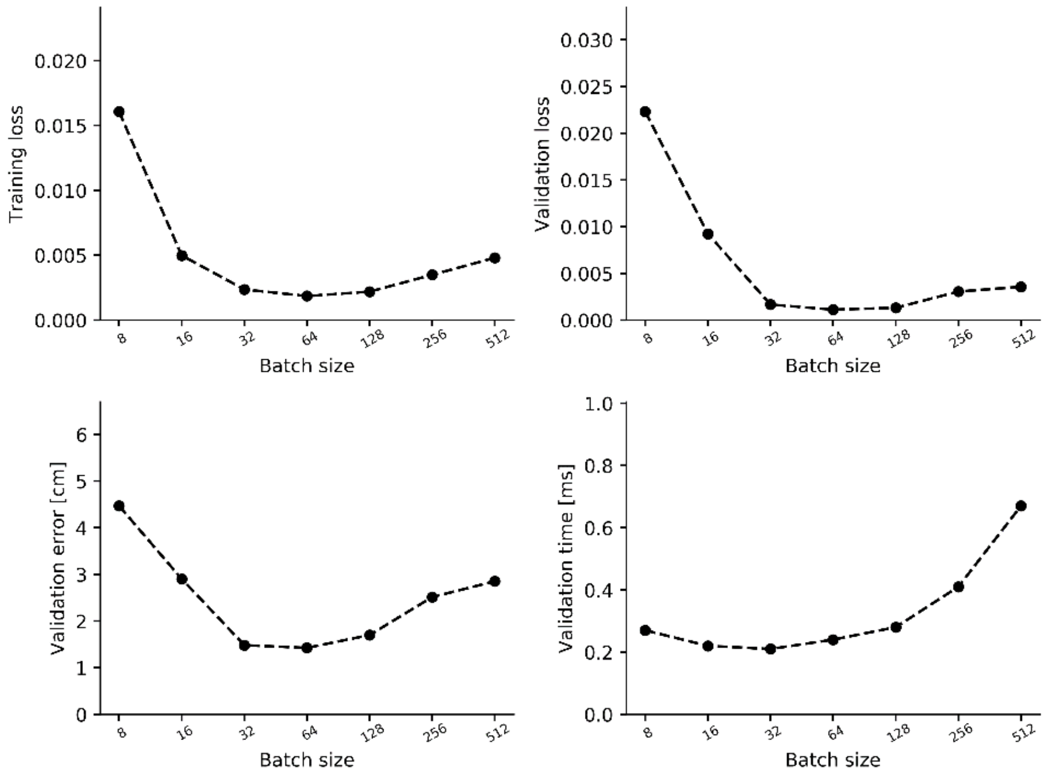

Figure 4-9 The training results of different batch sizes

To this end, the network with two residual units and 1024-width layers has the best performance. The learning rate and batch size were set as 0.001 and 64, respectively. Figure 4-10 shows the convergence process of the loss function.

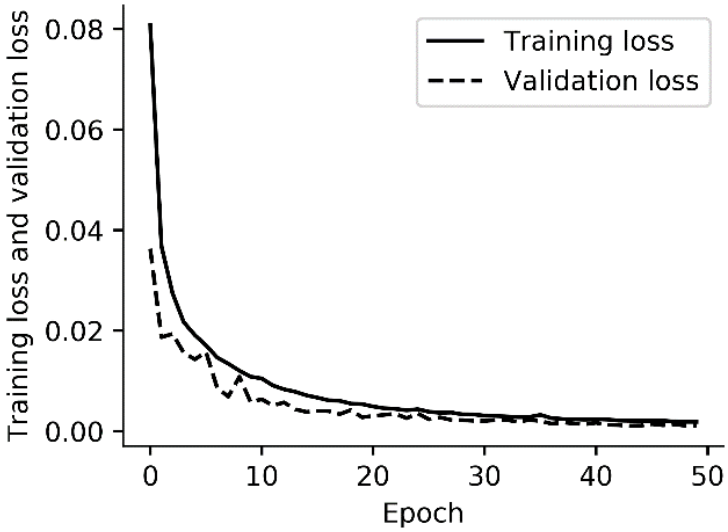

Figure 4-10 The convergence process of the loss function

4.6 Summary

In this chapter, a computer vision algorithm is designed and trained based on deep learning neural network and a construction working posture dataset. This algorithm could collect 3D working postures from RGB construction site images, which solves the posture data collection problem in the PFA method. The mean position per joint error and the estimation time of each frame are 1.26 cm and 0.24 s, respectively. In the following chapter, the estimated 3D posture data will be used in joint calculation for physical fatigue assessment.

Chapter 5 Inverse dynamics and physical fatigue assessment[5]

5.1 Introduction

This chapter aims to propose a new external force estimation method (section 5.2), which, together with the 3D posture data collection method, serves as the data foundation of the PFA method. Given the external force data and posture data, a human body skeleton model is built in section 5.3 to support the joint torque calculation in section 5.4. After calculating the joint torques, a PFA indicator is proposed in section 5.5.

---

[5] This chapter is based on the following published study and being reproduced with the permission of Elsevier and The International Association for Automation and Robotics in Construction.

Yu, Y., Li, H., Yang, X., Kong, L., Luo, X., & Wong, A. Y. L. (2019). An automatic and non-invasive physical fatigue assessment method for construction workers. Automation in Construction, 103, 1–12. https://doi.org/10.1016/j.autcon.2019.02.020

Yu, Y., Li, H., Yang, X., & Umer, W. (2018). Estimating Construction Workers' Physical Workload by Fusing Computer Vision and Smart Insole Technologies. In 2018 Proceedings of the 35th ISARC (pp. 1212–1219). Berlin: International Association for Automation and Robotics in Construction. https://doi.org/10.22260/ISARC2018/0168

5.2 External force measurement

The novel insoles with plantar pressure sensors, named *Moticon*, are used to measure the worker's total weight in Figure 5-1. The insole can be used in virtually any footwear. These commercial available smart insoles can transfer data wirelessly through an ANT radio service [136].

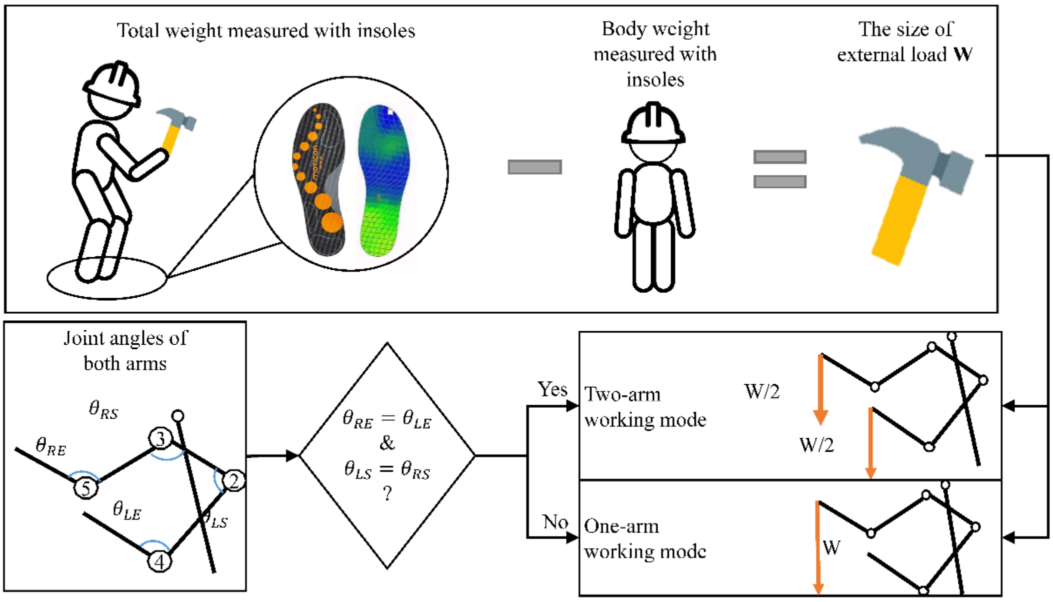

Figure 5-1 Calculation of external forces with smart insoles

Each pair of insoles contain 26 pressure sensors (13 in each insole) as shown in Figure 5-2 to measure the average pressure of the corresponding area. The total ground reaction force of equals the pressure measured by each sensor multiplied by the sensor area with

$$\begin{bmatrix} \boldsymbol{F}_{\mathrm{L}} \\ \boldsymbol{F}_{\mathrm{R}} \end{bmatrix} = \frac{A}{Q+1} \sum_{\mathrm{q}=0}^{\mathrm{Q}} \begin{bmatrix} \boldsymbol{f}_{\mathrm{L,q}} \\ \boldsymbol{f}_{\mathrm{R,q}} \end{bmatrix}, \tag{5-1}$$

where $\boldsymbol{F}_{\mathrm{L}}$ and $\boldsymbol{F}_{\mathrm{R}}$ are the ground reaction force of the left foot (L) and right foot (R); A is the plantar contact area of each foot (A =150 cm^2); Q is the largest sensor number (#), (Q =12; Q+1=13 is the total number of sensors in each insole); q is the number of each sensor, $\boldsymbol{f}_{\mathrm{L,q}}$ and $\boldsymbol{f}_{\mathrm{R,q}}$ are the pressure value measured by sensor n in the left (L) or right insole (R).

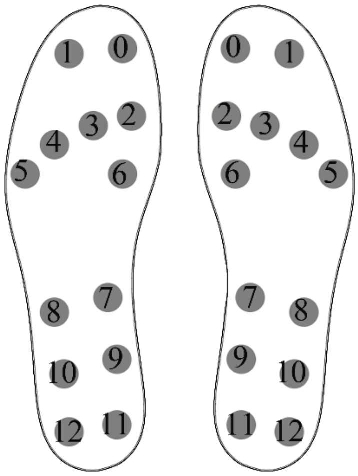

Figure 5-2 Distribution of sensors in a pair of smart insoles

It should be noted that the insole-based weight and external burden estimation method involves assumption 3 and assumption 4 in section 3.2.

The amount of external force is the total weight minus the worker's self-weight. In construction tasks, external forces are usually located at the hands and feet (the ground reaction forces). For the force located at the hands, two-arm and one-arm working patterns are taken into consideration. The angles of the shoulder joints and elbow joints on both sides are compared to identify the pattern. If the angles of the left and right arm are the same, the working pattern is considered a two-arm working pattern. Otherwise, a one-arm working pattern is identified, and the external force is considered at the worker's dominant hand.

5.3 Inverse dynamics of human body skeleton

The biomechanics of human musculoskeletal system are complex because the mechanical properties of bones, joints, tendons, and muscles of individuals are affected by various factors (e.g., age, gender, weight and height). Additionally, the stress-strain relations of bones, joints, tendons, and muscles also vary with the exerted forces. Based on assumption 1 and assumption 2 in section 3.2, the force balance equation and torque balance equation were used in this section to calculate the joint torques. Figure 5-3 presents the simplified human skeleton model for the biomechanical analysis, which contains 15 key joints including the torso and four limbs. The coordinates are a right-hand-rule system. The positive direction of the y-axis is upward.

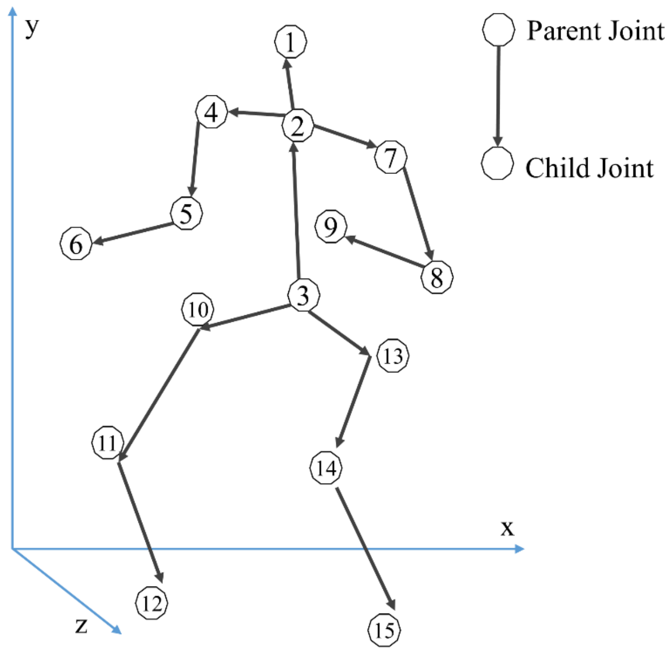

No.	Joint
1	Head
2	Neck
3	Waist
4	Right Shoulder (RS)
5	Right Elbow (RE)
6	Right Wrist (RW)
7	Left Shoulder (LS)
8	Left Elbow (LE)
9	Left Wrist (LW)
10	Right Hip (RH)
11	Right Knee (RK)
12	Right Ankle (RA)
13	Left Hip (LH)
14	Left Knee (LK)
15	Left Ankle (LA)

Figure 5-3 The simplified biomechanical human skeleton model

5.4 Computing joint torques

Newton equation was used to calculate joint reaction forces. For a given segment, the equation can be expressed as equation (5-2)

$$\boldsymbol{F}_{\mathrm{C}} + \boldsymbol{F}_{\mathrm{P}} + \boldsymbol{G} = \boldsymbol{0}, \tag{5-2}$$

where $\boldsymbol{F}_{\mathrm{C}}$ is the joint reaction force at the child joint of the segment [N]; $\boldsymbol{F}_{\mathrm{P}}$ is the joint reaction force at the parent joint [N]; $\boldsymbol{G}$ is the gravity of the segment [N]. The positive direction indicates the upward direction, which is the same as the positive direction of the y-axis in Figure 5-3.

In this research, the mass of each segment was calculated based on the segment percentage of total body weight, which could be referred to [137] for details. Briefly, according to the skeletal model in Figure 5-3, there is no child joint reaction force in the force equilibrium equations of lower arms and shanks. The forces are replaced with ground reaction forces and hand load forces due to the tools or materials holding in hands. In this research, the hand load force was assumed to be the weight of the tools/materials, and the ground reactions force was assumed to be the sum of hand load force and the participant's body weight. Given the ground reaction forces, the joint reaction forces of knees could first be calculated, while the joint reaction forces of other joints were estimated hieratically.

The torque balance equation was used to calculate joint torques. Figure 5-4 shows the torques on a given segment, where A is the parent joint, B is the child joint, and C is the gravity center point.

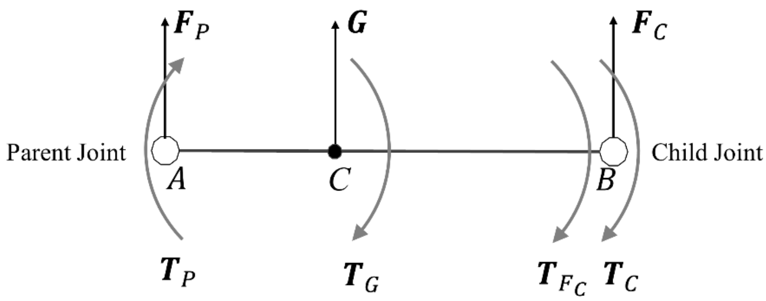

Figure 5-4 Forces and torques of a given segment

The sum of all the torques acting on the parent joint is equal to zero. The torques include the parent joint torque, the child joint torque, and the torques generated from the segment's self-weight and the joint reaction force on the child joint. The torque generated from the parent joint reaction force is zero. Equation (5-3) is the torque balance equation

$$\begin{aligned}&\boldsymbol{\Gamma}_{\mathrm{P}}+\boldsymbol{\Gamma}_{\mathrm{G}}+\boldsymbol{\Gamma}_{\boldsymbol{F}_{\mathrm{C}}}+\boldsymbol{\Gamma}_{\boldsymbol{F}_{\mathrm{P}}}=\boldsymbol{0},\\&\boldsymbol{\Gamma}_{\mathrm{G}}=\overrightarrow{AC}\times\boldsymbol{G}=r\overrightarrow{AB}\times\boldsymbol{G},\\&\boldsymbol{\Gamma}_{\boldsymbol{F}_{\mathrm{C}}}=\overrightarrow{AB}\times\boldsymbol{F}_{\mathrm{C}},\end{aligned}\tag{5-3}$$

where $\boldsymbol{\Gamma}_{\mathrm{P}}$ is the reaction torque at the parent joint A; $\boldsymbol{\Gamma}_{\mathrm{G}}$ is the torque produced by $\boldsymbol{G}$; $\boldsymbol{\Gamma}_{\boldsymbol{F}_{\mathrm{C}}}$ is the torque produced by $\boldsymbol{F}_{\mathrm{C}}$. The unit of torque is [N·m]. The positive direction is clockwise. $\overrightarrow{AC}$ is the vector from the parent joint to the center of mass of the segment; $\overrightarrow{AB}$ is the vector from the parent joint to the child joint; r is the ratio of $\overrightarrow{AC}$ to $\overrightarrow{AB}$, which represents the location of the center of mass. The value of r is given in [137].

5.5 Joint physical fatigue indicator

This module aims to determine joint physical fatigue according to the current loads on joints and the load history of these joints. The fatigue and recovery model developed by Ma et al. [50] was applied to predict construction workers instantaneous and cumulative fatigue alongside the posture and pressure data.

The instantaneous joint physical fatigue index IF is defined as the decrease of joint capacity in this paper (equation (5-4)). $\boldsymbol{\Gamma}_{\max}$ represents the maximum joint capacity, which means the maximum torque that the joint can hold. Γ_{cem} represents the current joint capacity. At the start of a task, the joint capacity Γ_{cem} equals to Γ_{max}, so $IF = 0$. In work status, the joint capacity Γ_{cem} will decrease, so IF will increase. In rest status, the joint capacity Γ_{cem} will increase, so IF will decrease. Figure 5-5 represents the above process.

$$IF(t) = \frac{\Gamma_{\max} - \Gamma_{\text{cem}}(t)}{\Gamma_{\max}} \times 100, \tag{5-4}$$

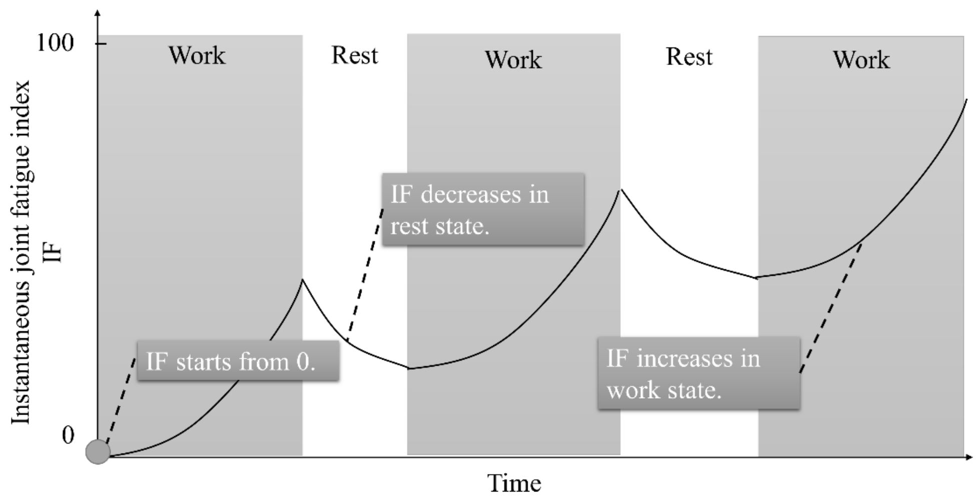

Figure 5-5 An example of the instantaneous joint physical fatigue index in work and rest status

The maximum joint capacity $\Gamma_{\max}$ is estimated based on the correlation between ages, gender, weights, height and ethnicities from Shaunak, Ang et al. (1987) and Meldrum, Cahalane et al. (2007) [46,138]. The basic assumption is that different people have different load tolerance, so workload assessment should consider not only external factors such as external forces and postures, but also the workers' capability to tolerate loads. Maximal isometric strength (MVIC) is a widely used indicator to measure the human body's biomechanical capacity. Consortium (1996) has developed a regression equation to predict MVIC based on gender, age, height, and weight, from the results of more than 500 experiments. This is used to estimate joint capability with

$$\Gamma_{\max} = \left(-c_1 \times age + c_2 \times gender + c_3 \times \frac{weight}{height^2} + c_4 \times l_{bone}\right), \tag{5-5}$$

where $\Gamma_{\max}$ represents the maximum torque the joint can tolerate (the unit is [N·m]); l_{bone} is the force arm length during measuring external forces (the unit is [m]) - as the joint angles in the experiment are right angles, the force arm is equal to the corresponding bone's length; gender =1 if the subject is a male; gender =0 if female; The units of age, weight, and height are [year], [kg], and [m] respectively; c_1, c_2, c_3, c_4 are the coefficients, whose values are given in Table 5-1.

Table 5-1 Joint capability regression coefficients

Joint	c_1	c_2	c_3	c_4
Right shoulder	0.17	c_7	0.17	23.35
Left shoulder	0.18	c_8	0.29	19.59
Right elbow	0.13	11.24	0.07	22.78
Left elbow	0.11	10.63	0.05	19.66
Right hip	0.33	19.19	0.66	34.44
Left hip	0.29	18.75	0.47	36.05
Right knee	0.16	8.78	0.08	22.47
Left knee	0.17	7.67	0.14	21.10

The current joint capacity Γ_{cem} *at work state* was simulated based on the muscle motor unit theory [51]. According to the theory, muscles generate torques because of the activation of motor units. Some units have a high muscle force generation capacity, but the capacity decreases rapidly (easy to fatigue). Other units have a lower muscle force generation capacity, which decreases slowly (fatigue resistant). When a given muscle is activated to work against a large external force, both type of motor units will be activated but the latter one would last longer. Based on the above theory, the joint capacity decreases more rapidly under a higher workload because motor units responsible for generating large force would show fatigue easier. Further, under the same constant workload, the rate of joint capacity reduction will decelerate [51]. Equation (5-6) depicts the above process, where c_5 is a constant value, and equals to 1 min^{-1}. $\boldsymbol{\Gamma}(t)$ means the joint torque at time *t*, which is the calculation results of 4.2.2. $\boldsymbol{\Gamma}_{\text{cem}}(t)$ can be calculated as the integral of $d\boldsymbol{\Gamma}_{\text{cem}}(t)/dt$ (equation (5-7)).

$$\frac{d\boldsymbol{\Gamma}_{\text{cem}}(t)}{dt} = -c_5 \frac{\boldsymbol{\Gamma}_{\text{cem}}(t)}{\boldsymbol{\Gamma}_{\text{max}}} \boldsymbol{\Gamma}(t) \tag{5-6}$$

$$\boldsymbol{\Gamma}_{\text{cem}}(t) = \boldsymbol{\Gamma}_{\text{cem}}(t_0)\exp\left(-\frac{c_5}{\boldsymbol{\Gamma}_{\text{max}}} \int_{t_0}^{t} \boldsymbol{\Gamma}(u)du\right) \tag{5-7}$$

The current joint capacity $\boldsymbol{\Gamma}_{\text{cem}}$ during rest. When the muscles of a certain body part are in a resting state, the respective joint capacity will recover. As shown in Figure 5-5, the joint muscle capacity increases when a worker is taking a rest. According to the muscle motor unit theory, the recovery process is represented by $\boldsymbol{\Gamma}_{\text{max}} - \boldsymbol{\Gamma}_{\text{cem}}(t)$ in equation (5-8), where c_6 is set as 2.4 min^{-1}, indicating the average rate of recovery [139]. $\boldsymbol{\Gamma}_{\text{cem}}(t)$ can be calculated as the integral of $d\boldsymbol{\Gamma}_{\text{cem}}(t)/dt$ (equation (5-9)).

$$\frac{d\boldsymbol{\Gamma}_{\mathrm{cem}}(t)}{dt}=\mathrm{c}_6\left(\boldsymbol{\Gamma}_{\max}-\boldsymbol{\Gamma}_{\mathrm{cem}}(t)\right), \tag{5-8}$$

$$\boldsymbol{\Gamma}_{\mathrm{cem}}(t)=\boldsymbol{\Gamma}_{\mathrm{cem}}(t_0)+\left(\boldsymbol{\Gamma}_{\max}-\boldsymbol{\Gamma}_{\mathrm{cem}}(t_0)\right)\left(1-e^{-\mathrm{c}_6 t}\right), \tag{5-9}$$

The cumulative joint physical fatigue index CF development speed is positively correlated with the external force and negatively related to muscle strength capacity [140]. The formula of the joint physical fatigue model is expressed in equation (5-10), where t represents time. CF represents cumulative joint physical fatigue level. In equation (5-10), $\boldsymbol{\Gamma}_{\max}/\boldsymbol{\Gamma}_{\mathrm{cem}}(t)$ is the reciprocal of current relative joint capacity, representing the personal factors. $\boldsymbol{\Gamma}(t)/\boldsymbol{\Gamma}_{\mathrm{cem}}(t)$ is the current relative joint load, representing the external factors.

$$\frac{dCF(t)}{dt}=\frac{\boldsymbol{\Gamma}_{\max}}{\boldsymbol{\Gamma}_{\mathrm{cem}}(t)}\frac{\boldsymbol{\Gamma}(t)}{\boldsymbol{\Gamma}_{\mathrm{cem}}(t)} \tag{5-10}$$

Finally, given $\boldsymbol{\Gamma}_{\mathrm{cem}}(t)$, the cumulative joint physical fatigue index $CF(t)$ can be calculated as the integration of $dCF(t)/dt$. Figure 5-6 is an example of the cumulative joint physical fatigue index $CF(t)$, which increases rapidly during work due to the decrease in muscle capacity and increases slowly or even decreases during rest due to the increase of the muscle capacity.

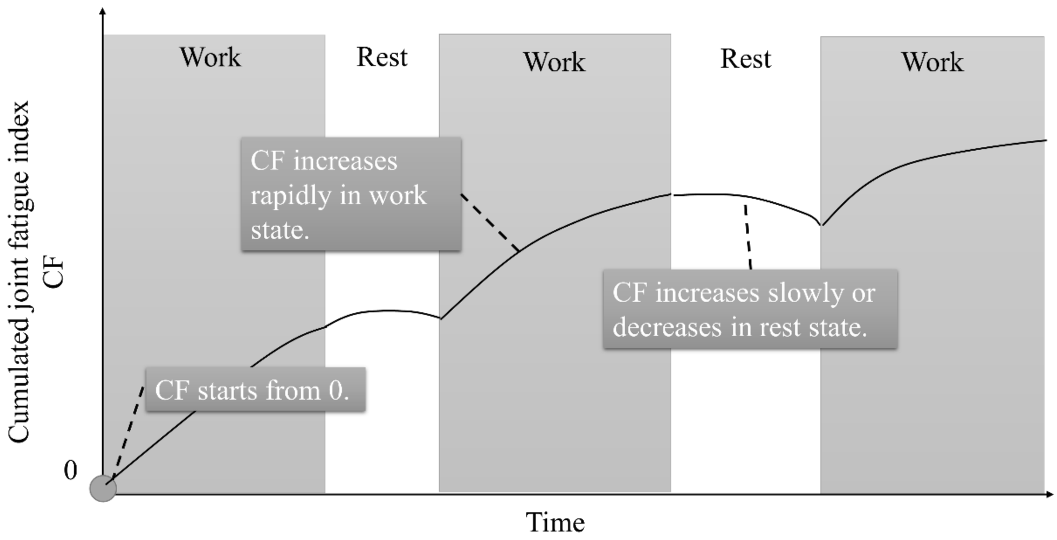

Figure 5-6 An example of the cumulative joint physical fatigue index at the work and rest states

In addition, in this study, the instantaneous/cumulative whole-body physical fatigue indices are defined as the average of the instantaneous/cumulative joint physical fatigue indices of all joints of an individual.

5.6 Summary

To this end, the new PFA method has been established, which includes a new PFA indicator and two novel data collection methods. The PFA indicator estimates joint physical fatigue level according to individual joint capacity and joint torque history. As for data collection, computer vision algorithm and smart insole-based method are used to collect posture data and external force data non-intrusively. Theoretically, the new PFA method could measure personalized physical fatigue level accurately and could work well in construction site situations. The accuracy and usability on sites are tested in the next chapter.

PART III DISCUSSION AND CONCLUSION

Chapter 6 Experiments and results[6]

6.1 Introduction

To validate the accuracy and usability of the proposed PFA method, four experiments were conducted to validate the proposed approach during construction tasks: 1) a field experiment to validate the accuracy of the motion capture method (section 6.2); 2) a laboratory experiment to validate the accuracy of the external force estimation method (section 6.3); 3) a laboratory experiment to validate the accuracy of the PFA method (section 6.4); and 4) a field experiment to validate the usefulness of the new approach in estimating physical fatigue (section 6.5).

[6] This chapter is based on the following published study and being reproduced with the permission of Elsevier and The International Association for Automation and Robotics in Construction.

Yu, Y., Li, H., Yang, X., Kong, L., Luo, X., & Wong, A. Y. L. (2019). An automatic and non-invasive physical fatigue assessment method for construction workers. Automation in Construction, 103, 1–12. https://doi.org/10.1016/j.autcon.2019.02.020

Yu, Y., Li, H., & Yang, X. (2019). 3D Posture Estimation from 2D Posture Data for Construction Workers. In M. Al-Hussein (Ed.), 2019 Proceedings of the 36th ISARC (pp. 26–34). Banff, AB, Canada: The International Association for Automation and Robotics in Construction. https://doi.org/10.22260/ISARC2019/0004

Yu, Y., Li, H., Yang, X., & Umer, W. (2018). Estimating Construction Workers' Physical Workload by Fusing Computer Vision and Smart Insole Technologies. In 2018 Proceedings of the 35th ISARC (pp. 1212–1219). Berlin: International Association for Automation and Robotics in Construction. https://doi.org/10.22260/ISARC2018/0168

6.2 Testing the accuracy of posture of the 3D motion estimation method

This study trained a deep learning network named RANN to estimate 3D construction workers postures from 2D postures. Combined with OpenPose, which could generate 2D postures from RGB images, RANN could estimate 3D postures from construction site videos or images. This section first demonstrates the integration of OpenPose and RANN, then tests the accuracy of the algorithm on the test dataset of ConPose.

6.2.1 Application of RANN on RGB images

The trained network was combined with OpenPose to estimate 3D working postures from RGB images. Five video clips were used to test the performance as shown in Figure 6-1. Six trades of construction workers were involved, including bricklayer, concreter, pipe layer, bar fixer, scaffolder and formwork erector. The authors shot a ten-minute video for each worker and then applied the proposed method to perform ergonomic assessments based on the videos. The video frequency is 25 fps. Generally speaking, integrating RANN and OpenPose could provide accurate 3D postures from construction site images or videos.

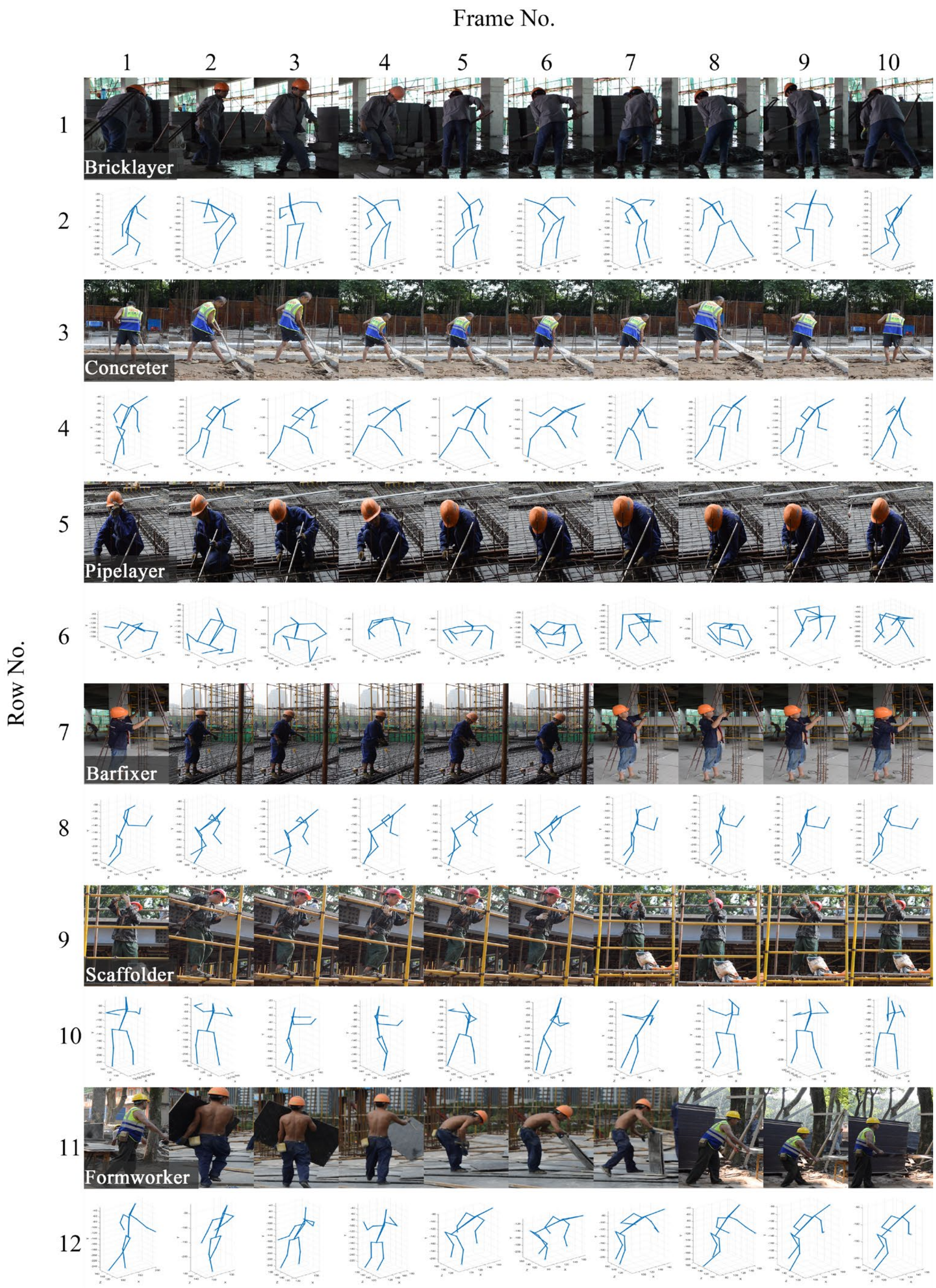

Figure 6-1 Example frames of generating 3D postures from RGB images by integrating the proposed network and Openpose

6.2.2 Network performance evaluation

The accuracy of the network was tested on the test dataset of ConPose. The predicted postures were compared with the ground truth postures. Mean per joint position error (MPJPE) was used to measure the differences. MPJPE for the n^{th} pose in the dataset is defined as the average of the Euclidean distances between the ground truth ($\boldsymbol{s}_{n,j}$) and estimation ($\hat{\boldsymbol{s}}_{n,j}$) of each joint location, as shown in equation (6-1).

$$e_n = \frac{1}{15}\sum_{j=1}^{15}\left\|\hat{\boldsymbol{s}}_{n,j} - \boldsymbol{s}_{n,j}\right\| \tag{6-1}$$

Figure 6-2 is the MPJPE of each frame and the histogram of the MPJPE. The mean of MPJPE is 1.26 cm, and the standard deviation is 0.43 cm. Most of the frames smaller than 3.00 cm.

Only one frame in Figure 6-3 has an MPJPE as high as 4.50 cm. Besides, there is one frame whose MPJPE is up to 9.98 cm, which is not shown in Figure 6-2. Figure 6-3 shows the two frames. The blue skeletons are the ground truth of the 3D postures, while the red skeletons are the estimated 3D postures. In both frames, the errors come from the limb joints, especially the knee joints and the elbow joints.

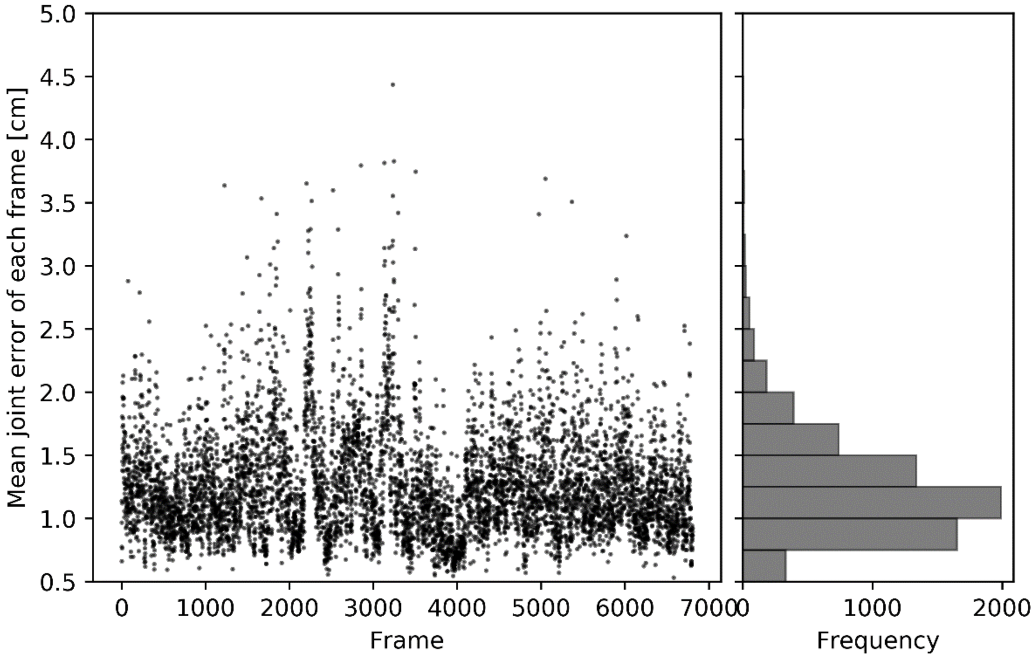

Figure 6-2 The mean per joint position error of each frame

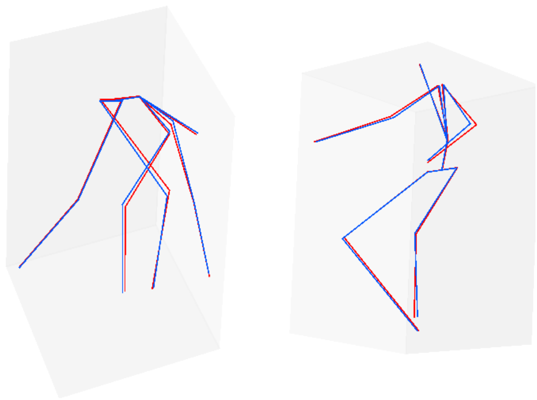

Figure 6-3 Two high-error frames

Figure 6-4 and Figure 6-5 are the mean and standard deviation of the errors for each joint and task in the testing data set. In Figure 6-4, the joints are sorted in the descending order of the mean error. The wrists and the ankles have the highest errors; the torso joints, such as the hip joints, the shoulders, neck and chest joints have lower errors. The reasons are that the wrists and the ankles have larger ranges of activity than the torso joints, which means the locations of the wrists and the ankles are more difficult for the network to learn and predict, resulting in higher errors. In Figure 6-5, calibrating and plaster have lower errors because the postures during the two tasks are less diversified. On the contrary, the postures of rebar tying, and material handling are more dynamic, resulting in higher errors.

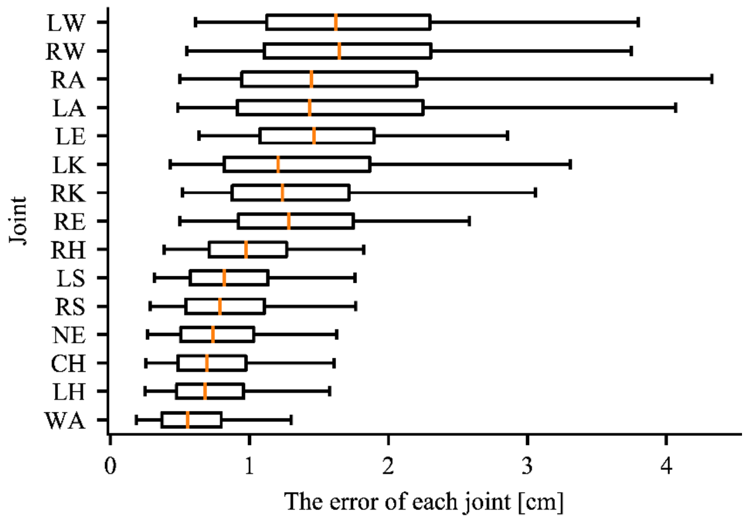

Figure 6-4 The error of each joint. R: Right; L: Left; H: Hip; K: Knee; A: Ankle; S: Shoulder; E: Elbow; WA: Wrist; NE: Neck; CH: Chest.

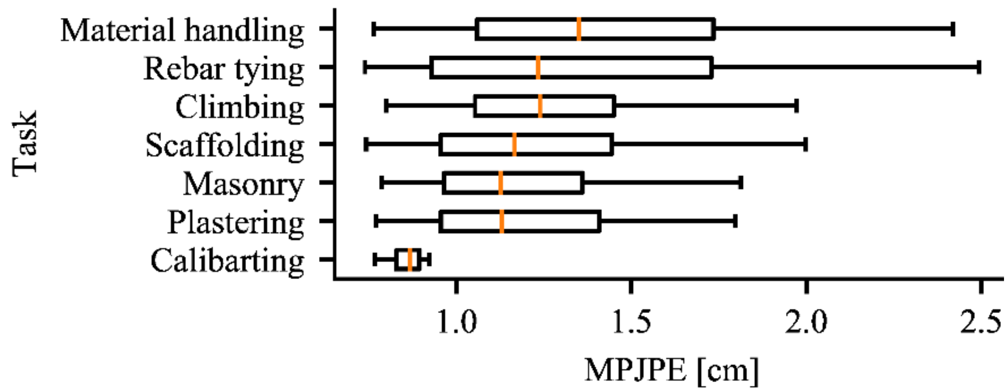

Figure 6-5 The MPJPE of each task

6.2.3 Comparison with other 3D posture estimation computer vision algorithms

Figure 6-6 is the comparison of 12 joints errors with a previous study that also estimated laborers' 3D postures according to RGB images. It could be found that our method outperforms the previous study in most of the joints. The reported error is 4.01 cm in [111], which is 2.75 cm higher than the proposed method. In addition, the output of the proposed network includes the 3D coordinates of 15 joints, while [111] includes 13 joints. What's more, the experiment in this study includes the posture data of six tasks from worksites, and the previous study only includes the posture data of three tasks collected in a laboratory, which means our network has better generalization ability for real-life application. In conclusion, our method has good performance considering the accuracy and the generalization ability.

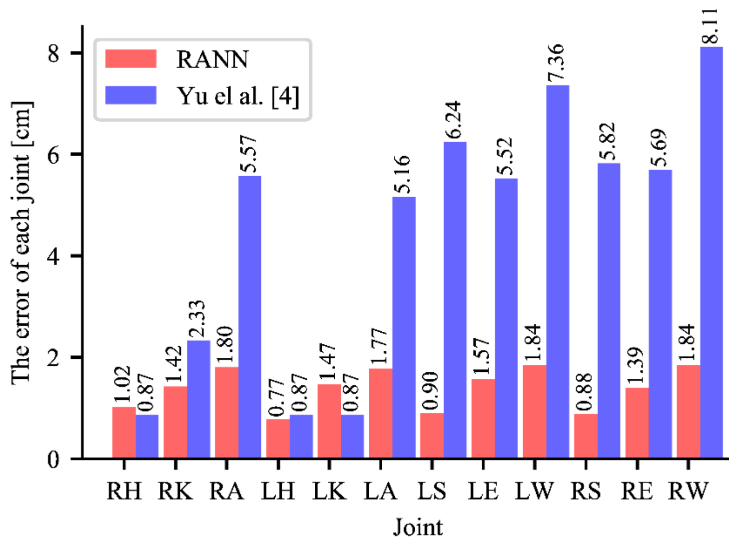

Figure 6-6 Comparison of the joint error with a previous study. R: Right; L: Left; H: Hip; K: Knee; A: Ankle; S: Shoulder; E: Elbow.

6.3 Testing the accuracy of the external forces and joint torques

Pressure data was used to evaluate the worker's self-weight and other forces. In the material handling experiment, the subjects were required to lift various numbers (0~4) of bricks and hold them for 10 seconds. Each brick weighs 2 kg, i.e., 19.6 N (g= 9.8 m/s^2)). Figure 6-7 shows the postures involved in holding the bricks.

Figure 6-7 Subject holding 0–4 bricks

At the same time, the total weight, i.e. the ground reaction force, was measured by the smart insoles. Each sensor recorded the corresponding area's average pressure data. Figure 6-8 presents an example of the pressure data recorded by the No. 8 sensor in the right insole when the subject was carrying 3 bricks. The pressure data was estimated as 2.5 N/cm^2. Table 6-1 provides the pressure values of all the 13 pressure sensors in the right insole.

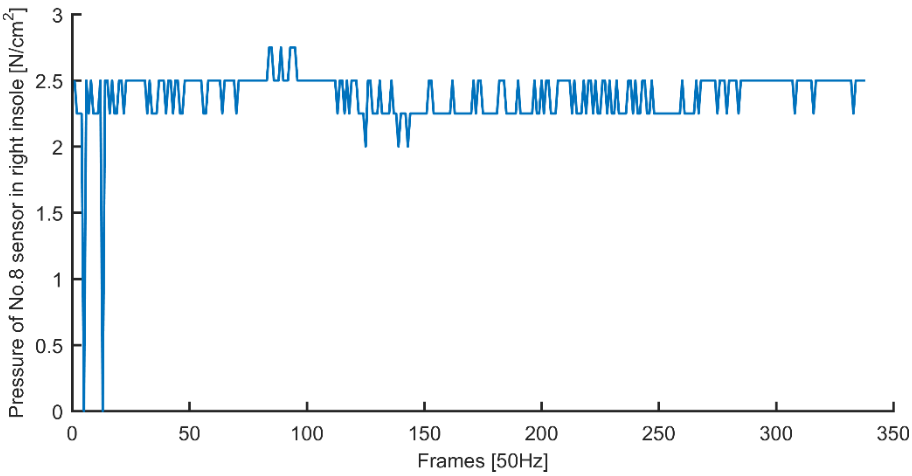

Figure 6-8 Pressure data of the No. 8 sensor in the right insole when the subject is carrying 3 bricks

Table 6-1 Values of all the right insole's 13 pressure sensors

Sensor Number	**Pressure [N/cm^2]**	**Sensor Number**	**Pressure [N/cm^2]**
0	1.25	7	5.25
1	1.50	8	2.50
2	1.00	9	5.75
3	0.50	10	5.5
4	1.00	11	4.24
5	3.00	12	5.25
6	0.25		

Figure 6-9 shows the ground reaction forces of both feet and the total ground reaction forces when the subject was holding 0~4 bricks. The brick weight was calculated as the difference between the ground reaction forces of consecutive liftings, as shown in Figure 6-10. The real weight of each brick is 19.6 N. The relative error is 5.99%, given by

$$\delta = \frac{1}{N}\sum_{i=1}^{N}\frac{|w_i - w|}{w} \times 100\%. \tag{6-2}$$

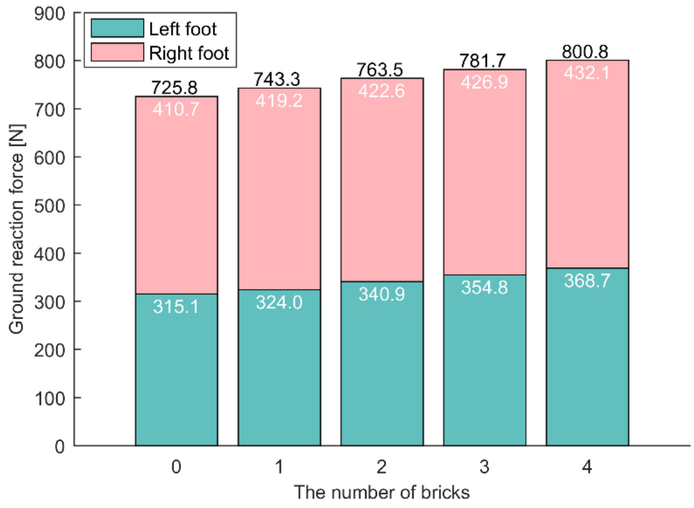

Figure 6-9 The ground reaction forces of both feet and total ground reaction forces when the subject is holding 0~4 bricks

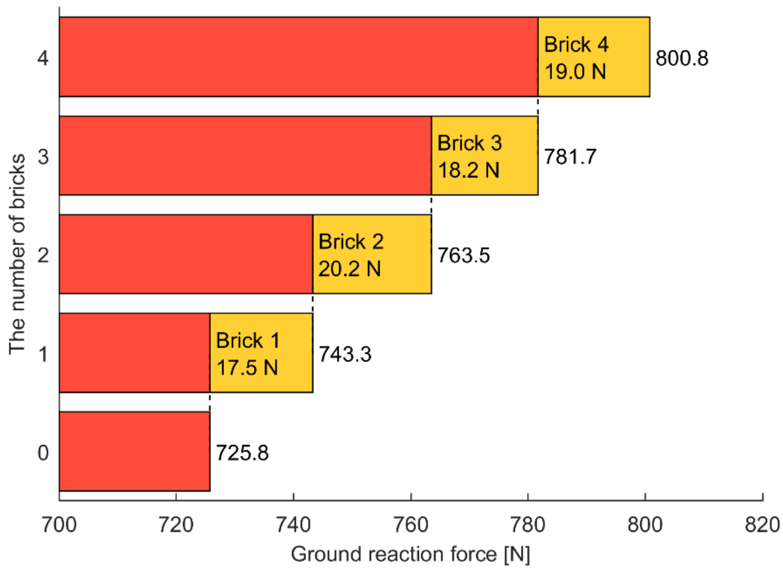

Figure 6-10 The ground reaction forces of both feet and total ground reaction forces when the subject is holding 0~4 bricks

Based on this analysis, the subject's self-weight was measured as 725.8N, and the weights of the four bricks were 17.5N, 20.2N, 18.2N, and 19.0N.

The error of joint torque was analyzed according to joint location and external force errors. As the forearm is the nearest joint with the external force in the experiment, and the self-weight of forearm is smaller than other body segments, the elbow torque was selected to calculate the maximum error of joint torque. Considering the forearm model when the elbow flexion angle is 90 degree, the elbow torque error can be calculated as

$$
\begin{aligned}
T &= \gamma l W_{\text{forearm}} + l W_{\text{brick}} = l\left(\gamma W_{\text{forearm}} + W_{\text{brick}}\right), \\
T + \Delta \mathrm{T} &= (l + \Delta \mathrm{l})(\gamma W_{\text{forearm}} + W_{\text{brick}} + \Delta W_{\text{brick}}), \\
\frac{\Delta \mathrm{T}}{T} &= \frac{\Delta \mathrm{l}}{l} + \frac{\Delta W_{\text{brick}} / W_{\text{brick}}}{\gamma W_{\text{forearm}} / W_{\text{brick}} + 1} + \frac{\Delta \mathrm{l}}{l} \times \frac{\Delta W_{\text{brick}} / W_{\text{brick}}}{\gamma W_{\text{forearm}} / W_{\text{brick}} + 1} \\
&\cong \frac{\Delta \mathrm{l}}{l} + \frac{\Delta W_{\text{brick}} / W_{\text{brick}}}{\gamma W_{\text{forearm}} / W_{\text{brick}} + 1},
\end{aligned}
\tag{6-3}
$$

where γ is the ratio of the force arm of $W_{forearm}$ and the force arm of W_{brick}; l is the force arm of W_{brick}; Δl , ΔW_{brick} and ΔT represent the errors of l , W_{brick} and T respectively .

According to the joint coordinate and external force errors, $\Delta W_{brick}/W_{brick}=$ 5.99% and Δl =3 cm. Assume l= 30 cm and $\gamma W_{forearm}$= 0.4 kg, then the elbow torque error was approximately 15%.

6.4 Testing the accuracy of physical fatigue assessment

This experiment aimed to validate the accuracy of the PFA method by comparing the average joint capacity with the participant's heart rate, which is a classical and widely-used assessment indicator for work load [23].

6.4.1 Experiment design

Participants: We recruited four health male participants, aged between 20 and 30 years to perform a simulated material handing task in a laboratory. They were allowed to terminate the task had they experienced intolerable fatigue, chest pain, shortness of breath, or muscle cramp. The demographic parameters (age, gender, height, and weight) of the participants were documented before the experiment.

Equipment: The participants wore a heart rate monitor at the chest (Equivital^{TM} LifeMonitor, UK) to monitor the heart rate. The task would be terminated had a participant's heart rate exceeded the corresponding maximum heart rate (90%* [(220 – age) - resting heart rate] + resting heart rate) for more than 2 minutes. The heart rate data was recorded every five seconds automatically by the heart rate monitor. At the same time, an RGB camera (1,920×1,080 pixels per frame, 50 frames per second) captured the participant's postures during the task.

Simulated material handling task: To ensure the accuracy of the heart rate monitoring, the experiment was conducted in a controlled laboratory environment (25°C). After putting on the heart rate monitor, participants were required to perform a simulated material handling task with both arms. Notably, the participant was instructed to lift a box (6 kg, 37 cm * 33 cm * 26 cm) from a 3 m x 4 m working platform (1 m height) and carried the box with bilateral elbows at 90° flexion to randomly walk around the platform with for about 5 minutes. The participant was given a five-second break every minute.

Data process: The normalized heart rate was standardized to the respective the heart rate at baseline (set as 100). The video data and the demographic data were used to calculate the current joint capacity and the maximum joint capacity of eight key joints (both shoulders, elbows, hips and knees). First, the eight joint capacity results were converted from 50 fps to 0.2 fps by averaging the results over every 250 frames. From the current joint capacity and the maximum joint capacity, the instantaneous joint physical fatigue indices were calculated according to section 5.5. Finally, the instantaneous whole-body physical fatigue index was calculated as the average of the eight instantaneous joint physical fatigue indices. Pearson correlation test was conducted to quantify the correlation between the average instantaneous whole-body physical fatigue index and normalized heart rate.

6.4.2 Experiment results

Four participants (mean age of 28.3 years, mean height of 1.73m, and mean weight of 60.33kg) were recruited (Table 6-2) participated in the study.

Table 6-2 The demographic parameters of the four male participants and the corresponding video records

Participant	Height [m]	Weight [kg]	Age [years]	Task duration [second]	Total number of frames
#1	1.78	69.3	30	326	16,300
#2	1.70	61	24	260	13,000
#3	1.73	60	29	298	14,900
#4	1.69	51	30	309	15,450

Figure 6-11shows the comparison between the opposite of capacity index and the heart rate index. The opposite of capacity index (solid blue line) is the opposite of the average of the physical fatigue assessment results of the eight key joints. The heat rate index (red dotted line) is normalized by setting the first heart rate value as 100 and calculating the other heart rate values according to their ratio to the first value. The opposite of capacity index increased in work state and decreased in rest state. Similarly, the heart rate index increased during work and decreased at rest. Figure 6-11 shows that the two lines have similar trends. Pearson correlation coefficients showed significant positive correlations between the opposite of capacity index and the heart rate index ($p < 0.01$, Table 6-3).

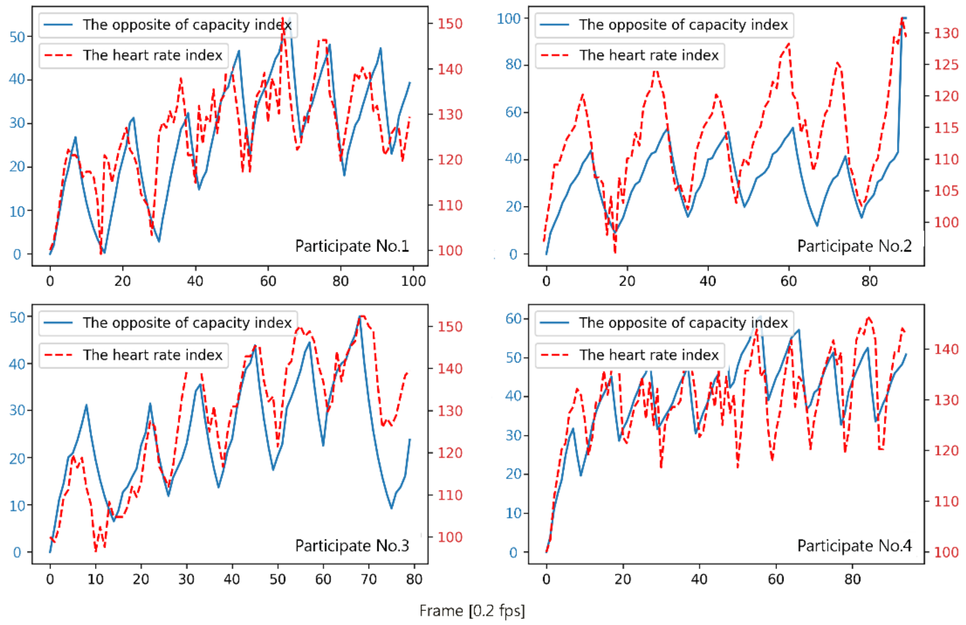

Figure 6-11 The comparisons of the opposite of capacity index and the heart rate index of the four participants

Table 6-3 The results of Pearson correlations between average instantaneous physical fatigue indices and normalized heart rates of different individuals

Participant	Correlation coefficient	*p*-value
#1	0.74	2.33×10^{-8}
#2	0.74	6.28×10^{-7}
#3	0.78	1.63×10^{-7}
#4	0.68	2.37×10^{-4}

6.5 Testing the usefulness of physical fatigue assessment

This experiment aimed to validate the usefulness of the PFA method through a scaffolding task and a masonry task. One participant was recruited to perform the scaffolding task and another participant was recruited to perform the masonry task.

6.5.1 Experiment design

For the scaffolding task, the participant was instructed to construct a cube with two-meter-long steel tubes and couplers, as shown in Figure 6-12. The construction site layout is shown in Figure 6-13. The working area was the location where the cube was built. The storage area was the place where the steel tubes and couplers were stored. The straight-line distance from the storage area to the work area was about 6 m. During the experiment, the participant first carried a tube weighted approximately 12 kg from the storage area to the working area, then assembled the tubes with couplers. This process was repeated for 16 times to finish the task. The 16 times were chosen because our pilot study showed that this number of repetitions caused fatigue in the participant. Two RGB cameras (smartphone cameras) were fixed on tripods to record the participants' motion. The height of the tripods was 1.2 m. The tripods were 3 meters away from the working area.

Figure 6-12 The process of the scaffolding task and the finished cube

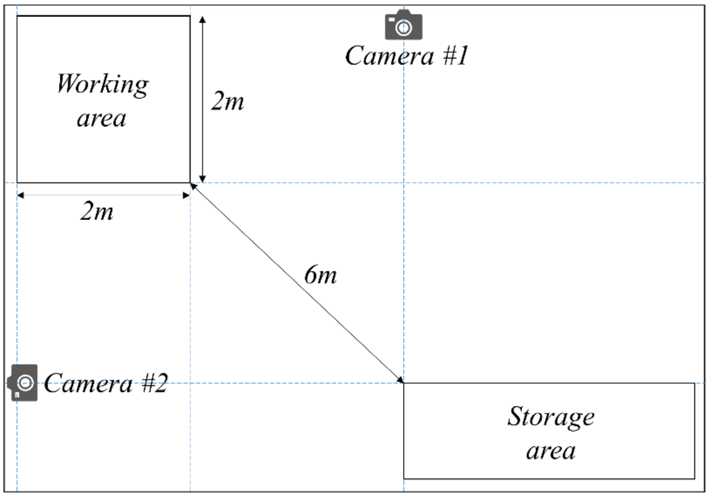

Figure 6-13 The site layout of the scaffolding task

For the masonry task, the participant was asked to build a concrete block wall as shown in Figure 6-14. Each concrete block weighted approximately 16 kg. Concrete blocks were placed 1 m away from the target concrete block wall location. The thickness of the wall was 190 mm. The height was 1,520 mm. The wall comprised eight layers. The width of each layer was either 780 mm or 970 mm (Figure 6-14). To build the wall, the participant first bent knees to pick up a block, then turned around to lay the block. The motion was repeated until a layer of the brick wall had been properly placed. Then the participant checked the layer with a level and evened it out with a thicker layer of mortar. The procedure was repeated until the target wall was built. Two RGB cameras (smartphone cameras) were fixed on tripods to record the participants' motion. The height of the tripods was 1.2 m. One of the tripods was 3 meters away from the working area, while the other one was 1 meter away from the working area (Figure 6-15).

Figure 6-14 The process of the masonry task and the finished concrete block wall

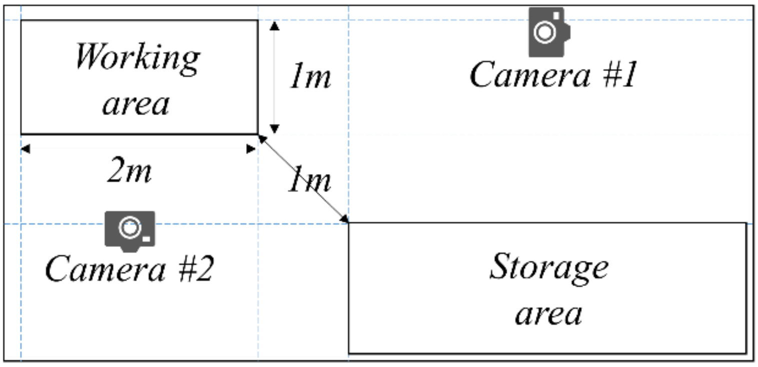

Figure 6-15 The site layout of the masonry task

6.5.2 Experiment data

The demographic data (Table 6-4) and the video records of the two tasks (Table 6-5) were entered to the fatigue model.

Table 6-4 The demographic parameters of the participants

Participant	Height [m]	Weight [kg]	Age	Gender
The scaffolder	1.70	75	27	Male
The masonry	1.75	71	40	Male

Table 6-5 The information of the video records of the two experiment tasks

Task	Duration [second]	Frame size	Data rate	Frame rate [fps]	No. of frames
Scaffolding	1,433	640×480	45,00kbps	30	42,990
Masonry	1134			10	11,330

Data processing. The anthropological parameters of the participants were used to estimate the respective body segment mass, the location of the center of mass of each body segment, and maximum joint capacity as explained in section 5.5. To eliminate the effects of visual obstruction, two cameras recorded the participants' motions simultaneously. The videos from two cameras were compared frame by frame and the one with fewer obstructions was selected to eliminate the effects of obstructions by the scaffold or the concrete brick wall.

6.5.3 Experiment results

Figure 6-16 to Figure 6-19 show the instantaneous and cumulative joint physical fatigue indices of eight joints during the scaffolding task and the masonry task. The instantaneous joint physical fatigue index reflects the specific fatigue level of each frame, while the cumulative joint physical fatigue index reflects the accumulated fatigue level from the start to a certain frame.

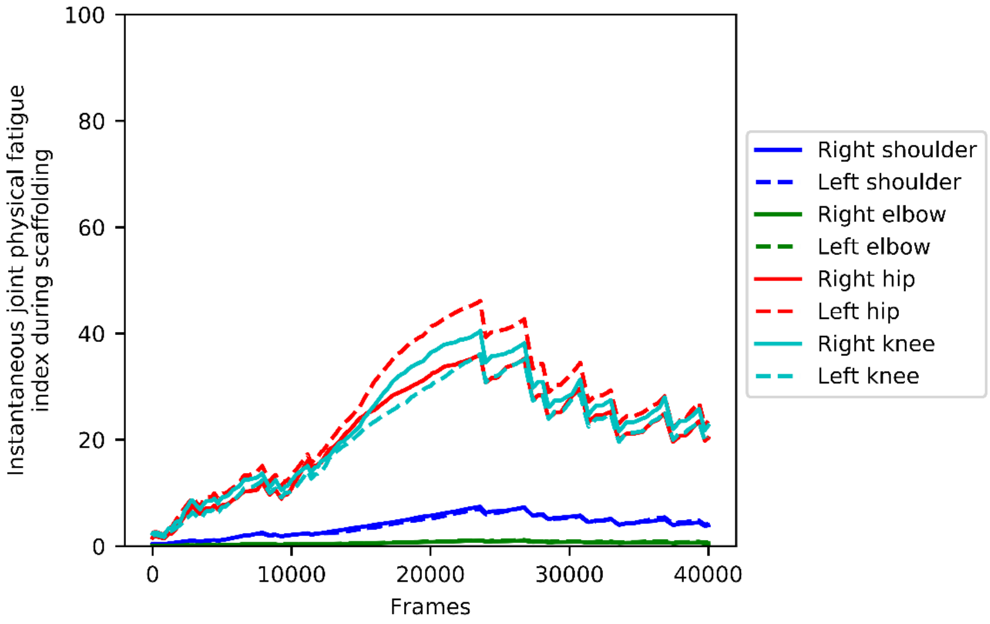

Figure 6-16 The instantaneous joint physical fatigue index of the key joints during scaffolding

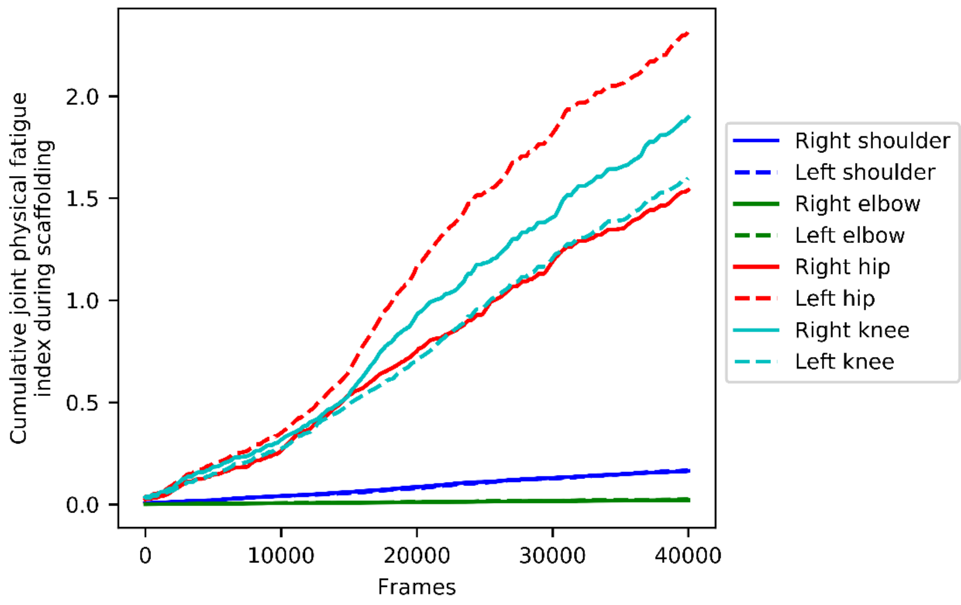

Figure 6-17 The cumulative joint physical fatigue index of the key joints during scaffolding

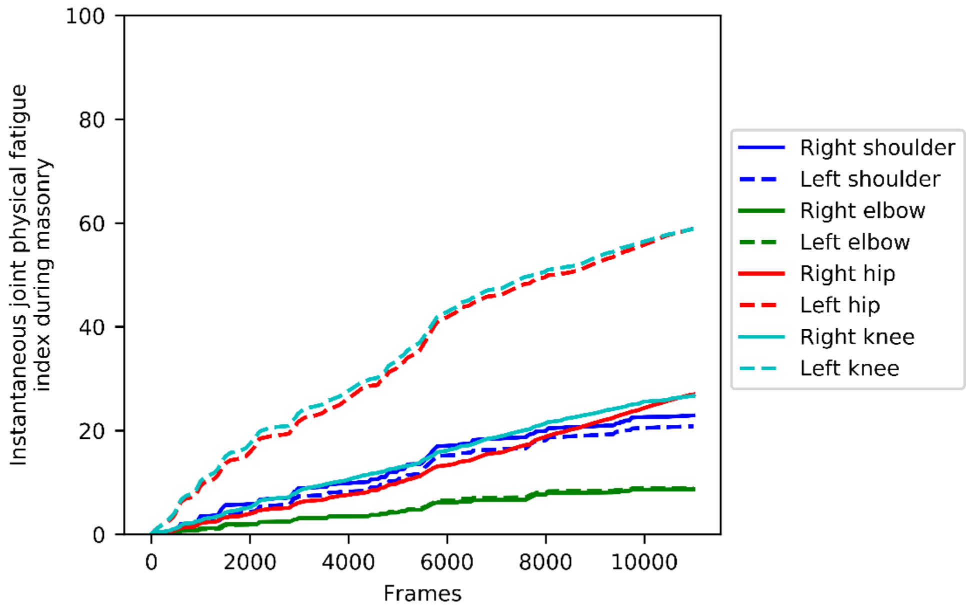

Figure 6-18 The instantaneous joint physical fatigue index of the key joints during masonry

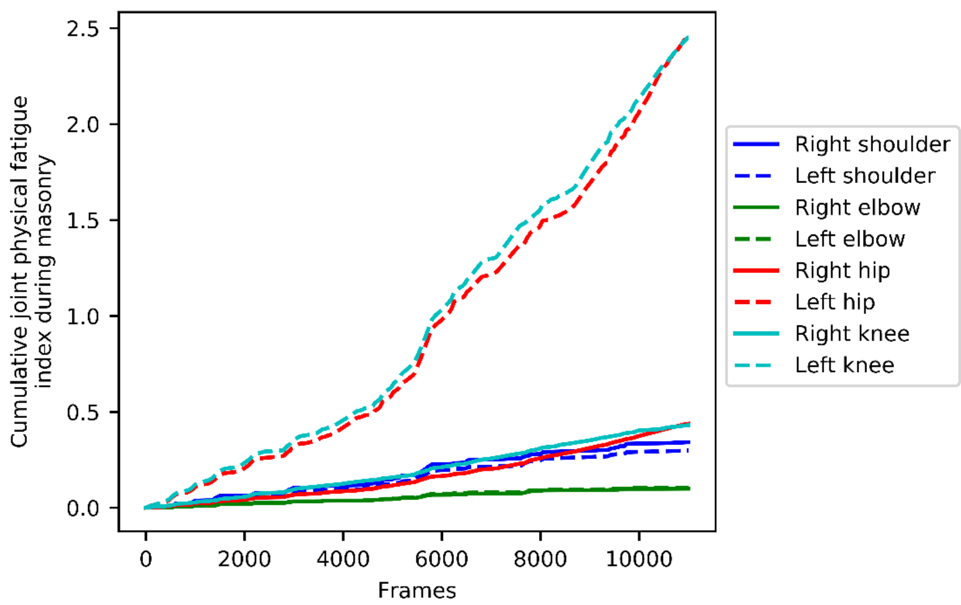

Figure 6-19 The cumulative joint physical fatigue index of the key joints during the masonry task

In Figure 6-16 and Figure 6-18, there was a general increase in the instantanuous joint phyiscal fatigue indices over time during both tasks. It is noteworthy that there were significant fluctuations in the instantaneous joint physical fatigue curves of hips and knees during the scaffolding task (Figure 6-16). The fluctuations might be attributed to the fact that the participant needed to return to the storage area without carrying any weights after fixing a steel tube. The participant's body segments were in a relaxed state without staying in an awkward posture or carrying an external force. Thereby, the instantaneous joint physical fatigue indices of the eight joints recovered during that period.

Figure 6-17 and Figure 6-19 show the cumulative fatigue levels of the eight key joints (bilateral shoulders/elbows/hips/knees) during the two tasks. All cumulative joint physical fatigue level curves during the two tasks show a continuous increasing trend. When the instantaneous joint physical fatigue indices increased, the cumulative joint physical fatigue indices increased sharply. Conversely, when the instantaneous joint physical fatigue indices decreased, the joint cumulative physical fatigue indices increased slowly or even decreased.

As is shown in the above four figures, the proposed PFA method could estimate joint-level physical fatigue development over time. Figure 6-17 and Figure 6-19 demonstrate that the participant's lower limbs (including both hips and knees joints) had higher cumulative fatigue levels than upper body joints. Specifically, the left hip and the left suffered from the highest workloads. In the masonry case (Figure 6-18 and Figure 6-19), the participant's left knee and left hip had the highest and the second highest fatigue levels. The final cumulative joint physical fatigue index of the left leg was about five times higher than the right leg. This indicated that the participant might involve more asymmetrical weightbearing during masonry task.

6.6 Summary

In this chapter, three laboratory experiments were conducted to test the accuracy of the data collection methods and PFA assessment method. The posture data collection method successfully generated 3D posture data given construction site images. The average distance error of each joint is as small as 1.26 cm, which outperforms pervious computer vision algorithms. In the brick holding experiments, the accuracy of the insole-based external force measurement is 5.99 %. The third laboratory experiment compared the PFA indicator to heart rate indicator and found that they had extremely similar fluctuation patterns. Finally, the usefulness of the proposed PFA method was validated through field experiments.

Chapter 7 Applications in construction site management[7]

7.1 Introduction

This chapter presents the applications of the proposed method in fatigue prevention in construction site management. Given construction site images, the proposed method could provide 3D posture data, external force data, joint torque data, and joint fatigue level data.

This chapter presents several application scenarios based on above data. Section 7.2 provides an automatic ergonomic scoring tool based on the 3D posture data collected with the computer vision algorithm; section 7.3 shows the application of

---

[7] This chapter is based on the following published study and being reproduced with the permission of Elsevier and American Society of Civil Engineers.

Yu, Y., Yang, X., Li, H., Luo, X., Guo, H., & Fang, Q. (2019). Joint-Level Vision-Based Ergonomic Assessment Tool for Construction Workers. Journal of Construction Engineering and Management, 145(5), 04019025. https://doi.org/10.1061/(ASCE)CO.1943-7862.0001647

Yu, Y., Li, H., Umer, W., Dong, C., Yang, X., Skitmore, M., & Wong, A. Y. L. (2019). Automatic Biomechanical Workload Estimation for Construction Workers by Computer Vision and Smart Insoles. Journal of Computing in Civil Engineering, 33(3), 04019010. https://doi.org/10.1061/(ASCE)CP.1943-5487.0000827

Yu, Y., Li, H., Yang, X., Kong, L., Luo, X., & Wong, A. Y. L. (2019). An automatic and non-invasive physical fatigue assessment method for construction workers. Automation in Construction, 103, 1–12. https://doi.org/10.1016/j.autcon.2019.02.020

the PFA method in ergonomic posture section; section 7.4 and 7.5 present how the PFA method could assist construction site layout and work-rest schedule.

7.2 Posture data based ergonomic assessment for construction workers

Given a construction site images, the posture estimation algorithm proposed in this study could accurately identity and localize the 3D joints of the construction workers captured in the image. The 3D joint locations satisfy the data demanding of a series of ergonomic assessment scales. As a result, the proposed method could be used to automize the manual observation based ergonomic assessments.

Figure 7-1 is the framework of the automatic ergonomic assessment method based on the 3D posture estimation algorithm proposed in this study. The method consists of a 3D posture estimator and a REBA score calculator. First, workers' joint 3D coordinates are estimated from 2D images. Then, joint angles are calculated based on the 3D coordinators. Finally, the Rapid Entire Body Assessment (REBA) scale, a classical whole-body fatigue level ergonomic posture assessment scale[39], provides the ergonomic status of a posture based on the joint angles.

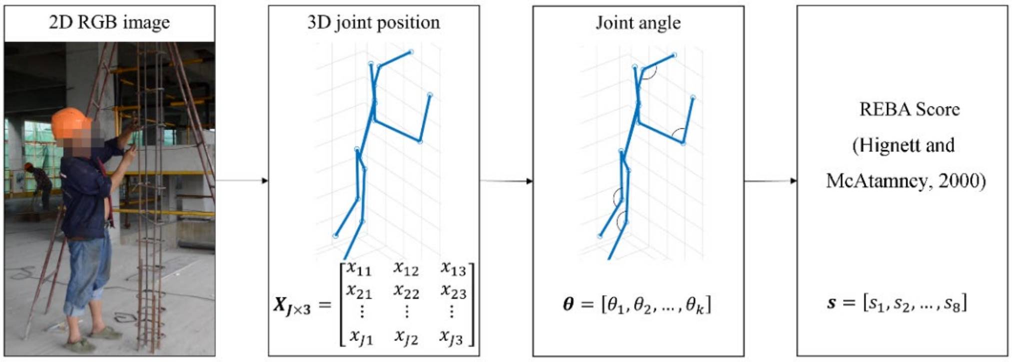

Figure 7-1 The framework of the ergonomic assessment methodology

Figure 7-2 illustrates the calculation process of REBA score. First, a joint-level score is given based on joint parameters. Take the trunk score for instance. A base trunk score is given based on trunk flexion angles; then the score will be added by 1 if trunk twist or side is found. Secondly, a body-part level is calculated according to the joint-level score. REBA divides human body into two parts. Part A includes trunk, neck and legs, and part B includes upper arms and lower arms. The scores of part A and part B are separately regulated by table A and table B in REBA. Finally, the whole-body level score, which also provides the urgency of ergonomic improvements, is calculated according to the scores of part A and part B based on table C in REBA. For more detailed explanation, please refer to [39].

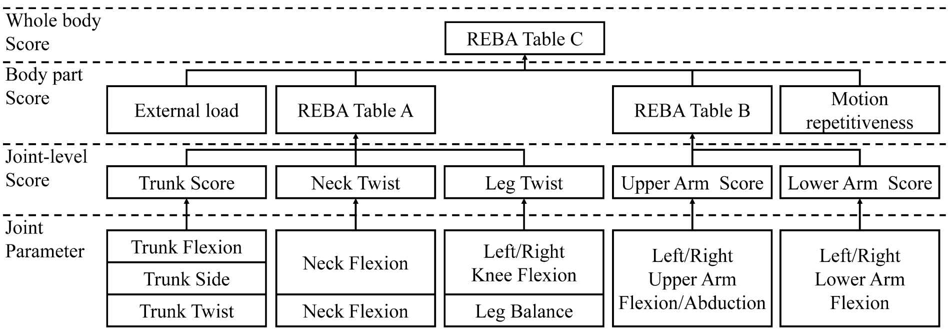

Figure 7-2 The structure of REBA

Trunk parameters. Trunk parameters include trunk flexion angle, side angle and twist angle. The calculation of trunk flexion and side is shown in Figure 7-3a. The numbers represent the corresponding joints in Figure 5-3. Plane $\boldsymbol{a}$ represents the upper body, which is defined by neck and two hips. Plane $\boldsymbol{b}$ is the lower body plane, which is defined by waist and two knees. α is the angle of plane $\boldsymbol{a}$ and plane $\boldsymbol{b}$. $\beta = 90 - \alpha$ is the trunk flexion angle. γ is the trunk side angle. To calculate γ, the line 3'-13 must be determined first, which represents the spine position without side. If we denote the norm vector of plane $\boldsymbol{a}$ as $\boldsymbol{n}$, vector 12-16 as $\boldsymbol{v}$, then vector 13-3' = $\boldsymbol{n} \times \boldsymbol{v}$. $\boldsymbol{\gamma}$ is the angle between line 13-3 and line 13-3', that is the angle between the real position of spine and that of the spine with no trunk side angle. Trunk twist is defined as the angles between shoulders vector 5-8 and hip vector 12-16, as shown in Figure 7-3b.

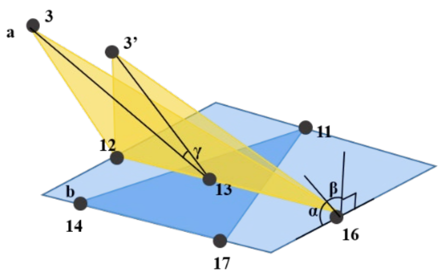

(a) Trunk flexion and side

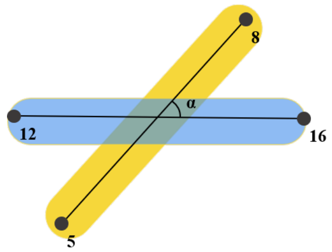

(b) Trunk side

Figure 7-3 The calculation of trunk flexion and trunk side angle

Neck parameters. Neck parameters include neck flexion and side. The calculation is similar with trunk flexion and side. The two planes are replaced with upper shoulder plane defined by point 1, 2, 4 and lower shoulder plane defined by point 2,4,11.

Upper arm parameters. Upper arm parameters include the flexion and abduction angles of both upper arms. Figure 7-4a illustrates how to calculate these angles. Plane $\boldsymbol{a}$ is the plane of frontal plane, which is the same as plane $\boldsymbol{a}$ in Figure 7-3a. Plane $\boldsymbol{c}$ is sagittal plane, which is perpendicular to plane $\boldsymbol{a}$. Line $\boldsymbol{l}$ is the intersecting line of plane $\boldsymbol{a}$ and plane $\boldsymbol{c}$. Line 8-9 represents the left upper arm. Line 8-9' is the projection on plane $\boldsymbol{a}$, and line 8-9'' is the projection on plane $\boldsymbol{c}$. Then the upper arm flexion is defined by angle η, i.e. the angle between line $\boldsymbol{l}$ and line 8-9''; the upper arm abduction is defined by angle ϕ, i.e. the angle between line $\boldsymbol{l}$ and line 8-9'.

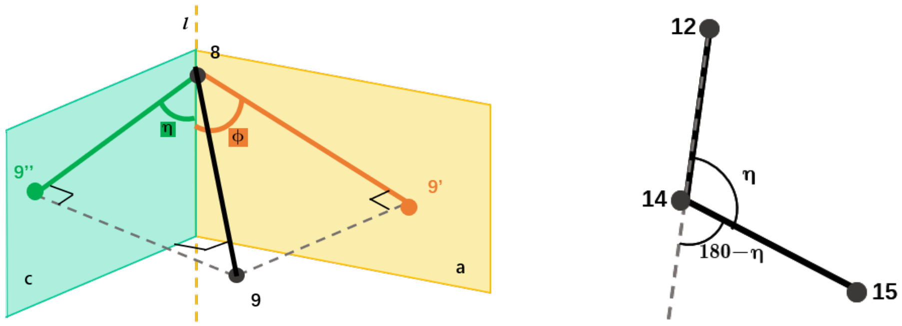

(a) Upper arm flexion and abduction (b) Knee flexion

Figure 7-4 The calculation of upper arm flexion, abduction and knee flexion

Lower arm parameters. Lower arm parameters include the flexion angles of both elbows. The calculation is similar with leg flexion angles.

Leg parameters. Leg parameters include the flexion angles of both knees and the balance of legs. As shown in Figure 7-4b, the flexion angles equal to the supplement of the angle between vector (12-14) and vector (14-15). The balance of legs is defined by the difference between two knee flexion angles.

Given above parameters, REBA scores were calculated based on the posture data from the experiment in section 6.4.

Figure 7-5 shows the whole-body ergonomic risk score of each frame, which demonstrates that the proposed methodology could provide a quantitative ergonomic risk score for each frame of videos on real construction site. Most of the scores were between 10 and 13, which is consistent with the observation results of the REBA scores of construction workers [141]. It could be observed from Figure 7-5 that the pipe layer, bar fixer, form worker and bricklayer seemed to have higher ergonomic risk than concreter and scaffolder during the on-site experiment, which means, during this experiment, the former four trades of workers were faced with higher ergonomic risk than concreters and scaffolders.

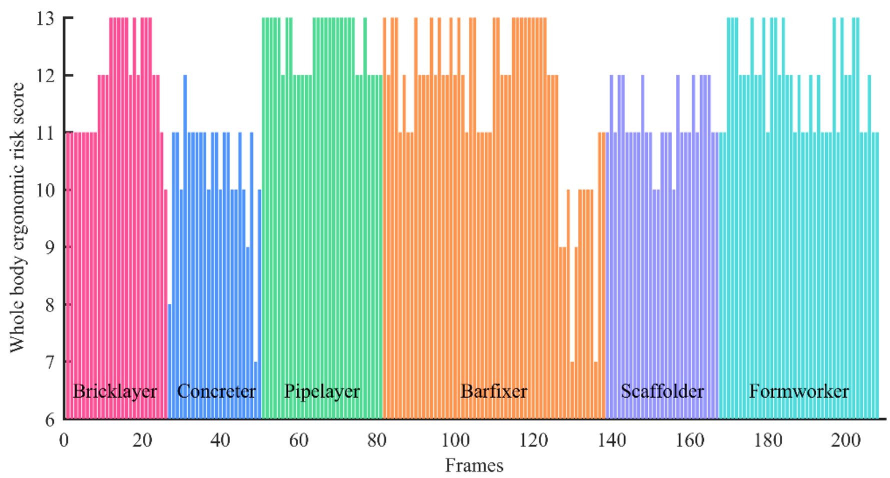

Figure 7-5 The whole body ergonomic risk score

Figure 7-6 shows more detailed results, which consist of 30 frequency histograms (5 body segment REBA score items × 6 construction trades). The pipe layer had the highest trunk and leg ergonomic risk score because the pipe layer was continuously squatting or bending during the experiment. The comparison of each column in Figure 7-6 suggested the ergonomic risk of each body segment. In the first and last column, the trunk score, upper arm score, and lower arm score tend to be higher than other scores, which suggested that the bricklayer and form erector should pay attention to their arms and trunks. Similarly, for the concreter and scaffolder, both neck and lower arms deserved more attention.

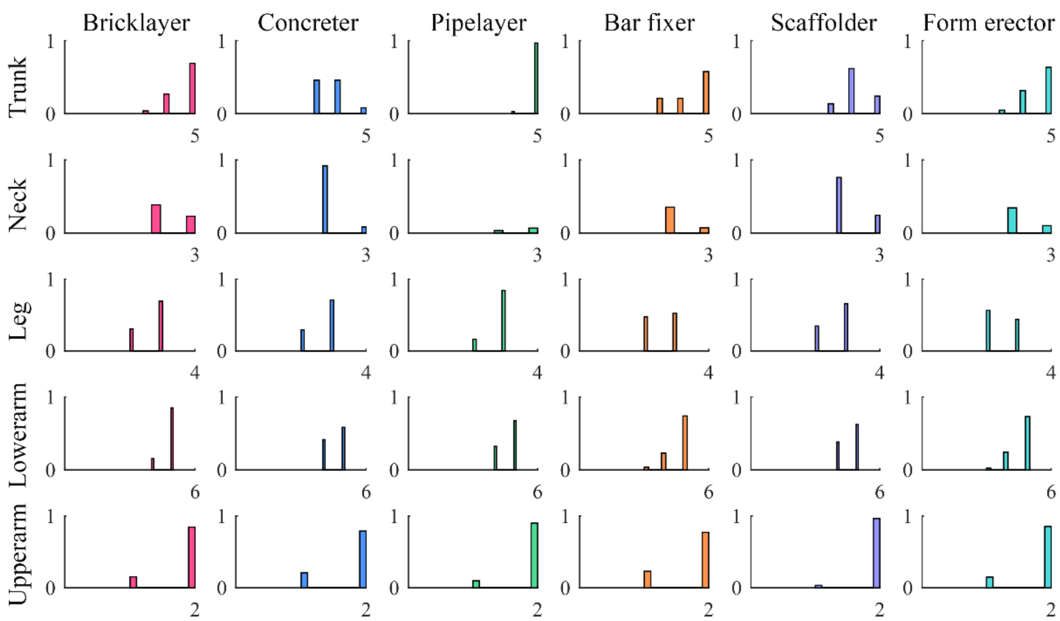

Figure 7-6 Eight score items of six construction trades

Above experiment results demonstrate that it can provide accurate and timely ergonomic assessment based on 2D videos by using a state-of-art 3D posture estimation algorithm to capture 3D joint positions from 2D images as well as adopting the REBA rule to get multi-level ergonomic risk scores. The site experiment demonstrates that the method is workable on construction sites as well.

7.3 Ergonomic posture suggestions based on individualized joint fatigue assessment

In addition to 3D posture data, the methodology also provides joint-level fatigue assessments. Through analyzing the joint fatigue level, the method could provide suggestions on working postures. Figure 7-7 provides detailed and intuitive information concerning material handling. In the experiment, two subjects were required to lift four bricks by bending lifting and squatting lifting. In the third column “Workload”, different joint varies in colors. The red joint represents high joint physical fatigue level, while the blue joint represents low physical fatigue level. It can be observed that the workloads of the squatting lifting were smaller, confirming the well-known fact that squatting lifting is a better posture for material handling.

7.4 The influence of construction site layout on physical fatigue level

Different construction site layout may result in different working postures and working durations, which may affect fatigue and productivity. Taking the scaffolding task as an example. If the distance between the working area and the storage area increases, workers need to carry the tubes for a longer period. However, workers also benefit from a longer resting period when they return to the storage area without carrying an external force. As such, the proposed PFA method can help provide objective comparisons between various construction site layouts to improve productivity and prevent physical fatigue. Given the above, the objective of this case study was to compare the effects of different distances between the work area and the storage area on physical fatigue level of an individual during a scaffolding task. In particular, the distances between the working area and the storage area was set at 3m, 6m and 12m (similar to the scaffolding task in section 6.5.

Figure 7-8 and Figure 7-9 illustrate the instantaneous and cumulative whole-body physical fatigue indices for completing the scaffolding task among three different site layout plans, which show that longer the distance between the work area and the storage area, lower the fatigue level. Figure 7-10 shows the final cumulative whole-body physical fatigue indices for completing the task under different conditions. Figure 7-11 demonstrates the durations for completing the task under the three conditions. Figure 7-10 and Figure 7-11 highlight that the longer the distances, the lower the final whole-body cumulative physical fatigue index, but the longer task completion time. In other words, there was a trade-off between alleviating the risk of physical fatigue and reducing productivity.

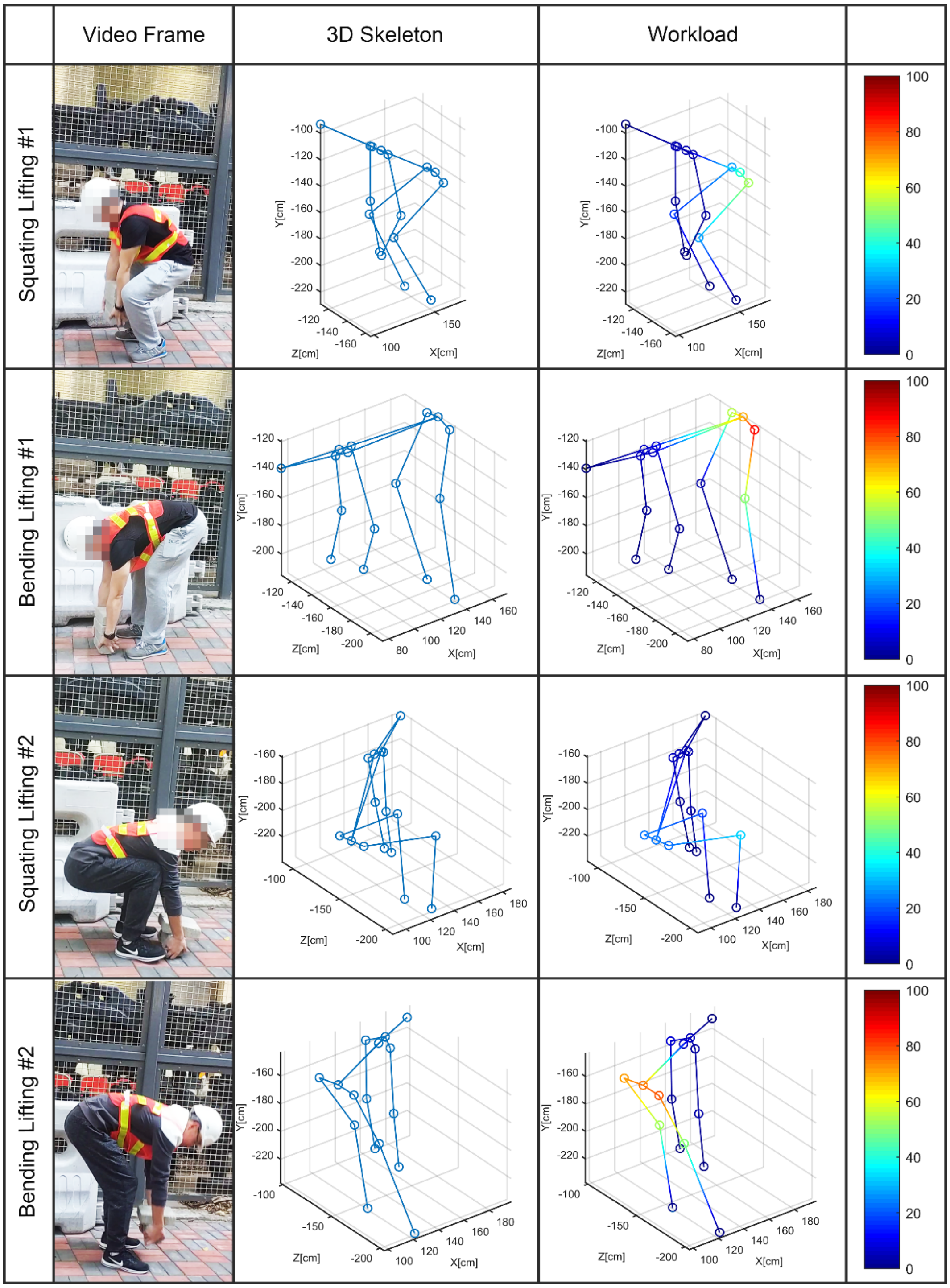

Figure 7-7 Joint physical fatigue of different lifting postures

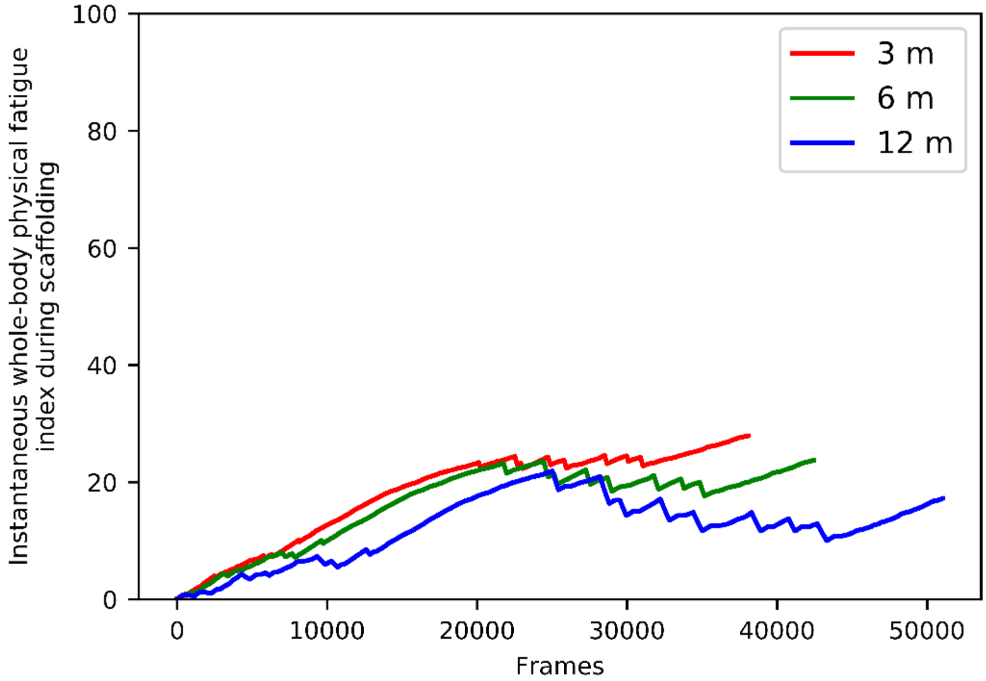

Figure 7-8 The comparison of the instantaneous whole-body physical fatigue indices during the scaffolding task with different distances between the working area and storage area (3m/6m/12m)

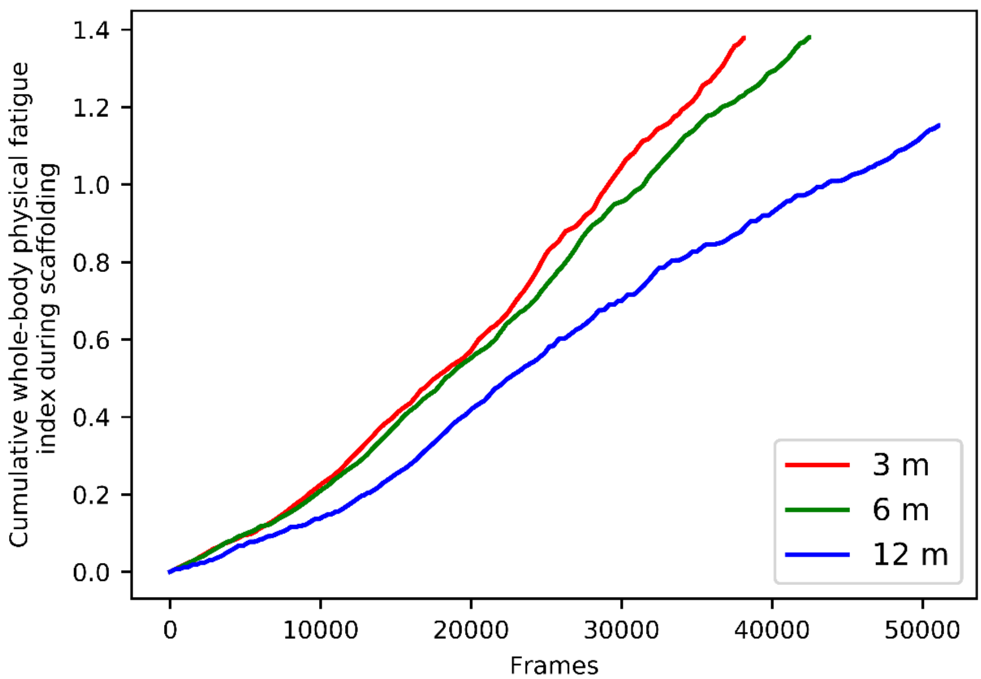

Figure 7-9 The comparison of the cumulative whole-body physical fatigue indices during the scaffolding task with different distances between the working area and storage area (3m/6m/12m)

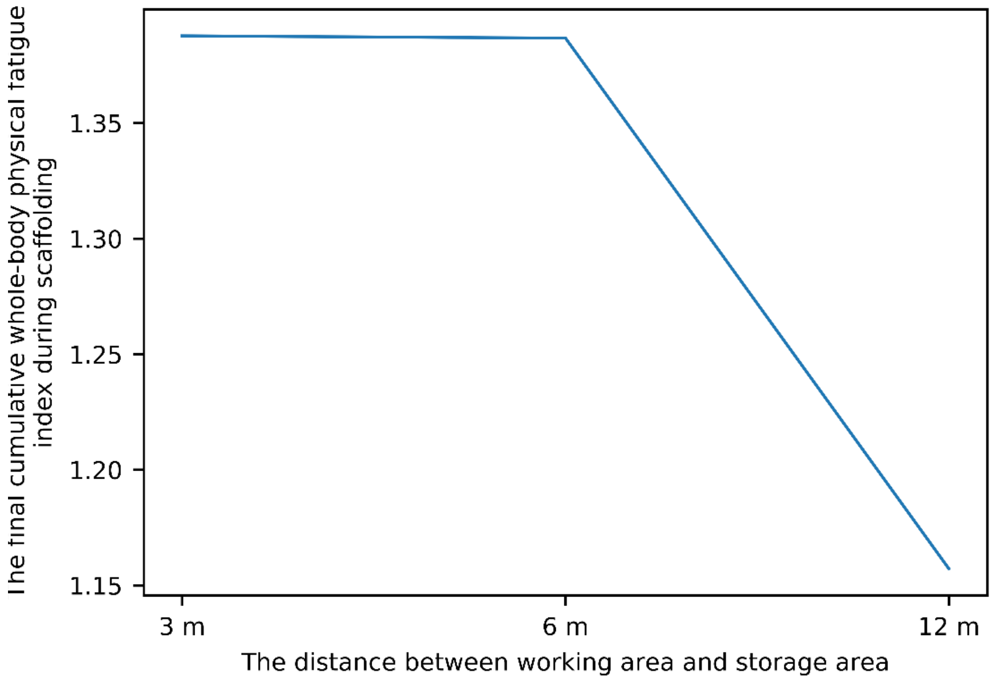

Figure 7-10 The comparison of the final cumulative whole-body physical fatigue indices after the scaffolding task with different distances between the working area and storage area (3m/6m/12m)

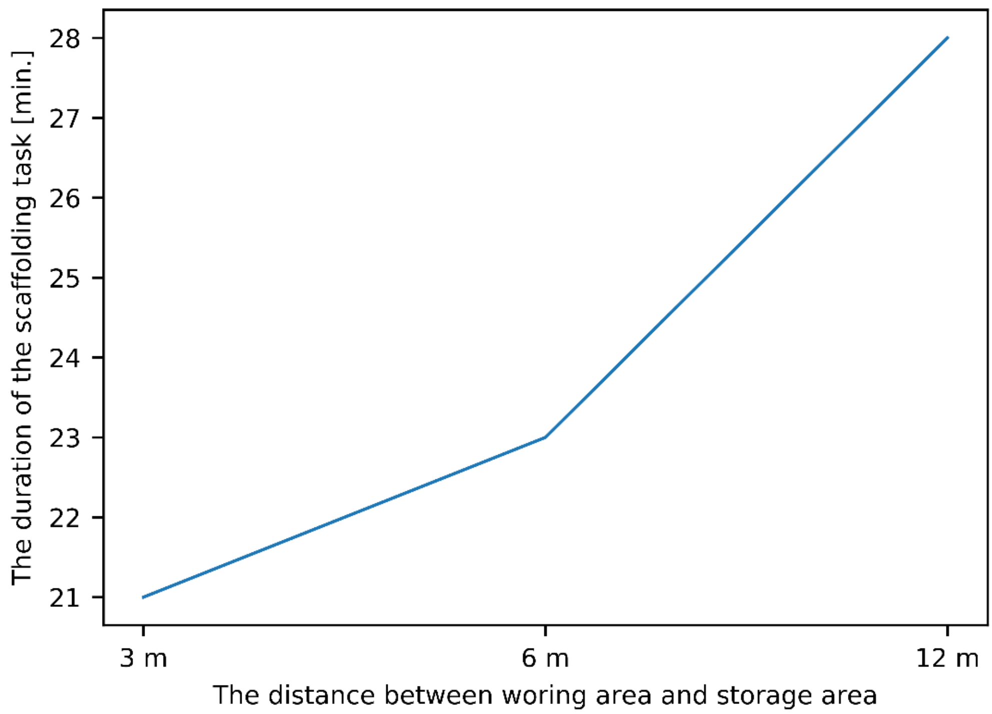

Figure 7-11 The comparison of the duration of the scaffolding task with different distances between working area and storage area

7.5 The influence of work-rest schedule on fatigue level

This experiment aimed to evaluate the influences of rest on fatigue mitigation by quantitative fatigue assessments. In the experiment in section 6.5, the worker performed the masonry task continuously without any breaks. In this case study, the worker had a rest after finishing each layer of the wall. The rest time was set at 5 and 10 seconds. The fatigue assessment results were shown in Figure 7-12. Compared with continuous working, taking short breaks slowed down the extent of instantaneous whole-body physical fatigue during the masonry task. Continuous working without a break led to approximately 75% decreases in worker's average maximum joint capacity at the end of the task. However, 5- and 10-second breaks could keep the worker's average joint capacity at 60% and 75% of the maximum capacity upon completion of the task.

7.6 Summary

This chapter shows the applications of the PFA method in construction site management. For individual workers, the method could help them to understand their ergonomic situations and injury risks in an accurate and intuitive manner. For construction site managers, the method could assist in data-based site layout and work-rest schedule to prevent physical fatigue and improve safety, health and productive performance.

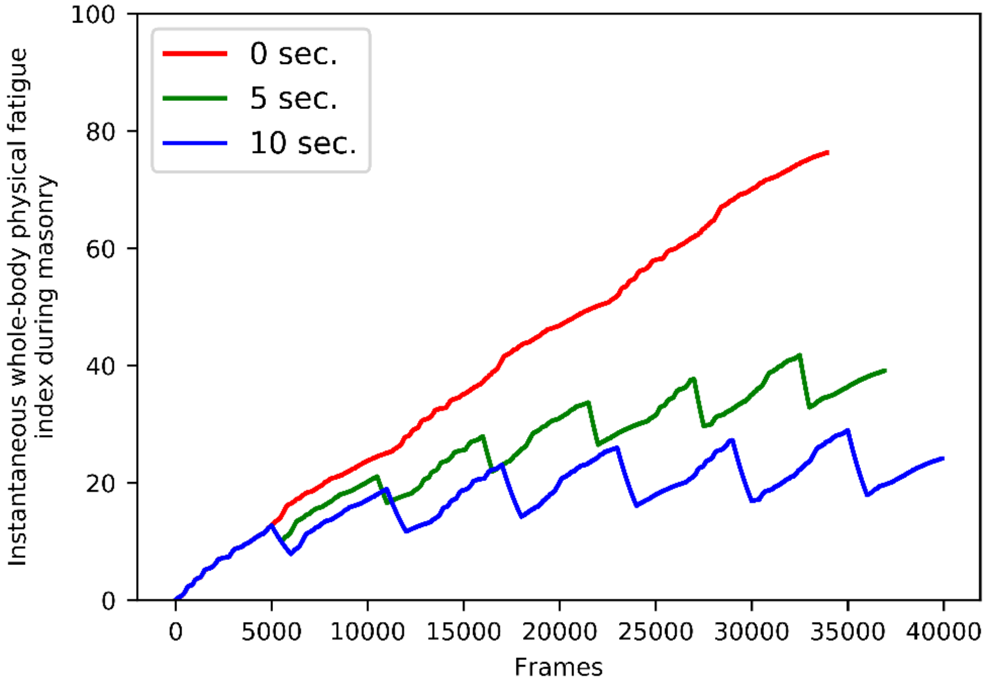

Figure 7-12 The comparison of the instantaneous whole-body physical fatigue indices during the masonry task with different rest time (0/5/10 seconds)

Chapter 8 Discussion and Conclusion

A non-invasive and automatic approach was proposed to assess construction workers' physical fatigue using computer vision, smart insoles and a biomechanics computation model. In laboratory experiments, the high correlation between the estimated physical fatigue index and heart rate data proved the accuracy of the approach. Field experiments explored the application of the approach in construction sites management. The results showed that the method could provide suggestions on working postures thorough analyzing joint fatigue level and assess construction workers' physical fatigue under different site-layout and work-rest schedule.

8.1 Contributions

This study provides a theoretical and practical contribution on construction site management aiming at fatigue prevention. First, this research provides an individualized and quantitative PFA indicator for construction workers. Compared with previous assessment indicators, the proposed one considers the individual variety in physical capability through involving the maximum joint capability in the fatigue assessment model. For practice, the indicator suits well to the complex and dynamic nature of construction activities because it has no limitations on working patterns (regular or repetitive working postures). For academic research, the indicators are quantitative, contributing to the further research on construction worker fatigue development and fatigue prevention.

Secondly, this research provides new types of workers research data, including the accurate and continuous 3D posture data and the plantar pressure data captured from construction sites, as well as joint angles and torque data generated from the posture and pressure data. Compared with conventional manual observation data and posture data collected from laboratories, the data collected in this research reflects the real situations of the workers status on construction sites, and thus could provide accurate and helpful suggestions on real construction site management. In addition to the application in construction worker health management as proposed in this research, the 3D posture data could also help to recognize the workers behavior, and in turn used in unsafe behavior identification and productivity management [142,143].

Thirdly, this study contributes to more accurate and robust 3D working posture estimation, which are non-invasive and economic. A deep learning algorithm, residual artificial neural network (RANN), was developed to accurately estimate laborers' 3D working postures from RGB images. The experiments demonstrated that RANN could estimate 3D working postures from worksite images accurately and timely. The mean position per joint error and the estimation time of each frame were 1.26 cm and 0.24 second, respectively. The comparison with previous deep-learning-based 3D posture estimation algorithms demonstrated the accuracy and generalization ability of the proposed network.

Finally, this study built a 3D working posture dataset for construction workers. Previous 3D posture dataset only includes only daily activities, such as talking on the phone, walking, siting and so on. The postures in construction activities, however, differ a lot from these activities. As a result, the accuracy of previous 3D posture estimation algorithms on construction activities could not be ensured. This research, for the first time, built a 3D posture dataset for construction workers, which could serve as the foundation for future computer vision algorithms for posture or activity identification for construction workers.

Compared to previous fatigue assessment methods for construction workers, the proposed approach has several advantages. First, the data collection is continuous and non-invasive. Second, the results are objective, and quantifiable. Third, the fatigue analysis has no limitations on working patterns (regular or repetitive working postures). Fourth, the method considers multiple factors including workers' capacity, postures and joint loading history. These advantages make this approach suitable for estimating physical fatigue of construction workers during complex and dynamic construction works.

8.2 Limitations

Despite numerous advantages, the current study had a few limitations. A limitation of the method is the assumption that motions are relatively slow and steady, and therefore we simply use statistics when calculating the joint torques; when the workers' motion is not steady, however, the acceleration will increase the joint torque. As a result, the proposed method might underestimate the physical fatigue level if there are accelerations of the joints motion.

Further, when estimating external forces, it was assumed that all worker pressure was on the feet. Although this assumption may be true for most construction works, it is not applicable for situations where workers are sitting or sharing their body weight on their knees, when the external forces cannot be simply estimated by subtracting a worker' self-weight from the total ground reaction force.

Thirdly, the training data set for 3D posture estimation from RGB images is not large enough. The data set used in this study only includes the postures of two participants during plastering, which may limit the generalization performance of the method. Besides, in the dataset, the 2D posture data was generated from projecting the 3D posture data in a horizontal view. However, on construction site, the cameras were usually installed at heights. The differences may decrease the accuracy of the 3D posture estimation method for images captured by top-down views.

Besides, there might exist privacy problems in collecting construction workers' pose data. Workers might feel offensive under the surveillance of sensors, cameras, or observers. In addition, age, gender, height and weight are required to estimate maximum joint capacity in the proposed method. However, getting and using the information can be difficult or even illegal in some countries. In that case, the proposed method will fail to provide individualized fatigue assessment results.

In addition, fatigue is a complex phenomenon, which includes physical fatigue, mental fatigue, and emotional fatigue. Considering that it is difficult to measure mental fatigue and emotional fatigue on construction sites, this study is only focused on physical fatigue. As a result, in the experiments, the study assumed that the participants experienced no emotional or mental fatigue, and all the participants are instructed to have a 5-min rest before the experiment to calm down. However, the author admit that construction workers might experience mental and emotional fatigue during work and leading to the increasement of physical fatigue, In conclusion, the proposed method might underestimates physical fatigue level.

Finally, personal fitness level can vary hugely among the individuals of the same age, gender, weight and height. So, estimating an individual’s maximum joint capacity based the above factors is not so accurate as the measurement in biomechanics through laboratory experiments. However, it is not practical to measure the maximum joint capacity for every construction worker, so the proposed method in this study is tradeoff between accuracy and feasibility.

8.3 Suggestions on future research directions

Considering above limitations on joint torque calculation, external force estimation and 3D posture estimation algorithms, future studies could work on the following topics.

For accurate joint torque calculation, further research could consider applying wearable sensors, such as smart watches to collect the acceleration data and using dynamics to analyze the joint torques. For accurate external force estimation methods, future research could consider first identifying the carried object with deep learning algorithms and using the information to help estimate the weight of the tool or material hold in the worker's hand.

The 3D posture estimation method could be improved from the aspects of dataset and algorithm design. In future, a more diversified training data set should be established, which includes the posture data of different construction tasks collected from participants of different heights, weights and BMIs. Besides, future studies should train a 3D motion estimation model with more on-site pictures, especially those with obstructions and/or top-down angles.

The algorithm could be improved from the following aspects. Firstly, current 3D posture estimation method is based on individual frames. Considering the continuity of the joint trajectories, the information of nearby frames may benefit the joint location estimation in the current frame. Future works could involve algorithms for time series data, such as Long Short Term Memory (LSTM) [144], to achieve better 3D posture estimation performance. In addition, the generalization ability and accuracy of the proposed network could be further improved through redesigning the loss function. Different from other 3D reconstruction problems, human body posture's 3D reconstruction has more constraints, such as constant bone length and maximum joint angle. These constraints could be added to the loss function in the training period, which might increase the accuracy. Besides, since these constraints are generalized rules, which are independent of the training data set, so applying the constraints in the training period may increase the generalization ability.

Finally, further large-scale experiments are needed in order to develop an industry-level guideline for managing and preventing physical fatigue. Field experiments are needed to 1) test the robustness of the proposed PFA method, 2) enhance the accuracy of posture estimation algorithms and joint physical fatigue indicators module and 3) explore the rules of physical fatigue among construction workers, such as fatigue-prone joints of each crew, dangerous postures in each construction, and data-based work-rest schedule guidelines. In the long term, this study would contribute to industry-wide guidance and legislative improvement on fatigue prevention. Such efforts will significantly reduce the possibility of non-fatal and fatal injuries, reduce the time loss and various costs of construction companies caused by workers’ injuries, and improve occupational safety, health and productivity in the construction industry.

References

[1] W. Umer, M.F. Antwi-Afari, H. Li, G.P. Szeto, A.Y. Wong, The prevalence of musculoskeletal disorders in the construction industry: A systematic review and meta-analysis, International Archives of Occupational and Environmental Health. 91 (2018) 125–144. doi:10.1007/s00420-017-1273-4.

[2] U.S. Bureau of Labor Statistics, Nonfatal Occupational Injuries and Illnesses Requiring Days Away From Work, (2016). https://www.bls.gov/news.release/osh2.toc.htm (accessed April 20, 2018).

[3] D. Wang, F. Dai, X. Ning, Risk Assessment of Work-Related Musculoskeletal Disorders in Construction: State-of-the-Art Review, Journal of Construction Engineering and Management. 141 (2015) 04015008. doi:10.1061/(ASCE)CO.1943-7862.0000979.

[4] Construciton Industry Council, Forecast of manpower situation of skilled construction workers, Construciton industry council, Hong Kong, 2016. http://www.cic.hk/Forecast_SkilledWorkers_e/20161216_Forecast_Skilled Workers_e.pdf (accessed June 26, 2018).

[5] Census and Statistics Department, Selected Statistics for All Establishments in the Industry Section of Construction, The Goverment of the Hong Kong Special Administrative Region. (2018) https://www.censtatd.gov.hk/hkstat/sub/so330.jsp. https://www.censtatd.gov.hk/hkstat/sub/so330.jsp (accessed December 24, 2018).

[6] Research Office of Legislative Council Secretariat, Construction industry in Hong Kong, Hong Kong, 2018. https://www.legco.gov.hk/research-publications/english/1819issh07-construction-industry-in-hong-kong-20181121-e.pdf (accessed April 28, 2019).

[7] R.H. Fitts, Cellular mechanisms of muscle fatigue, Physiological Reviews. 74 (1994) 49–94. doi:10.1152/physrev.1994.74.1.49.

[8] M.R. Frone, M.-C.O. Tidwell, The meaning and measurement of work fatigue: Development and evaluation of the Three-Dimensional Work Fatigue Inventory (3D-WFI)., Journal of Occupational Health Psychology. 20 (2015) 273–288. doi:10.1037/a0038700.

[9] T. Åkerstedt, A. Knutsson, P. Westerholm, T. Theorell, L. Alfredsson, G. Kecklund, Mental fatigue, work and sleep, Journal of Psychosomatic Research. 57 (2004) 427–433. doi:10.1016/j.jpsychores.2003.12.001.

[10] U.D. Techera, Measuring and Managing Construction Worker Fatigue, Polytechnic University of Catalonia, 2017. https://scholar.colorado.edu/cven_gradetds/98 (accessed May 7, 2018).

[11] A. Golabchi, S. Han, J. Seo, S. Han, S. Lee, M. Al-Hussein, An Automated Biomechanical Simulation Approach to Ergonomic Job Analysis for Workplace Design, Journal of Construction Engineering and Management. 141 (2015) 04015020. doi:10.1061/(ASCE)CO.1943-7862.0000998.

[12] H. Lingard, R. Wakefield, Integrating Work Health and Safety into Construction Project Management, Wiley, 2019. doi:10.1002/9781119159933.

[13] J.E. Ware Jr., SF-36 Health Survey., The Use of Psychological Testing for Treatment Planning and Outcomes Assessment, 2nd Ed. (1999) 1227–1246.

[14] G.A. Borg, Psychophysical bases of perceived exertion, Medicine and Science in Sports and Exercise. 14 (1982) 377–81. http://www.ncbi.nlm.nih.gov/pubmed/7154893.

[15] D. Minichberger, Indicators and data collection, Florence, 2017. http://www.interact-eu.net/.

[16] M. Zhang, E.H. Sparer, L.A. Murphy, J.T. Dennerlein, D. Fang, J.N. Katz, A.J. Caban-Martinez, Development and validation of a fatigue assessment scale for U.S. construction workers, American Journal of Industrial Medicine. 58 (2015) 220–228. doi:10.1002/ajim.22411.

[17] P. Mitropoulos, B. Memarian, Task Demands in Masonry Work: Sources, Performance Implications, and Management Strategies, Journal of Construction Engineering and Management. 139 (2013) 581–590. doi:10.1061/(ASCE)CO.1943-7862.0000586.

[18] W. Umer, H. Li, G.P.Y. Szeto, A.Y.L. Wong, Low-Cost Ergonomic Intervention for Mitigating Physical and Subjective Discomfort during Manual Rebar Tying, Journal of Construction Engineering and Management. 143 (2017) 04017075. doi:10.1061/(ASCE)CO.1943-7862.0001383.

[19] A. Aryal, A. Ghahramani, B. Becerik-Gerber, Monitoring fatigue in construction workers using physiological measurements, Automation in Construction. 82 (2017) 154–165. doi:10.1016/j.autcon.2017.03.003.

[20] W. Lee, K.-Y. Lin, E. Seto, G.C. Migliaccio, Wearable sensors for monitoring on-duty and off-duty worker physiological status and activities in construction, Automation in Construction. 83 (2017) 341–353. doi:10.1016/j.autcon.2017.06.012.

[21] C. Tao, M.G. C., T. Jochen, G.U. C., Data Fusion of Real-Time Location Sensing and Physiological Status Monitoring for Ergonomics Analysis of Construction Workers, Journal of Computing in Civil Engineering. 27 (2013) 320–335. doi:10.1061/(ASCE)CP.1943-5487.0000222.

[22] W. Yi, A.P.C. Chan, X. Wang, J. Wang, Development of an early-warning system for site work in hot and humid environments: A case study, Automation in Construction. 62 (2016) 101–113. doi:10.1016/j.autcon.2015.11.003.

[23] G. Borg, Borg's perceived exertion and pain scales, Human kinetics, Champaign, IL, US, 1998.

[24] U.C. Gatti, S. Schneider, G.C. Migliaccio, Physiological condition monitoring of construction workers, Automation in Construction. 44 (2014) 227–233. doi:http://dx.doi.org/10.1016/j.autcon.2014.04.013.

[25] P.M. Kirk, M.J.M. Sullman, Heart rate strain in cable hauler choker setters in New Zealand logging operations, Applied Ergonomics. 32 (2001) 389–398. doi:https://doi.org/10.1016/S0003-6870(01)00003-5.

[26] M.R. Al-Mulla, F. Sepulveda, M. Colley, A Review of Non-Invasive Techniques to Detect and Predict Localised Muscle Fatigue, Sensors. 11 (2011) 3545–3594. doi:10.3390/s110403545.

[27] H.N. Alyea, Basics of sEMG, Journal of Chemical Education. 43 (1966).

[28] H.J. Hermens, B. Freriks, C. Disselhorst-Klug, G. Rau, Development of recommendations for SEMG sensors and sensor placement procedures, Journal of Electromyography and Kinesiology. 10 (2000) 361–374.

[29] M.F. Antwi-Afari, H. Li, J. Seo, A.Y.L. Wong, Automated detection and classification of construction workers' loss of balance events using wearable insole pressure sensors, Automation in Construction. 96 (2018) 189–199. doi:10.1016/j.autcon.2018.09.010.

[30] C.S. Moriguchi, L. Carnaz, K.B. Veiersted, T.N. Hanvold, L.B. Hæg, G.-Å. Hansson, H.J. Cote Gil Coury, Occupational posture exposure among construction electricians, Applied Ergonomics. 44 (2013) 86–92. doi:10.1016/j.apergo.2012.05.002.

[31] X. Yan, H. Li, C. Wang, J. Seo, H. Zhang, H. Wang, Development of ergonomic posture recognition technique based on 2D ordinary camera for construction hazard prevention through view-invariant features in 2D skeleton motion, Advanced Engineering Informatics. 34 (2017) 152–163. doi:10.1016/j.aei.2017.11.001.

[32] X. Yan, H. Li, A.R. Li, H. Zhang, Wearable IMU-based real-time motion warning system for construction workers' musculoskeletal disorders prevention, Automation in Construction. 74 (2017) 2–11. doi:10.1016/j.autcon.2016.11.007.

[33] N.D. Nath, R. Akhavian, A.H. Behzadan, Ergonomic analysis of construction worker's body postures using wearable mobile sensors, Applied Ergonomics. 62 (2017) 107–117. doi:10.1016/j.apergo.2017.02.007.

[34] D. Roman-Liu, Comparison of concepts in easy-to-use methods for MSD

risk assessment, Applied Ergonomics. 45 (2014) 420–427. doi:10.1016/j.apergo.2013.05.010.

[35] T.R. Waters, V. Putz-Anderson, A. Garg, L.J. Fine, Revised NIOSH equation for the design and evaluation of manual lifting tasks, Ergonomics. 36 (1993) 749–776. doi:10.1080/00140139308967940.

[36] O. Karhu, R. Härkönen, P. Sorvali, P. Vepsäläinen, Observing working postures in industry: Examples of OWAS application, Applied Ergonomics. 12 (1981) 13–17. doi:10.1016/0003-6870(81)90088-0.

[37] E. Occhipiniti, OCRA: a concise index for the assessment of exposure to repetitive movements of the upper limbs, Ergonomics. 41 (1998) 1290–1311. doi:10.1080/001401398186315.

[38] L. McAtamney, E. Nigel Corlett, RULA: a survey method for the investigation of work-related upper limb disorders, Applied Ergonomics. 24 (1993) 91–99. doi:10.1016/0003-6870(93)90080-S.

[39] S. Hignett, L. McAtamney, Rapid Entire Body Assessment (REBA), Applied Ergonomics. 31 (2000) 201–205. doi:10.1016/S0003-6870(99)00039-3.

[40] The University of Michigan, 3D Static Strength Predication Program, Ver. 2.0, User's Manual, (1995). https://c4e.engin.umich.edu/tools-services/3dsspp-software/ (accessed April 18, 2018).

[41] S.L. Delp, F.C. Anderson, A.S. Arnold, P. Loan, A. Habib, C.T. John, E. Guendelman, D.G. Thelen, OpenSim: Open-Source Software to Create and Analyze Dynamic Simulations of Movement, IEEE Transactions on Biomedical Engineering. 54 (2007) 1940–1950. doi:10.1109/TBME.2007.901024.

[42] The AnyBody Modeling System, (2018). https://www.anybodytech.com/software/ams/ (accessed April 19, 2018).

[43] J. Seo, M. Moon, S. Lee, Construction Operation Simulation Reflecting Workers' Muscle Fatigue, in: Computing in Civil Engineering, American Society of Civil Engineers, Reston, VA, 2015: pp. 515–522. doi:10.1061/9780784479247.064.

[44] J. Seo, R. Starbuck, S. Han, S. Lee, T.J. Armstrong, Motion Data-Driven Biomechanical Analysis during Construction Tasks on Sites, Journal of Computing in Civil Engineering. 29 (2015) B4014005. doi:10.1061/(ASCE)CP.1943-5487.0000400.

[45] C. John, S. Hammer, Collecting Experimental Data - OpenSim 3.3 Documentation -, (2017). https://simtk-confluence.stanford.edu:8443/display/OpenSim33/Collecting+Experimental+Data (accessed November 13, 2018).

[46] D. Meldrum, E. Cahalane, R. Conroy, D. Fitzgerald, O. Hardiman, Maximum voluntary isometric contraction: Reference values and clinical

application, Amyotrophic Lateral Sclerosis. (2007). doi:10.1080/17482960601012491.

[47] J. Ding, A.S. Wexler, S.A. Binder-Macleod, A predictive fatigue model - II: Predicting the effect of resting times on fatigue, IEEE Transactions on Neural Systems and Rehabilitation Engineering. 10 (2002) 59–67. doi:10.1109/TNSRE.2002.1021587.

[48] D.G. Allen, G.D. Lamb, H. Westerblad, Skeletal Muscle Fatigue: Cellular Mechanisms, Physiological Reviews. 88 (2008) 287–332. doi:10.1152/physrev.00015.2007.

[49] Y. Giat, J. Mizrahi, M. Levy, A musculotendon model of the fatigue profiles of paralyzed quadriceps muscle under FES, IEEE Transactions on Biomedical Engineering. 40 (1993) 664–674. doi:10.1109/10.237696.

[50] L. Ma, W. Zhang, S. Wu, Z. Zhang, A new simple local muscle recovery model and its theoretical and experimental validation, International Journal of Occupational Safety and Ergonomics. (2015). doi:10.1080/10803548.2015.1017961.

[51] F. Buchthal, H. Schmalbruch, Motor unit of mammalian muscle., Physiological Reviews. 60 (1980) 90–142. doi:10.1152/physrev.1980.60.1.90.

[52] D. Seth, D. Chablat, S. Sakka, F. Bennis, Experimental Validation of a New Dynamic Muscle Fatigue Model, in: International Conference on Digital Human Modeling and Applications in Health, Safety, Ergonomics and Risk Management, 2016: pp. 54–65. doi:https://doi.org/10.1007/978-3-319-40247-5_6.

[53] J. Seo, S. Lee, J. Seo, Simulation-Based Assessment of Workers' Muscle Fatigue and Its Impact on Construction Operations, Journal of Construction Engineering and Management. 142 (2016) 04016063. doi:10.1061/(ASCE)CO.1943-7862.0001182.

[54] S. McCaw, Biomechanics For Dummies, Wiley, 2014https://books.google.com.hk/books?id=6S7qAgAAQBAJ.

[55] C.A. Oatis, Kinesiology : the mechanics and pathomechanics of human movement, Third edit, Wolters Kluwer, Philadelphia, 2017.

[56] M. Dalstra, R. Huiskes, L. van Erning, Development and Validation of a Three-Dimensional Finite Element Model of the Pelvic Bone, Journal of Biomechanical Engineering. 117 (1995) 272–278. doi:10.1115/1.2794181.

[57] G. Li, J. Gil, A. Kanamori, S.L.-Y. Woo, A Validated Three-Dimensional Computational Model of a Human Knee Joint, Journal of Biomechanical Engineering. 121 (1999) 657–662. doi:10.1115/1.2800871.

[58] A. Rajagopal, C.L. Dembia, M.S. DeMers, D.D. Delp, J.L. Hicks, S.L. Delp, Full-Body Musculoskeletal Model for Muscle-Driven Simulation of Human

Gait, IEEE Transactions on Biomedical Engineering. 63 (2016) 2068–2079. doi:10.1109/TBME.2016.2586891.

[59] J. Hicks, Preparing your data for OpeinSim 3.3, National Center for Simulation in Rehabilitation Research (NCSRR), US. (2018). https://simtk-confluence.stanford.edu:8443/display/OpenSim33/Preparing+Your+Data (accessed December 24, 2018).

[60] R. Feyen, Y. Liu, D. Chaffin, G. Jimmerson, B. Joseph, Computer-aided ergonomics: a case study of incorporating ergonomics analyses into workplace design, Applied Ergonomics. 31 (2000) 291–300. doi:10.1016/S0003-6870(99)00053-8.

[61] D.B. Chaffin, Development of computerized human static strength simulation model for job design, Human Factors and Ergonomics in Manufacturing. 7 (1997) 305–322. doi:10.1002/(SICI)1520-6564(199723)7:4<305::AID-HFM3>3.0.CO;2-7.

[62] Y.-K. Kong, D.-M. Kim, The relationship between hand anthropometrics, total grip strength and individual finger force for various handle shapes, International Journal of Occupational Safety and Ergonomics. 21 (2015) 187–192. doi:10.1080/10803548.2015.1029726.

[63] R. Merletti, A. Botter, A. Troiano, E. Merlo, M.A. Minetto, Technology and instrumentation for detection and conditioning of the surface electromyographic signal: State of the art, Clinical Biomechanics. 24 (2009) 122–134. doi:10.1016/j.clinbiomech.2008.08.006.

[64] E.R. Komi, J.R. Roberts, S.J. Rothberg, Evaluation of thin, flexible sensors for time-resolved grip force measurement, Proceedings of the Institution of Mechanical Engineers, Part C: Journal of Mechanical Engineering Science. 221 (2007) 1687–1699. doi:10.1243/09544062JMES700.

[65] S. Sundaram, P. Kellnhofer, Y. Li, J.-Y. Zhu, A. Torralba, W. Matusik, Learning the signatures of the human grasp using a scalable tactile glove, Nature. 569 (2019) 698–702. doi:10.1038/s41586-019-1234-z.

[66] W. Umer, H. Li, W. Lu, G. Pui, Y. Szeto, A.Y.L. Wong, Development of a tool to monitor static balance of construction workers for proactive fall safety management, Automation in Construction. 94 (2018) 438–448. doi:10.1016/j.autcon.2018.07.024.

[67] M. Saito, K. Nakajima, C. Takano, Y. Ohta, C. Sugimoto, R. Ezoe, K. Sasaki, H. Hosaka, T. Ifukube, S. Ino, K. Yamashita, An in-shoe device to measure plantar pressure during daily human activity, Medical Engineering & Physics. 33 (2011) 638–645. doi:10.1016/j.medengphy.2011.01.001.

[68] M.F. Antwi-Afari, Y. Yu, H. Li, A. Darko, J. Seo, Y.L.A. Wong, Automated Detection and Classification of Potential Biomechanical Risk Factors for Work-Related Musculoskeletal Disorders Using Wearable Insole Pressure Sensors, in: 1st Postgraduate Applied Research Conference in Africa,

Applied Research Conference in Africa, Accra, Ghana, 2018.

[69] P.I. Simeonov, H.W. Hsiao, B.W. Dotson, D.E. Ammons, Control and perception of balance at elevated and sloped surfaces, HUMAN FACTORS. 45 (2003) 136–147. doi:10.1518/hfes.45.1.136.27232.

[70] M.F. Antwi-Afari, H. Li, D.J. Edwards, E.A. Pärn, J. Seo, A. Wong, Effects of different weights and lifting postures on balance control following repetitive lifting tasks in construction workers, International Journal of Building Pathology and Adaptation. 35 (2017) 247–263. doi:10.1108/IJBPA-05-2017-0025.

[71] A.J. Caban-Martinez, K.M. Santiago, J. Stillman, K.J. Moore, D.A. Sierra, J. Chalmers, M. Baniak, M.M. Jordan, Physical Exposures, Work Tasks, and OSHA-10 Training Among Temporary and Payroll Construction Workers, Journal of Occupational and Environmental Medicine. 60 (2018) E159–E165. doi:10.1097/JOM.0000000000001267.

[72] L.A.M. Elders, A. Burdorf, Interrelations of risk factors and low back pain in scaffolders, Occupational and Environmental Medicine. 58 (2001) 597–603. doi:10.1136/oem.58.9.597.

[73] A. DiDomenico, R.W. McGorry, Y.H. Huang, M.F. Blair, Perceptions of postural stability after transitioning to standing among construction workers, Safety Science. 48 (2010) 166–172. doi:10.1016/j.ssci.2009.07.006.

[74] R.A. Rwamamara, O. Lagerqvist, T. Olofsson, B.M. Johansson, K.A. Kaminskas, Evidence-Based Prevention of Work-Related Musculoskeletal Injuries in Construction Industry, Journal of Civil Engineering and Management. 16 (2010) 499–509. doi:10.3846/jcem.2010.56.

[75] American Psychological Association, Systematic observation – APA Dictionary of Psychology, American Psychological Association. (2019). https://dictionary.apa.org/systematic-observation (accessed August 6, 2019).

[76] L. Rose, R. Ortengren, M. Ericson, Endurance, pain and resumption in fully flexed postures, Applied Ergonomics. 32 (2001) 501–508. doi:10.1016/S0003-6870(01)00016-3.

[77] H. Sporrong, L. Sandsjo, R. Kadefors, P. Herberts, Assessment of workload and arm position during different work sequences: a study with portable devices on construction workers, Applied Ergonomics. 30 (1999) 495–503. doi:10.1016/S0003-6870(99)00016-2.

[78] B. Buchholz, V. Paquet, L. Punnett, D. Lee, S. Moir, PATH: A work sampling-based approach to ergonomic job analysis for construction and other non-repetitive work, Applied Ergonomics. 27 (1996) 177–187. doi:10.1016/0003-6870(95)00078-X.

[79] B. Gram, K. Westgate, K. Karstad, A. Holtermann, K. Sogaard, S. Brage, G. Sjogaard, Occupational and leisure-time physical activity and workload

among construction workers - a randomized control study, International Journal of Occupational and Environmental Health. 22 (2016) 36–44. doi:10.1080/10773525.2016.1142724.

[80] S. Tak, B. Buchholz, L. Punnett, S. Moir, V. Paquet, S. Fulmer, H. Marucci-Wellman, D. Wegman, Physical ergonomic hazards in highway tunnel construction: Overview from the Construction Occupational Health Program, Applied Ergonomics. 42 (2011) 665–671. doi:10.1016/j.apergo.2010.10.001.

[81] R. Rwamamara, P. Simonsson, Self-Compacting Concrete Use for Construction Work Environment Sustainability, Journal of Civil Engineering and Management. 18 (2012) 724–734. doi:10.3846/13923730.2012.723399.

[82] A. Golabchi, S. Han, A.R. Fayek, A fuzzy logic approach to posture-based ergonomic analysis for field observation and assessment of construction manual operations, Canadian Journal of Civil Engineering. 43 (2016) 294–303. doi:10.1139/cjce-2015-0143.

[83] G. Dudek, M. Jenkin, Inertial Sensors, GPS, and Odometry, in: B. Siciliano, O. Khatib (Eds.), Springer Handbook of Robotics, Springer Berlin Heidelberg, Berlin, Heidelberg, 2008: pp. 477–490. doi:10.1007/978-3-540-30301-5_21.

[84] Yost Labs, 3-Space™ Blue Tooth, (2019). https://yostlabs.com/product/3-space-bluetooth/ (accessed January 10, 2020).

[85] H. Jebelli, C.R. Ahn, T.L. Stentz, Fall risk analysis of construction workers using inertial measurement units: Validating the usefulness of the postural stability metrics in construction, Safety Science. 84 (2016) 161–170. doi:10.1016/j.ssci.2015.12.012.

[86] H. Kim, C.R. Ahn, K. Yang, Identifying Safety Hazards Using Collective Bodily Responses of Workers, Journal of Construction Engineering and Management. 143 (2017). doi:10.1061/(ASCE)CO.1943-7862.0001220.

[87] J.A. Hess, L.D. Kincl, K. Davis, The impact of drywall handling tools on the low back, Applied Ergonomics. 41 (2010) 305–312. doi:10.1016/j.apergo.2009.08.001.

[88] E. Valero, A. Sivanathan, F. Bosche, M. Abdel-Wahab, Analysis of construction trade worker body motions using a wearable and wireless motion sensor network, Automation in Construction. 83 (2017) 48–55. doi:10.1016/j.autcon.2017.08.001.

[89] A. Alwasel, A. Sabet, M. Nahangi, C.T. Haas, E. Abdel-Rahman, Identifying poses of safe and productive masons using machine learning, Automation in Construction. 84 (2017) 345–355. doi:10.1016/j.autcon.2017.09.022.

[90] J. Chen, J. Qiu, C. Ahn, Construction worker's awkward posture recognition through supervised motion tensor decomposition, Automation in

Construction. 77 (2017) 67–81. doi:10.1016/j.autcon.2017.01.020.

[91] S.S. Chiou, C.S. Pan, A. Bhattacharya, Kinematics and kinetics of gait on stilts: Identification of risk factors associated with construction stilt use, Ergonomics. 51 (2008) 1814–1829. doi:10.1080/00140130801961885.

[92] P. Simeonov, H. Hsiao, J. Powers, D. Ammons, T. Kau, A. Amendola, Postural stability effects of random vibration at the feet of construction workers in simulated elevation, Applied Ergonomics. 42 (2011) 672–681. doi:10.1016/j.apergo.2010.10.002.

[93] Z. Wang, G. Liu, G. Tian, A Parameter Efficient Human Pose Estimation Method Based on Densely Connected Convolutional Module, IEEE Access. 6 (2018) 58056–58063. doi:10.1109/ACCESS.2018.2874307.

[94] H. Sarbolandi, D. Lefloch, A. Kolb, Kinect range sensing: Structured-light versus Time-of-Flight Kinect, Computer Vision and Image Understanding. 139 (2015) 1–20. doi:10.1016/j.cviu.2015.05.006.

[95] S. Han, S. Lee, F. Peña-Mora, Vision-Based Detection of Unsafe Actions of a Construction Worker: Case Study of Ladder Climbing, Journal of Computing in Civil Engineering. 27 (2013) 635–644. doi:10.1061/(ASCE)CP.1943-5487.0000279.

[96] M. Liu, S. Han, S. Lee, Tracking-based 3D human skeleton extraction from stereo video camera toward an on-site safety and ergonomic analysis, Construction Innovation. 16 (2016) 348–367. doi:10.1108/CI-10-2015-0054.

[97] S. Han, S. Lee, A vision-based motion capture and recognition framework for behavior-based safety management, Automation in Construction. 35 (2013) 131–141. doi:10.1016/j.autcon.2013.05.001.

[98] H. Guo, Y. Yu, Q. Ding, M. Skitmore, Image-and-Skeleton-Based Parameterized Approach to Real-Time Identification of Construction Workers' Unsafe Behaviors, Journal of Construction Engineering and Management. 144 (2018) 04018042. doi:10.1061/(ASCE)CO.1943-7862.0001497.

[99] Y. Yu, H. Guo, Q. Ding, H. Li, M. Skitmore, An experimental study of real-time identification of construction workers' unsafe behaviors, Automation in Construction. 82 (2017) 193–206. doi:10.1016/j.autcon.2017.05.002.

[100] G. Diraco, A. Leone, P. Siciliano, Human posture recognition with a time-of-flight 3D sensor for in-home applications, Expert Systems with Applications. 40 (2013) 744–751. doi:10.1016/j.eswa.2012.08.007.

[101] Y. He, B. Liang, Y. Zou, J. He, J. Yang, Depth Errors Analysis and Correction for Time-of-Flight (ToF) Cameras, Sensors. 17 (2017) 92. doi:10.3390/s17010092.

[102] M.-W. Park, I. Brilakis, Construction worker detection in video frames for

initializing vision trackers, Automation in Construction. 28 (2012) 15–25. doi:10.1016/j.autcon.2012.06.001.

[103] M. Memarzadeh, M. Golparvar-Fard, J.C. Niebles, Automated 2D detection of construction equipment and workers from site video streams using histograms of oriented gradients and colors, Automation in Construction. 32 (2013) 24–37. doi:http://dx.doi.org/10.1016/j.autcon.2012.12.002.

[104] Y. Bai, J. Huan, S. Kim, Measuring Bridge Construction Efficiency Using the Wireless Real-Time Video Monitoring System, Journal of Management in Engineering. 28 (2012) 120–126. doi:10.1061/(ASCE)ME.1943-5479.0000061.

[105] S.J. Ray, J. Teizer, Real-time construction worker posture analysis for ergonomics training, Advanced Engineering Informatics. 26 (2012) 439–455. doi:10.1016/j.aei.2012.02.011.

[106] H. Zhang, X. Yan, H. Li, Ergonomic posture recognition using 3D view-invariant features from single ordinary camera, Automation in Construction. 94 (2018) 1–10. doi:10.1016/j.autcon.2018.05.033.

[107] Y. Yu, H. Li, X. Yang, L. Kong, X. Luo, A.Y.L. Wong, An automatic and non-invasive physical fatigue assessment method for construction workers, Automation in Construction. 103 (2019) 1–12. doi:10.1016/j.autcon.2019.02.020.

[108] Y. Chung, P.J. Haas, E. Upfal, T. Kraska, Unknown Examples & Machine Learning Model Generalization, (2018) 1–11. http://arxiv.org/abs/1808.08294.

[109] N. Askham, D. Cook, M. Doyle, H. Fereday, M. Gibson, U. Landbeck, R. Lee, C. Maynard, G. Palmer, J. Schwarzenbach, The six primary dimensions for data quality management, The Global Data Management Community. (2013) 6. https://www.whitepapers.em360tech.com/wp-content/files_mf/1407250286DAMAUKDQDimensionsWhitePaperR37.pdf.

[110] H. Guo, Y. Yu, T. Xiang, H. Li, D. Zhang, The availability of wearable-device-based physical data for the measurement of construction workers' psychological status on site: From the perspective of safety management, Automation in Construction. 82 (2017) 207–217. doi:10.1016/j.autcon.2017.06.001.

[111] Y. Yu, X. Yang, H. Li, X. Luo, H. Guo, Q. Fang, Joint-Level Vision-Based Ergonomic Assessment Tool for Construction Workers, Journal of Construction Engineering and Management. 145 (2019) 04019025. doi:10.1061/(ASCE)CO.1943-7862.0001647.

[112] K. Ball, Workplace surveillance: an overview, Labor History. 51 (2010) 87–106. doi:10.1080/00236561003654776.

[113] Y. Khosravi, H. Asilian-Mahabadi, E. Hajizadeh, N. Hassanzadeh-Rangi, H. Bastani, A.H. Behzadan, Factors influencing unsafe behaviors and accidents on construction sites: A review, International Journal of Occupational Safety and Ergonomics. 20 (2014) 111–125. doi:10.1080/10803548.2014.11077023.

[114] P.J. Holland, B. Cooper, R. Hecker, Electronic monitoring and surveillance in the workplace, Personnel Review. 44 (2015) 161–175. doi:10.1108/PR-11-2013-0211.

[115] C.-H. Chen, D. Ramanan, 3D Human Pose Estimation = 2D Pose Estimation + Matching, in: 2017 IEEE Conference on Computer Vision and Pattern Recognition (CVPR), IEEE, 2017: pp. 5759–5767. doi:10.1109/CVPR.2017.610.

[116] X. Zhou, Q. Huang, X. Sun, X. Xue, Y. Wei, Towards 3D Human Pose Estimation in the Wild: A Weakly-Supervised Approach, in: 2017 IEEE International Conference on Computer Vision (ICCV), IEEE, 2017: pp. 398–407. doi:10.1109/ICCV.2017.51.

[117] MVN, MVN Analyze, (2019). https://www.xsens.com/products/mvn-analyze (accessed January 10, 2020).

[118] MotionNode, MotionNode Miniature Inertial Measurement Unit, (2019). https://www.motionnode.com/ (accessed January 10, 2020).

[119] OptiTrack, OptiTrack - Build Your Own Motion Capture System, (2019). https://optitrack.com/systems/ (accessed January 10, 2020).

[120] Nokov Mocap, About Nokov Motion Capture System, (2019). https://www.nokov.com/en/about (accessed January 10, 2020).

[121] Vicon, Vicon Visualization Tool | Build Your Ideal Motion Capture System, (2019). https://www.vicon.com/visualization/ (accessed January 10, 2020).

[122] Microsoft, Kinect for Windows v2 Xbox Sensor with Kinect Adapter for Windows, (2019). https://support.xbox.com/en-HK/xbox-on-windows/accessories/kinect-for-windows-v2-setup#c8652d85386a4baba138b73ac11e0899 (accessed January 10, 2020).

[123] Intel® RealSense™, Depth Camera D435 – Intel® RealSense™ Depth and Tracking Cameras, (2019). https://www.intelrealsense.com/depth-camera-d435/ (accessed January 10, 2020).

[124] TVico, TVico - Interactive Android™ Box, (2019). https://tvico.io/ (accessed January 10, 2020).

[125] Hikvision, DS-2CE56C0T-IT3 1MP CMOS EXIR Turret Camera Key Features, 2019. https://www.hikvision.com/hk/products/Turbo-HD-Products/Turbo-HD-Cameras/Value-Series/DS-2CE56C0T-IT3/ (accessed January 10, 2020).

[126] Dahua Technology USA, Eyeball Cameras – Dahua Technology USA Inc, (2019). https://us.dahuasecurity.com/product-category/network-products/fixed-cameras/pro/eyeball-cameras-pro/ (accessed January 10, 2020).

[127] Hikvision, DS-2DE3304W-DE 3MP Network Mini PTZ Dome Camera Key Features, 2019. https://www.hikvision.com/en/products/IP-Products/PTZ-Cameras/Pro-Series/DS-2DE3304W-DE/ (accessed January 10, 2020).

[128] C.S. Pan, K.M. Miller, S. Chiou, J.Z. Wu, EVALUATION OF A COMPUTER-SIMULATION MODEL FOR HUMAN AMBULATION ON STILTS, JOURNAL OF MECHANICS IN MEDICINE AND BIOLOGY. 4 (2004) 283–303. doi:10.1142/S0219519404001041.

[129] Z. Cao, G. Hidalgo, T. Simon, S.-E. Wei, Y. Sheikh, OpenPose: Realtime Multi-Person 2D Pose Estimation using Part Affinity Fields, (2018). http://arxiv.org/abs/1812.08008.

[130] Yost Labs, 3-Space^{TM} Sensors, Yost Labs. (2017). https://yostlabs.com/3-space-sensors/ (accessed April 19, 2018).

[131] A. Grinciunaite, A. Gudi, E. Tasli, M. den Uyl, Human Pose Estimation in Space and Time using 3D CNN, (2016). doi:10.1007/978-3-319-49409-8_5.

[132] G. Legnani, F. Casolo, P. Righettini, B. Zappa, A homogeneous matrix approach to 3D kinematics and dynamics — I. Theory, Mechanism and Machine Theory. 31 (1996) 573–587. doi:10.1016/0094-114X(95)00100-D.

[133] S. Ioffe, C. Szegedy, Batch Normalization: Accelerating Deep Network Training by Reducing Internal Covariate Shift, (2015). http://arxiv.org/abs/1502.03167.

[134] J. Martinez, R. Hossain, J. Romero, J.J. Little, A Simple Yet Effective Baseline for 3d Human Pose Estimation, in: 2017 IEEE International Conference on Computer Vision (ICCV), IEEE, 2017: pp. 2659–2668. doi:10.1109/ICCV.2017.288.

[135] D.P. Kingma, J. Ba, Adam: A Method for Stochastic Optimization, (2014). http://arxiv.org/abs/1412.6980.

[136] T. Stöggl, A. Martiner, Validation of Moticon's OpenGo sensor insoles during gait, jumps, balance and cross-country skiing specific imitation movements, Journal of Sports Sciences. 35 (2017) 196–206. doi:10.1080/02640414.2016.1161205.

[137] Standardization Administration of China, Human Dimensions of Chinese Adults, http://www.gb688.cn, 1988. doi:ICS 13.180.

[138] S. Shaunak, L. Ang, K. Colston, S. Patel, M. Bland, J.D. Maxwell, Muscle strength in healthy White and Asian subjects: The relationship of quadriceps maximum voluntary contraction to age, sex, body build and vitamin D, Clinical Science. 73 (1987) 541–546. doi:10.1042/cs0730541.

[139] J.Z. Liu, R.W. Brown, G.H. Yue, A dynamical model of muscle activation, fatigue, and recovery., Biophysical Journal. 82 (2002) 2344–2359. doi:10.1016/S0006-3495(02)75580-X.

[140] L. Ma, D. Chablat, F. Bennis, W. Zhang, F. Guillaume, A new muscle fatigue and recovery model and its ergonomics application in human simulation, Virtual and Physical Prototyping. 5 (2010) 123–137. doi:10.1080/17452759.2010.504056.

[141] V.S. Kulkarni, R. V Devalkar, Postural analysis of building construction workers using ergonomics, International Journal of Construction Management. (2018) 1–8. doi:10.1080/15623599.2018.1452096.

[142] D. Fang, Z. Jiang, M. Zhang, H. Wang, An experimental method to study the effect of fatigue on construction workers' safety performance, Safety Science. 73 (2015) 80–91. doi:10.1016/j.ssci.2014.11.019.

[143] T. Cheng, J. Teizer, G.C. Migliaccio, U.C. Gatti, Automated task-level activity analysis through fusion of real time location sensors and worker's thoracic posture data, Automation in Construction. 29 (2013) 24–39. doi:http://dx.doi.org/10.1016/j.autcon.2012.08.003.

[144] H. Sak, A. Senior, F. Beaufays, Long Short-Term Memory Based Recurrent Neural Network Architectures for Large Vocabulary Speech Recognition, (2014). https://arxiv.org/abs/1402.1128 (accessed April 26, 2018).